Università degli Studi di Roma "La Sapienza"

Dottorato di Ricerca in Astronomia XXV Ciclo

SAPIENZA
UNIVERSITÀ DI ROMA

Geophysical History of Asteroids 4 Vesta and 21 Lutetia

Tutors:

Dott. Fabrizio Capaccioni

Prof. Costanzo Federico

Dott. Diego Turrini

PhD Coordinator:

Prof. Roberto Capuzzo Dolcetta

PhD Student

Michelangelo Formisano

Matricola 1309816

2011-2012

"*Stars are small slits through which the light comes out of the infinite*".

(**Confucio)**

Contents

Introduction

English Version

In my work I analyzed the geophysical and thermal history of asteroids *4 Vesta* and *21 Lutetia*, two asteroids of the Main Belt, representing two important case study.

Vesta is one of the largest asteroid of the Main Belt and plays an important role in the comprehension of the primordial stages of the planetary formation. Spectroscopic studies of the HEDs (Howardite - Eucrite - Diogenite) indicate that Vesta is the source of the bulk of these meteorites and as a consequence we know it was one of the first bodies to have formed and differentiated in the Solar System. Therefore Vesta can be used as case study to investigate the primordial stages of the evolution of the terrestrial planets and of the Solar System in general.

Lutetia is a border-line object: it belong to those objects that survived to the collisional evolution of the Main Belt and possibly differentiated. Moreover it could be used as a case study to investigate the minimal conditions to obtain a differentiated object. Since the only data about Lutetia were provided by a single *Rosetta* flyby, theoretical models are needed to build a reference framework to correctly interpret the observational data.

To study the geophysical histories of these two asteroids I developed a numerical 1D model for the contemporary solution of the heat equation with radiogenic heat source and the advection equation, which controls the percolation of the metals inside the asteroids. The numerical solution is obtained using a finite difference method in radial direction (*FTCS scheme*). I investigated the link between the evolution of the internal structure and

thermal heating due to ^{26}Al and ^{60}Fe and long-lived radionuclide (e.g. ^{238}U and ^{235}U), taking into account the chemical differentiation of the body and the affinity of ^{26}Al with silicates: our simulation covered a timespan of 5 Ma starting from the condensation of CAIs. I considered primordial Vesta and Lutetia as spherical bodies with fixed radius (270 km and 50 km, respectively) and composed of a homogenous mixture of two components, the first one generically referred to as metals and the second generically referred to as silicates. This composition is similar to those of the H and L classes of the ordinary chondrites. I explored several thermal and structural scenarios differing in the available strength of energy due to the radiogenic heating and in the post-sintering macroporosity. In the case of Vesta, by comparing them with the data supplied by the HEDs, I used my results to constrain the accretion and differentiation time as well as the physical properties of the core, while in the case of Lutetia this comparison is not possible since we do not possess " *rock samples*" and the available data are quite limited. Nevertheless, I could constrain its formation time in case the asteroid partially differentiated.

My work is structured as following: in Cap.1 I report an overview regarding the Dawn and the Rosetta missions; in Cap.2 I describe the classification and main properties of the Main Belt asteroids, including Vesta and Lutetia; in Cap.3 I explore the thermal evolution of rocky asteroids, including the main source of energy and introduce the model I developed; in Cap.4 I describe the numerical procedure and, finally, in Cap.5 and Cap.6 I report the results obtained for Vesta and Lutetia and discuss them. Conclusions and an appendix, regarding on Von Neumann stability analysis for FTCS scheme, end my work.

Italian Version

In questo lavoro ho studiato l'evoluzione geofisica e termica degli asteroidi rocciosi 4 Vesta e 21 Lutetia, nelle fasi primordiali della loro esistenza. L'importanza di studiare Vesta è legata al fatto che questo asteroide presenta una struttura interna simile a quella della Terra ed inoltre è considerato, grazie a studi spettroscopici della missione Dawn della NASA, la sorgente

delle meteoriti HED (Howardite-Eucrite-Diogenite) raccolte sul nostro pianeta. Vesta è uno dei pochi oggetti intatti del Sistema Solare ad essere differenziato e di cui si dispone di materiale campione: può essere utilizzato come caso studio per investigare le fasi primordiali dell'evoluzione dei pianeti terrestri. Discorso diverso per Lutetia, di cui non si dispone di materiale campione e di cui si conosce ancora poco sulla struttura interna e sulla composizione superficiale. Dati osservativi sulla struttura interna, in particolare sulla densità, forniti dalla missione Rosetta dell'ESA fanno propendere per l'idea che Lutetia sia parzialmente differenziato e che disponga di un nucleo prevalentemente metallico.

In questo lavoro, ho sviluppato un codice per la risoluzione numerica contemporanea dell'equazione del calore, con termine di sorgente radiogenico, e dell'equazione di advezione, che regola la migrazione della componente metallica verso il centro dell'asteroide. Il metodo utilizzato è quello delle differenze finite ed il codice è stato sviluppato in linguaggio Python. Gli scenari esplorati differiscono per il differente contenuto iniziale di ^{26}Al (la sorgente principale di energia) nei due asteroidi considerati, e per la differente macroporosità post sintering. I due asteroidi, all'inizio delle simulazioni, sono considerati dei corpi sferici, con raggio fissato, e composti essenzialmente da due componenti: la prima è quella genericamente chiamata *metallica* e la seconda genericamente chiamata *silicatica*. Il tipo di composizione scelto è simile a quella delle classi H e L delle condriti ordinarie. La temperatura alla superficie è regolata dal bilancio tra il calore prodotto all'interno degli asteroidi e quello irraggiato alla superficie come un corpo nero.

Dagli scenari esplorati è possibile ricavare i tempi di accrescimento e differenziazione dei due asteroidi, oltre ai tempi di formazione e proprietà fisiche (dimensione, densità, momento di inerzia) del nucleo. Per Vesta, è possibile selezionare scenari compatibili con i vincoli osservativi forniti dalla missione *Dawn* della *NASA*. Per Lutetia, invece, i vincoli sulla struttura interna e sulla composizione superficiale, con cui discriminare gli scenari esplorati, sono forniti dalla missione *Rosetta* dell'*ESA*.

Chapter 1

Dawn and Rosetta missions

1.1 Dawn

1.1.1 Overview

Dawn is a NASA (in progress) mission whose goal is to explore Vesta and Ceres, two of the largest protoplanets of the Main Belt, remaining intact since their formation, in order to answer several important questions related to the formation and evolution of Solar System. The name Dawn is appropriate: in fact the mission will explore the *dawn* of our Solar System, trying to add important elements to our knowledge (Raymann et al., 2006). Vesta and Ceres are complementary asteroids and between the first bodies to form in the history of the Solar System. Vesta is a rocky body and it is considered the progenitor of HED meteorites (HEDs, in the following), while Ceres is believed to contain large quantities of ice. The profound differences in geology between these two protoplanets that formed and evolved so close to each other form a bridge from the rocky bodies of the inner Solar System to the icy bodies, all of which lay beyond in the outer Solar System. Dawn was launched on 27 September 2007, from pad 17-B at the Cape Canaveral Air Force Station on a Delta 7925-H rocket. The spacecraft flies by Mars in 2009 enroute to Vesta. Dawn made its closest approach (549 km) to Mars on 17 February 2009 during a successful gravity assist. After being captured by Vesta's gravity and entering its orbit on 16 July, 2011, Dawn moved itself to a lower, closer orbit, entering in a 4.3-hour low-

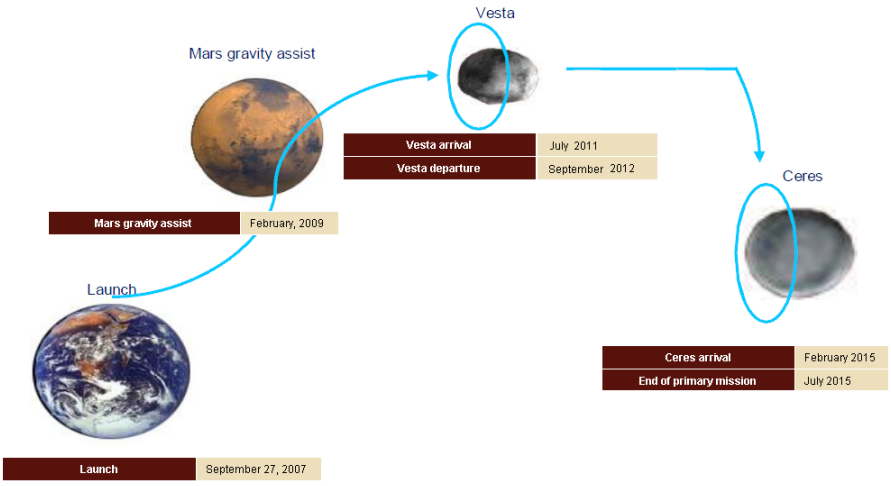

Figure 1.1: Overview of Dawn mission.

altitude mapping orbit at 21 km on 8 December 2011. Dawn left Vesta on September 2012. It is scheduled to arrive at Ceres in 2015: Dawn will thus be the first mission to study a dwarf planet at close range. A high-level mission timeline is shown in Fig.1.1. Dawn spacecraft carries three science instruments whose data will be used in combination to characterize these bodies. The instrument suite consists of redundant Framing Cameras (FC), a Visible and InfraRed mapping spectrometer (VIR) and a Gamma Ray and Neutron Detector (GRaND). In addition to these instruments, radiometric and optical navigation data will be used to determine the gravity field and thus bulk properties and internal structure of the two bodies.

1.1.2 Science Objectives

Dawn spacecraft images the surfaces of *Vesta* and *Ceres* to determine their bombardment, thermal, tectonic and possible volcanic history. It determines the topography and internal structure of these two complementary protoplanets that have remained intact since their formation, by measuring their mass, shape, volume and spin rate with navigation data and imagery. Dawn determines mineral and elemental composition from infrared, gamma ray and neutron spectroscopy to constrain the thermal history and compositional evolution of Ceres and Vesta and in addition provides context for

meteorites. It also uses the spectral information to search for water-bearing minerals. The objectives that are primarily answered by the redundant framing camera instruments are:

- To determine the origin and evolution of Vesta and Ceres by mapping the extent of geologic processes on the asteroid surfaces and by using the cratering record to establish a relative chronology of the crustal units and population of impactors in the early Solar System.
- To map the shape, determine the spin rate and establish the degree of cratering of the asteroids visited.
- To map the topography of Vesta and Ceres.
- To search for dust and satellites in the environment of the asteroid visited.

The framing camera will also contribute to answering some of the broader objectives:

- To provide a geologic, compositional and geophysical context for the HEDs.
- To provide an opportunity to identify Ceres-derived meteorites in their geologic context.

The visible and infrared spectrometer scientific objectives are:

- To provide a geologic, compositional and geophysical context for the HEDs.
- To provide an opportunity to identify Ceres-derived meteorites in their geologic context.
- To map the thermophysical properties of Vesta and Ceres.
- To determine the origin and evolution of Vesta and Ceres by mapping the mineralogical composition and its spatial variation across the asteroid surface.

The gamma ray and neutron spectrometer scientific objectives are:

- To map the major elemental composition of O, Si, Fe, Mg, Ti, Al, Ca and H on Vesta and Ceres.
- To map the trace elements U, Th, K, Gd and Sm on Vesta and Ceres.
- To provide a geologic, compositional and geophysical context for the HEDs.

The gravity science scientific objectives are:

- To determine the masses of the asteroid visited.
- To measure the bulk density of Vesta and Ceres, in conjunction with topography and determine its heterogeneity.
- To determine the gravitational fields of Vesta and Ceres.

In the best of scenarios, observations will enable informed contemplation of even more difficult questions. Arguably the most fascinating question is *Why did only one Vesta survive to the present day*? *How many differentiated parent bodies formed in the nascent Solar System*? *If there were many, then were the preponderance gravitationally perturbed out of Main Belt*? Scott et al. (2009) *Is Vesta really unique, or did its survival somehow defy probability*?
For more complex details see the website of the NASA Dawn mission: *http://dawn.jpl.nasa.gov/* .

1.2 Rosetta

1.2.1 Overview

ESA's Rosetta spacecraft will be the first to undertake the long-term exploration of a comet at close quarters. It comprises a large orbiter, which is designed to operate for a decade at large distances from the Sun, and a small lander. Each of these carries a large complement of scientific experiments designed to complete the most detailed study of a comet ever attempted. After entering orbit around Comet 67P Churyumov-Gerasimenko in 2014, the spacecraft will release a small lander onto the icy nucleus, then spend

the next two years orbiting the comet as it heads towards the Sun. On the way to Comet Churyumov-Gerasimenko, Rosetta will receive gravity assists from Earth and Mars, and will fly past Main Belt asteroids. Rosetta was launched as flight 158 on 2 March 2004 by an Ariane-5G rocket from Kourou, French Guiana. The spacecraft has already performed two successful asteroid flyby missions on its way to the comet. In 2007, Rosetta performed a Mars swingby (flyby), and returned images. The craft completed its fly-by of asteroid 2867 Steins in September 2008 and of 21 Lutetia in July 2010 and is presently in " hibernation" mode and on-target for its final destination. The spacecraft will remain in this state until 20 January 2014 when the hibernation exit sequence will be initiated (see Fig.1.2).

1.2.2 Science Objectives

Once attached to the comet, expected to take place in November 2014, the lander will begin its science mission:

- Characterization of the nucleus.
- Determination of the chemical compounds present.
- Study of comet activities and developments over time.

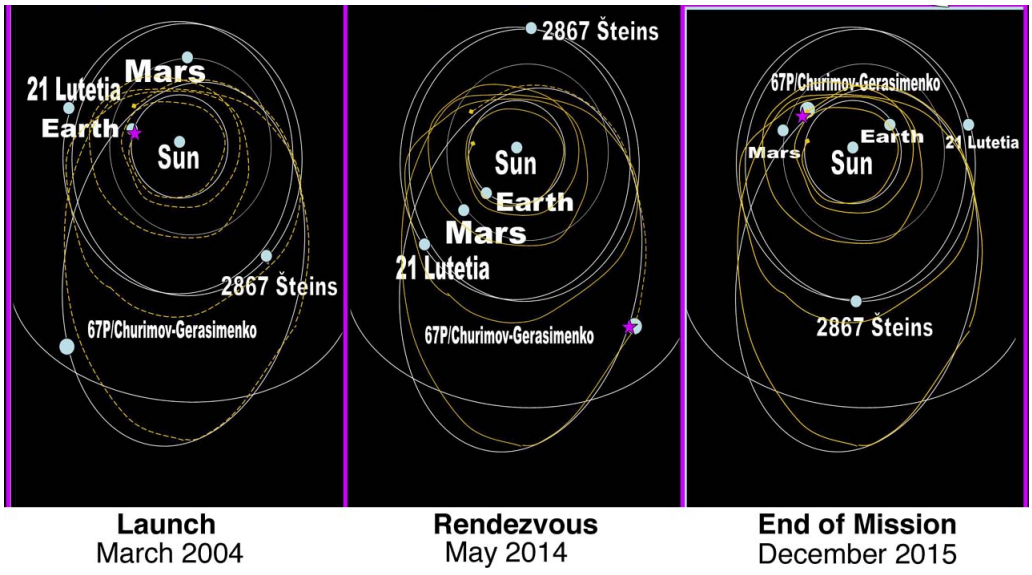

Figure 1.2: Trajectory of the Rosetta Space Probe.

Chapter 2

The Asteroids: Classification and Main Properties

2.1 Introduction

Any natural Solar System object other than the Sun, a planet, a dwarf planet or a moon is called a small body: these include asteroids, meteoroids and comets. Asteroids are minor planets that orbit the Sun at distances ranging from inside Mercury's orbit to outside the orbit of Neptune. Most known asteroids, however, are concentrated in the Main Belt, between the orbits of Mars and Jupiter, a demarcation point between the inner Solar System (consisting mainly of the terrestrial planets) and the outer Solar System (see Fig.2.1). By the end of the eighteenth century, especially after the discovery of Uranus, it was strongly believed that *Bode's Law* was fundamental in nature and that the gap between Mars and Jupiter should be occupied. Astronomers searched for the missing body and on 1 January 1801 such a body was found by Giuseppe Piazzi (1746-1826) who called it *Ceres*, after the guardian god of his native Sicily. On 24 January 1801, 23 days after, Piazzi commented: " *I have announced this star as a comet, but since it is not accompanied by any nebulosity and, further, since its movement is so slow and rather uniform, it has occurred to me several times that it might be something better than a comet.*" (Foderà Serio et al., 2003). The discover of other similar, if even smaller, bodies over the next few years was the prelude

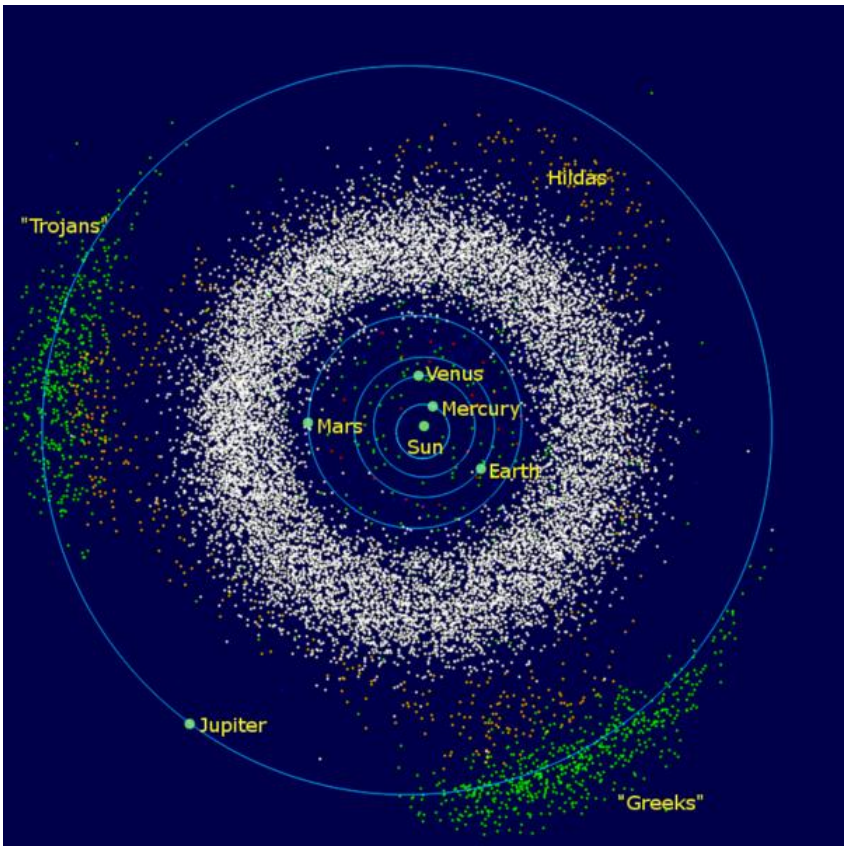

Figure 2.1: Main Belt (white) between inner and outer Solar System.

of many other discoveries of asteroids, which continues to the present day. These bodies have a variety of characteristics in terms of orbit, shape, size and composition.

2.2 Why studying Asteroids?

One of the main reason for studying the asteroids is that their physical properties, distribution, formation and evolution, are fundamental in our knowledge about planetary formation and emergence of life on Earth. In the Solar System the asteroids are, along with the comets, the most important remains of the original constituents of the planets. They preserved, in fact, pristine informations about the initial conditions of the Solar Nebula, about 4.6 Ga ago. The survived asteroids, however, underwent many ther-

mal and dynamic events that have determined their current form and orbital parameters. Interpreting these informations through observations and theoretical models we can improve our knowledge about the evolution of these small bodies in the Solar System. Even if the asteroids represent a very small fraction of the total mass of the Solar System, their amount, different composition and orbital distribution provide important constraints for the theoretical models of planetary formation, discerning about the several possible scenarios and trying to explain why life developed on Earth. Another more practical reason for the study and the monitoring of the asteroids is linked to the fact that some of these small bodies could impact with the Earth, procuring more o less irreparable damages. It is fairly diffuse the idea according to which, for example, dinosaurs are extinct precisely due to the impact of a large asteroid with the Earth (Bottke et al., 2003; Milani et al., 2003).

2.3 Origin and Evolution

The basic idea is that infall and rotation of the turbulent, protosolar molecular cloud caused flattening in a disk (Weidenschilling & Cuzzi, 1993). Dust grains from the protoplanetary disk collide, stick together and form clumps that progressively grow in size and mass. As material accumulated, more planetesimal surface area became available to add material so the process accelerated. There is much uncertainty in growth through centimeter and meter sizes because of lack of understanding of the relative importance of contributing processes that include collision and impact melting, charge exchange, gas drag and gravitational instability. Modeling growth to 1 to 10 km-sized bodies is also problematic. But beyond that point gravity becomes important and runaway growth can take place, though in the Main Belt perturbations from Jupiter likely complicate the situation. In this phase, collisional velocity relative to escape velocity is the major factor that determined whether collisional interactions led to net accretion or disruption of planetesimals (Leinhardt et al., 2000). During this phase gravitational focusing caused the largest planetesimals to quickly outgrow the rest of the population. Radiogenic isotope data from meteorites provide the best

constraints on timescales of protoplanet accretion. The earliest formed material in the Solar System, calcium-aluminum-rich inclusions (CAIs, in the following), are either high temperature condensates or refractory evaporative residues mostly formed within a few $\times 10^5$ years (Amelin et al., 2002) at 4.567 Ga, which is taken as the age of the Solar System . The age limits set by short-lived isotopic signatures in meteorites are all consistent with model predictions that it would take 10^5 to a few times 10^6 years to assemble km-sized to embryo-sized objects, respectively, in the Main Belt (Lugmair & Shukolyukov, 2001). At least two asteroids with basaltic surfaces, Vesta and Magnya, survive to this day. Other differentiated asteroids, were disrupted by collisions that stripped away their crusts and mantles and exposed their iron cores.

2.4 Classification

In the mid-1970s astronomers, using information gathered from studies of color, spectral reflectance and albedo, recognized that asteroids could be grouped into three broad taxonomic classes, designated C, S and M. At that time they estimated that about 75% belonged to class C, 15% to class S and 5% to class M. The remaining 5% were unclassifiable owing to either poor data or genuinely unusual properties. Furthermore, they noted that the S class dominated the population at the inner edge of the Main Belt, whereas the C class was dominant in the middle and outer region of the belt. Within a decade this taxonomic system was expanded and it was recognized that the Main Belt comprised overlapping rings of differing taxonomic classes, with classes designated S, C, P and D dominating the populations at distances from the Sun of about 2, 3, 4 and 5 AU, respectively (Tholen, 1989).

2.4.1 Rotation and Shape

The rotation periods and shapes of asteroids are determined primarily by monitoring their changing brightness on timescales of minutes to days. Short-period fluctuations in brightness caused by the rotation of an irregular shaped asteroid of a spherical spotted asteroid (i.e. one with albedo differences) produce a light curve that repeats at regular intervals correspond-

ing to an asteroid's rotation period. The range of brightness variation is closely related to an asteroid's shape or spottedness but is more difficult to interpret. The largest asteroids may have preserved the rotation rates they had when they were formed, but the smaller ones almost certainly have had theirs modified by subsequent collisions and, in the case of the very smallest, perhaps also by the radiation effects. The difference in rotation periods between 200-km-class and 100-km-class asteroids is believed to stem from the fact that large asteroids retain all of the collision debris from minor collisions, whereas smaller asteroids retain more of the debris ejected in the direction opposite to that of their spins, causing a loss of angular momentum and thus a reduction in speed of rotation. Major collisions can completely disrupt smaller asteroids. The debris from such collisions makes still smaller asteroids, which can have virtually any shape or spin rate (Pravec et al., 2003).

2.4.2 Mass and Density

Most asteroid masses are low, although present-day observations show that the asteroids measurably perturb the orbits of the major planets. Except for Mars, however, these perturbations are too small to allow the masses of the asteroids in question to be determined. The mass of the largest asteroid, Ceres, is 9.1×10^{20} kg, or less than 10^{-4} the mass of Earth. The masses of the second and third largest asteroids, Pallas and Vesta, are each only about one-fourth the mass of Ceres (see Fig.2.2). The mass of the entire Main Belt is roughly three times that of Ceres (see Fig.2.3). Most of the mass in the Main Belt is concentrated in the larger asteroids, with about 90% of the total in asteroids having diameters greater that 100 km. Of the total mass of the asteroids, 90% is located in the Main Belt (Hilton, 2003). The density of Ceres is similar to that of a class of meteorites known as carbonaceous chondrites, which contain a larger fraction of volatile material than do ordinary terrestrial rocks and hence have a somewhat lower density. The density of Pallas and Vesta are similar to those of Mars and the Moon. Insofar as Ceres, Pallas and Vesta are typical of asteroids in general, it can be concluded that Main Belt asteroids are rocky bodies. We want to stress

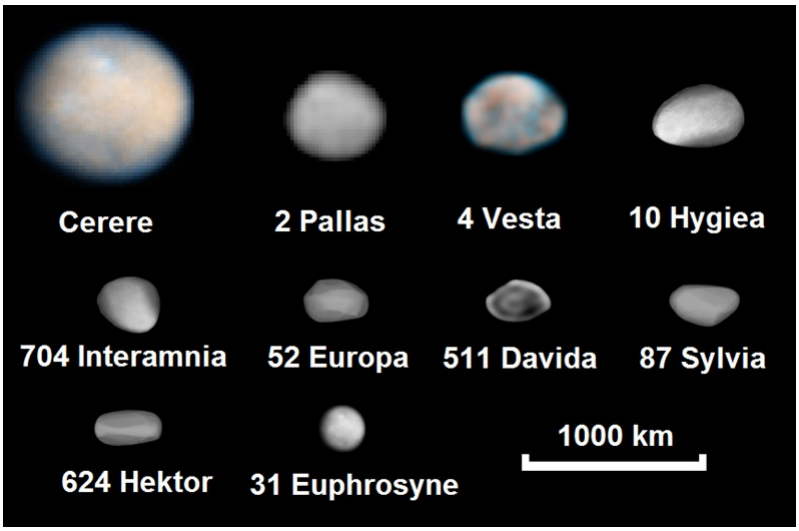

Figure 2.2: Comparison in scale between the ten largest asteroids in Main Belt.

that Vesta never grew to planetary size because of the formation of Jupiter at 5.2 AU, which caused disruptive resonance in the Main Belt. A recent paper investigated the bombardment on Vesta due to Jupiter formation and to its gradual displacement (Turrini et al., 2012).

2.4.3 Composition

The combination of albedos and spectral reflectance measurements specifically, measures of the amount of reflected sun-light at wavelengths between about 0.3 and 1.1 μm is used to classify asteroids into various taxonomic groups, as mentioned above. If sufficient spectral resolution is available, especially extending to wavelengths of about 2.5 μm, these measurements also can be used to infer the composition of the surface reflecting the light. This can be done by comparing the asteroid data with data obtained in the laboratory using meteorites or terrestrial rocks or minerals. Asteroids of the B, C, F, and G classes have low albedos and spectral reflectances similar to those of carbonaceous chondritic meteorites and their constituent assemblages produced by hydrothermal alteration and/or metamorphism of carbonaceous precursor materials. Some C class asteroids are known to have hydrated minerals on their surfaces, whereas Ceres, a G class aster-

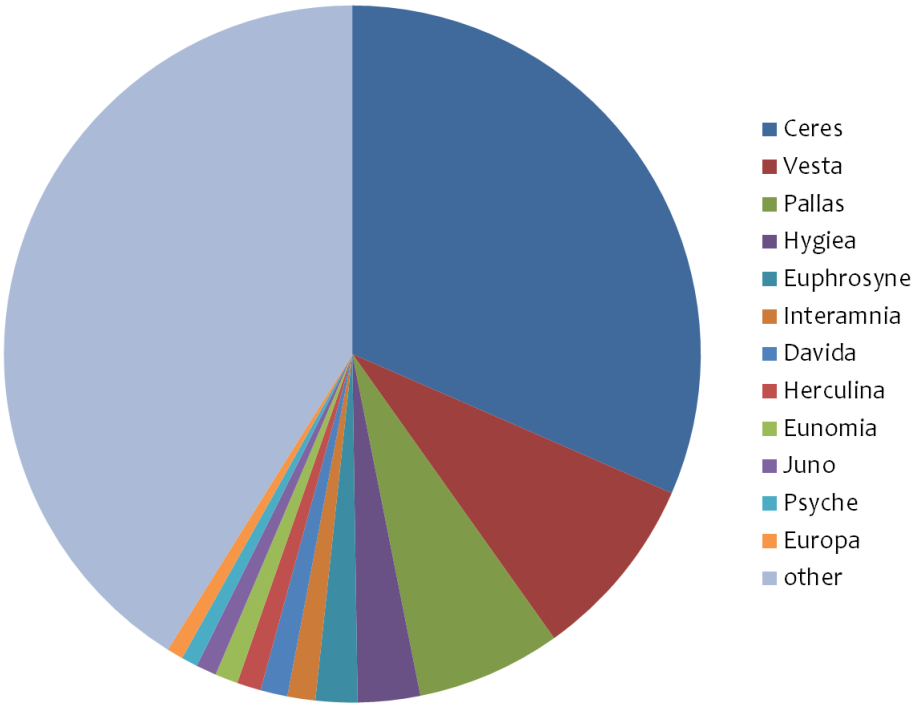

Figure 2.3: The mass of the twelve biggest asteroid compared to the rest one of the Main Belt.

oid, probably has water present as a layer of permafrost. K and S class have moderate albedos and spectral reflectances similar to the stony iron meteorites, and they are known to contain significant amounts of silicates and metals, including the minerals olivine and pyroxene on their surfaces. M class asteroids are moderate-albedo objects, may have significant amounts of nickel-iron metal in their surface material, and exhibit spectral reflectances similar to the nickel-iron meteorites. Paradoxically, however, some M class asteroids have spectral features due to the presence of hydrated minerals. D class asteroids have low albedos and show reflectance spectra similar to the spectrum exhibited by a relatively new type of carbonaceous chondrite, represented by the Tagish Lake meteorite, which fell in January 2000. Remaining classes constitute less than 4% of the population by number. P and T class asteroids have low albedos and no known meteorite or naturally occurring mineralogical counterparts, but they may contain a large fraction of carbon polymers or organic-rich silicates or both in their surface material. R class asteroids are very rare. Their surface material has been identified as being most consistent with a pyroxene and olivine-rich composition analogous to the pyroxene-olivine achondrite meteorites. The E class asteroids have the highest albedos and have spectral reflectances that match those of the enstatite achondrite meteorites. V class asteroids have reflectance properties closely matching those of one particular type of basaltic achondritic meteorite, the eucrites. The match is so good that some believe that the eucrites exhibited in museums are chips from the surface of a V class asteroid that were knocked off during a major collision. The V class had been thought confined to the large asteroid Vesta and a few very small Earth-approaching asteroids until 2000, when asteroid 1459 Magnya located at 3.15 AU from the Sun was discovered also to have a basaltic surface. Among the larger asteroids (those with diameters greater than about 25 km), the C class asteroids are the most common, accounting for about 65% by number. This is followed, in decreasing order, by the S class, at 15%; the D class, at 8%; and the P and M classes, at 4% each. The remaining classes constitute less than 4% of the population by number. In fact, there are no A, E, or Q class asteroids in this size range, only one member of the R and V classes, and between two and five members of each of the B, F, G, K, and

T classes. The distribution of the taxonomic classes throughout the Main Belt is highly structured. Some believe this variation with distance from the Sun means that the asteroids formed at or near their present locations and that a detailed comparison of the chemical composition of the asteroids in each region will provide constraints on models for the conditions that may have existed within the contracting solar nebula at the time the asteroids were formed. For more details on the taxonomic classification of asteroids see Barucci et al. 1987; Tholen 1989; Tedesco et al. 1989; Howell et al. 1994; Xu & Binzel 1995; Bus & Binzel 2002; Lazzaro 2009; De Meo et al. 2009.

2.5 Vesta

2.5.1 The connection with the HEDs

Vesta is one of the largest Main Belt asteroid, considered the parent of the HED (Howardite - Eucrite - Diogenite) meteorite, accreted from the protoplanetary disk (Wetherill, 1989; Lissauer, 1993) during the final stage of processing of the pre-solar molecular cloud (Lunine, 1997). Spectroscopic studies, in fact, show the presence of the 0.9 and 1.9 μm absorption bands for pyroxene in the spectra of Vesta that match those observed in the spectra of HEDs (Gaffey, 1997; De Sanctis et al., 2012). For this reason has been assumed that Vesta is the source of the HEDs collected on the Earth. This scenario is supported by diverse facts: first, the oxygen isotope data of the HEDs suite indicate an unique origin for these meteorites as stated by Greenwood et al. 2005 that reported a study of oxygen isotopes in two basaltic meteorite suites, the HEDs (which are thought to sample the asteroid Vesta) and the angrites (from an unidentified asteroidal source). Their results seem to demonstrate that these meteorite suites formed in early, global-scale (i.e covering 50% or more of the surface) melting events. In the Fig.2.4 a composite Dawn spacecraft image of Vesta is shown. The second reason is that a family of asteroids dynamically linked to Vesta has been identified (Williams, 1989; Zappalà et al., 1990). The members of the family, called *Vestoids*, seem to have a surface composition similar to Vesta (Binzel & Xu, 1993). The large impact basin discovered on Vesta stimulated the idea

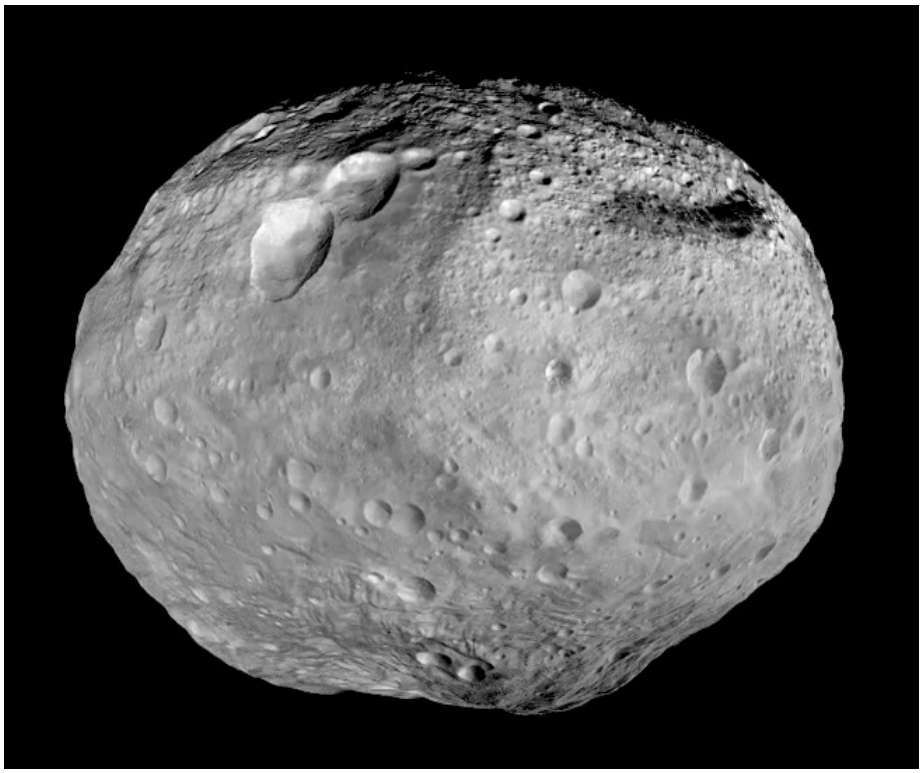

Figure 2.4: Composite Dawn spacecraft image of Vesta. Rheasilvia crater, with its massive central peak, covers much of the southern hemisphere.

that this large crater could be the source of Vestoids (Thomas et al., 1997a). The Vestoids could have been spread, not forming a specific dynamic family due to Yarkovsky effect (Farinella & Vokrouhlick, 1999) and to the mean motion and secular resonances able to transport fragments to near-Earth orbits (Marzari et al., 1996; Migliorini et al., 1997). Recent ground based measurements on Vestoids by De Sanctis et al. 2011 seem to indicate mineralogical differences between Vestoids and Vesta. The observed differences are attributed by the authors to the variegation of the Vesta surface or to the displacement of material excavated from different layers, and not to their possible origins from different parent bodies. As discussed by Coradini et al. 2011a, also these measurements support the idea that Vesta is deeply differentiated. The crater at the south pole of Vesta shows that about 1 vol.% of the asteroid was lost, and the amount of ejected material is enough to account for the HEDs (Drummond et al., 1988; Schenk et al., 2012). Their absolute ^{207}Pb -^{206}Pb age is 4568.5 $\pm$ 0.5 Ma (Bouvier et al., 2007), and CAIs have the ^{26}Al/^{27}Al ratios found in chondrites (Chaudisson & Gounelle, 2007). If HEDs are from Vesta, then we can infer from their absolute ages that Vesta's heating occurred early in its life (Thomas et al., 1997b), at time of rocky planets formation. This would make Vesta one of few intact bodies in the Solar System that differentiated and for which rock samples are available and it shows a surface geology as the one of the Moon and Mars. Vesta plays a unique role in the reconstruction of the physical and chemical processes that comprise collectively terrestrial planet accretion. The spectral connection between Vesta and the HEDs suite of meteorites suggests that Vesta formed very early in the history of the Solar System and differentiated on a Ma-long timescale due to the decay of short lived radionuclides (Keil et al., 1997). Recent results Schiller et al. 2011, however, indicate a faster cooling of the interior of Vesta than previously thought. If confirmed, this would imply that the thermal history of Vesta diverges from the generally accepted picture (Ghosh & McSween, 1998). In Fig.2.5 Vesta is compared with other asteroids of Main Belt, including Lutetia.

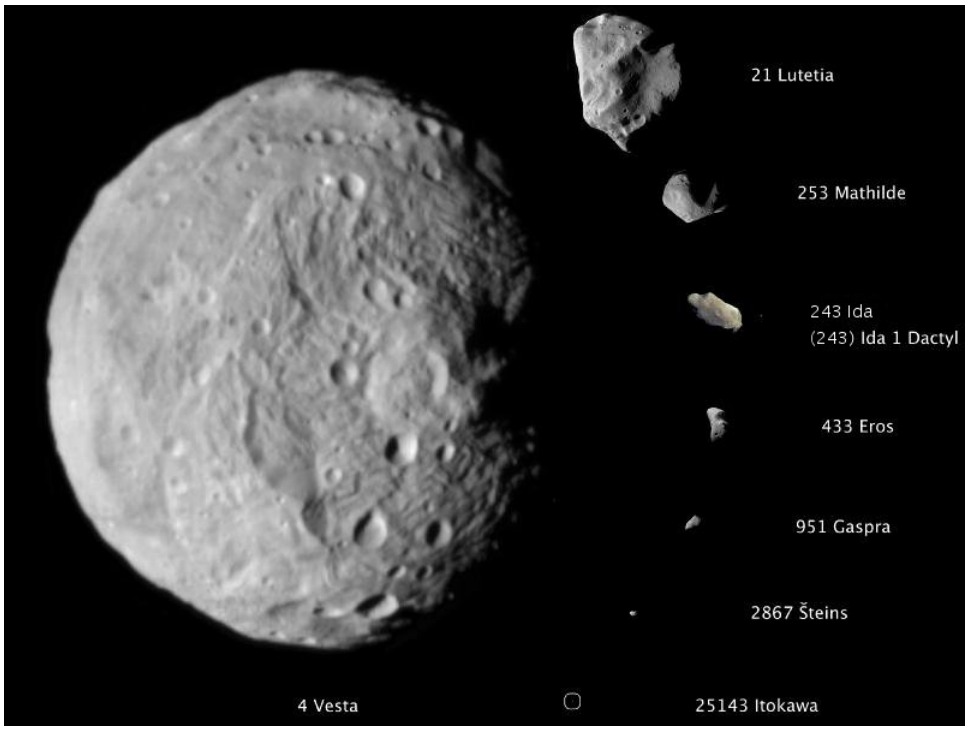

Figure 2.5: Vesta's image, compared with other asteroids, including Lutetia.

2.5.2 Physical and Chemical Properties

The composition of the HEDs have been used to estimate the asteroid's bulk composition and core mass (McSween et al., 2011). Some additional informations on bulk composition has been gleaned from models based on chondrites (Alexander et al., 2001; Scott, 2007). Current best estimates are summarized in Tab.2.1. Before Dawn's arrival, the best estimates of Vesta's mass depended on the asteroid perturbation of Mars, whose position can be determined to within about 5 m from landers and orbiters. Other measurements were provided by the perturbation of the orbit of asteroid 433 Eros by Vesta using the range data from the *Near Earth Asteroid Rendezvous* (NEAR) spacecraft. The perturbation of the Dawn spacecraft by Vesta's gravitational field yields a mass within the bounds of errors of estimates from the Mars data but with significantly reduced uncertainty: in fact, currently Vesta's mass has an uncertainty of only 0.00001 ± 10^{20} (see Russel et al. 2012 and Tab.2.1): it is the second most massive asteroid, though its mass

Parameter	Dawn	Previous knowledge
Major axes (km)	(286.3/278.6/223.2) ± 0.1	(280 × 289 × 229) ± 5 (*15*)
Mean radius (km)	262.7 ± 0.1	264.6 ± 5 (*15*)
Volume (km^3)	74.970×10^6	$77.60 \pm 8.7 \times 10^6$ (*15*)
Mass (kg)	$2.59076 \pm 0.00001 \times 10^{20}$	$2.6 \pm 0.3 \times 10^{20}$ (*13*)
Bulk density (kg m^{-3})	3456 ± 1%	3800 ± 15.8% (*15*)
Gravitational flattening ($\overline{J}_2$)	0.0317799 ± 0.0005%	—
Spin pole right ascension (deg)	309.03 ± 0.01	301° ± 5° (*15*)
Spin pole declination (deg)	42.23 ± 0.01	41° ± 5° (*15*)
Rotation rate (deg/day)	1617.333119 ± 0.000003	1617.332776 (*15*)

Table 2.1: Vesta physical parameters from Dawn compared to the previous HST values. Table from Russel et al. 2012.

is only 28% of Ceres. The best model of the shape of Vesta was derived from *Hubble Space Telescope* (HST) images and indicates that the asteroid can be fitted by tri-axial ellipsoid. The new volume estimate, using the previous HST shape model to fill in the unmapped northern polar region, is 74.970 $\times 10^6$ km^3, yielding an average density of 3456 kg m^{-3}. This value is at the lower end of the bulk densities previously derived, which ranged from 3500 to 3900 kg m^{-3} and were uncertain within a range of 3100 to 4700 kg m^{-3}. It is comparable to bulk silicates compositions having densities of 3320 to 3630 kg m^{-3} predicted by HEDs analysis that assume negligible porosity and it is consistent with the notation of a differentiated silicate-metal interior.

Geologic mapping using the HST during the 1994 apparition showed Vesta to be geologically dichotomous (Gaffey, 1997; Binzel et al., 1997). This has been confirmed also by recent HST observations (Li et al., 2010). The eastern hemisphere is dominated by units composed of Mg-rich and Ca-poor pyroxene interpreted to be similar in composition to diogenites. The western hemisphere is dominated by an Fe-rich and Ca-rich pyroxene, analogous to eucrites, and an olivine component. An hypothetical cross section of the equatorial part of Vesta drawn from the interpretative lithologic maps of Gaffey 1997 and Binzel et al. 1997, shows that eucrites (basalts, either near-surface or cumulates former deeper in the crust, composed of Ca-poor pyroxene, piogenite and Ca-rich plagioclase (anorthite); a number of these meteorites are regolith breccias) sample the surface and upper crust; diogenites (plutonic rocks made primarily of Mg-rich orthopyroxene, with small

amounts of plagioclase and olivine, derived from deep layers in the parent asteroid) sample the lower crust and finally peridotite (mostly olivine) sample the mantle. On the surface are found howardites (polymict eucrite-diogenite breccias) that consist of re-accreted material, reprocessed after ejection from parent body (Asphaug et al., 1997). Diogenites have the highest bulk and grain densities, with howardites tending to average the eucrite and diogenite values. Porosity and magnetic susceptibility are similar in the three classes. In Fig.2.7 HEDs stratigraphy is represented. The composition of the HEDs indicates that Vesta experienced melting. The abundances of Ni, Co, Mo, W and P in the Vesta mantle are consistent with equilibrium between metal and molten silicates (Drake, 2001). The differentiation from the molten material caused the heavy elements, and especially Fe, to separate and sink toward the center to form a core. Evidence of this metallic core has been supplied by the studies of Sr abundances and metal/silicate partitioning. A large amount of work has been devoted in the last years in order to infer from geochemical considerations the size of the Vesta core, and of its mantle and crust. As an example Ruzicka et al. 1997, assumed that the interior includes a metal core ($<$ 130 km in radius), an olivine-rich mantle ($\sim$ 65-220 km thick) a lower crustal unit ($\sim$ 12-43 km thick) composed of pyroxenite from which diogenite were derived and an upper crustal unit ($\sim$ 23-42 km thick) from which eucrites originated. A " base" model of the interior, also consistent with HEDs compositions (Ruzicka et al., 1997) is given in Tab.2.2. In Fig.2.6 the range of plausible bulk densities of ranges of polar moment of inertia and core density is shown(Zuber et al., 2011).

	Thickness [km]	**Density** [kg m^{-3}]	**Mass** [kg]
Upper crust	Shape-214[a]	2800	8.0
Lower crust	14	3200	2.6
Mantle	80	3976	10.4
Core	120	7870	5.7

Table 2.2: Base model of the internal structure. [a]shape-214 is a spherical harmonic expansion of the Thomas et al. (1997b) shape model.

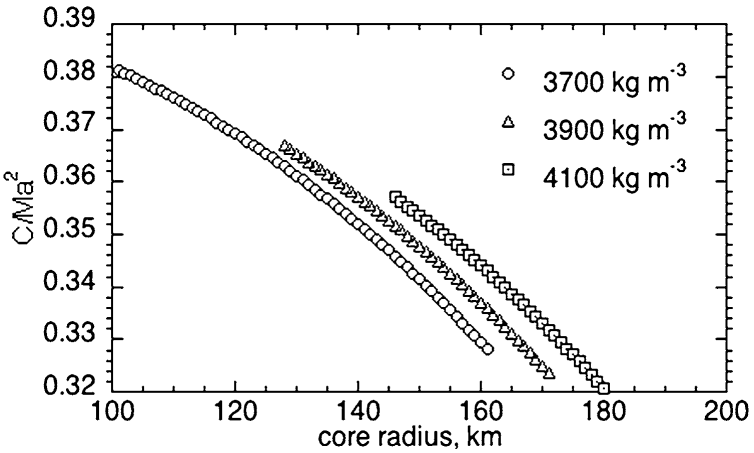

Figure 2.6: Calculation assumes a model of Vesta of 2700 kg m^{-3} to 3500 kg m^{-3} and a core density of 7000 kg m^{-3}. Figure from (Zuber et al., 2011).

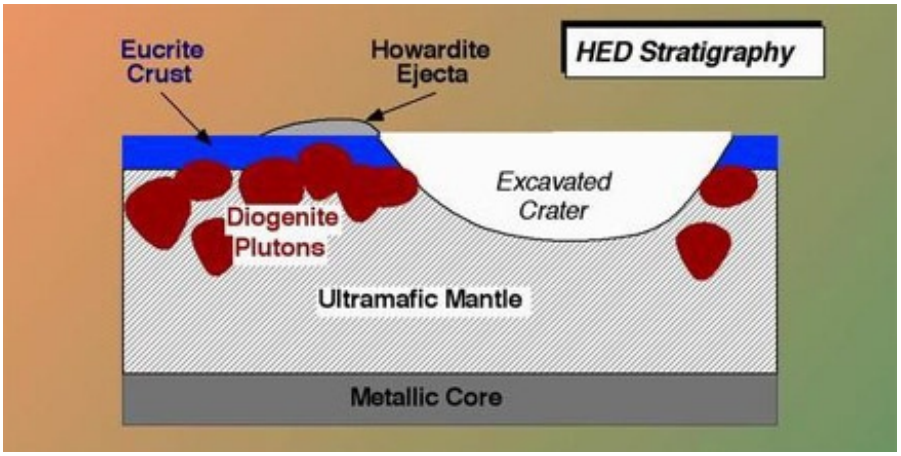

Figure 2.7: HEDs schematic stratigraphy. Credit: Harry Y. McSween, Jr., Department of Earth and Planetary Sciences, University of Tennessee.

2.6 Lutetia

2.6.1 Introduction

The asteroid 21 Lutetia (see Fig.2.8) plays an important role, like Vesta, in the comprehension of the origin and evolution of the planetary objects. Unlike Vesta, there are some experimental evidences (Weiss et al., 2011) suggesting the partial differentiation of this asteroid. In fact, data provided by Rosetta spacecraft measured mass and volume of the asteroid giving a high bulk density which exceeds that of most known chondritic meteorite groups. This suggests the presence of a metallic core overlain by a primitive chondritic crust. Lutetia is at the limit of the differentiation: very little variation in its original properties could make it differentiated or not, so it is the first asteroid unambiguously in the size regime capable of large scale melting and metallic core formation to be visited by a spacecraft. The size of Lutetia is sufficient to retain most of its original large scale structure against impact disruption (Bottke et al., 2005): this means that Lutetia may have retained a mostly intact record of any metamorphic and melting processes.

2.6.2 Physical and Chemical Properties

Earlier studies of its color and surface properties showed that Lutetia is an unusual and rather mysterious member of the Main Belt. Previous surveys have shown that similar asteroids are rare and represent less than 1% of the asteroid population of the Main Belt. The north pole region is covered by a thick layer of regolith, which is seen to flow in major landslides associated with albedo variation. Its geologically complex surface, ancient surface age, and high density suggest that Lutetia is most likely a primordial planetesimal. Lutetia's true nature has always been far from clear-cut. One difficulty in unambiguously classifying Lutetia is the lack of clear features in the spectrum of this asteroid. Ground-based visible-near infrared reflectance spectra and new infrared spectra from VIRTIS onboard Rosetta (Coradini et al., 2011b) are flat and nearly featureless compatible with some carbonaceous chondrites (Belskaya et al., 2010) and enstatite chondrites (Ockert-Bell et al., 2010) but distinct from all other meteorite groups with

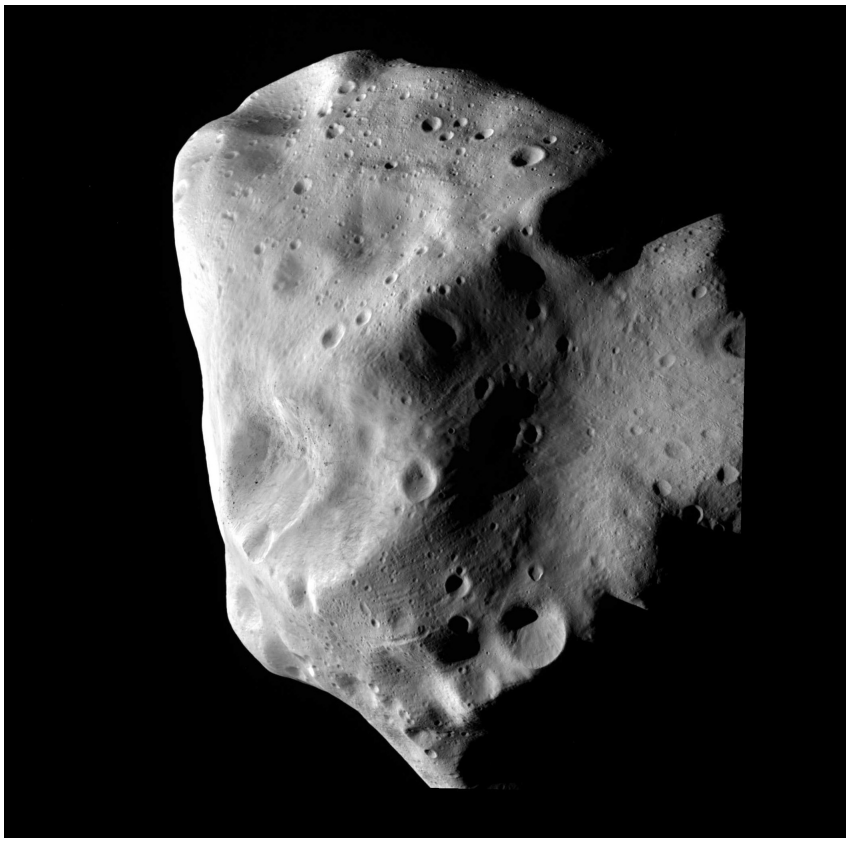

Figure 2.8: Image of Lutetia from Rosetta spacecraft.

the possible exception of iron meteorites (Cloutis et al., 2010). The Rosetta OSIRIS and RSI experiments have now determined that Lutetia has a bulk density of 3400 ± 300 kg m^{-3} (Patzold et al., 2011). This high bulk density together with surface properties (carbonaceous or enstatite chondrites) suggest that Lutetia might have experienced partial differentiation. In Fig.2.9 there are reported three end-member scenarios producing high bulk density through partial differentiation (figure from Weiss et al. 2011). Partial differentiation and core formation on Lutetia would be consistent with the proposal that some chondrites and achondrites could have a common parent body origin and also support recent arguments that the remanent magnetization observed in some metamorphosed carbonaceous chondrites could be the product of an internal core dynamo rather than the early nebula or Sun (Carpozen et al., 2011; Elkins-Tanton et al., 2011; Weiss et al., 2010). The value of the macroporosity of Lutetia is very uncertain. It could be similar to the asteroids having abundant fractures and joints (Asphaug et al., 2009). These bodies were inferred to have macroporosities of $6 \sim 40\%$ (Consolmagno et al., 2008), suggesting that Lutetia may have similarly substantial porosity. A stringent upper limit on Lutetia's macroporosity of $\sim 52\%$ is provided by a model in which the entire asteroid below a very thin chondritic surface layer is made of pure iron. However, given that impact craters visible on Lutetia have excavated hundreds of meters to several km deep into Lutetia, the lack of exposures of differentiated rocks suggest that the chondritic crust is likely at least several km thick. For such a body with an enstatite or non-CB/CH carbonaceous chondrite-like bulk metal content, a more realistic upper limit on the macroporosity is $\sim 25\%$ (Weiss et al., 2011) and for this is unlikely that Lutetia has a rubble pile structure. If Lutetia even has $>\sim 13\%$ macroporosity, a value modest for asteroids of Lutetia's size and consistent with indications that it is thoroughly fractured, then it likely has a melted interior including a metallic core or at least large, metal-rich regions. Such a partially differentiated structure is predicted to be a natural outgrowth of prolonged accretion beginning before 1.5 Ma and extending for several Ma (Elkins-Tanton et al., 2011; Sahijpal et al., 2011). This contrasts with smaller asteroids visited by previous spacecraft, which are probably shattered bodies, fragments of larger parents, or reaccumulated

rubble piles. Lutetia parameters are reported in Tab.2.3 (table from Weiss et al. 2011).

Parameter	**Value**	**Unit**	**Reference**
Mean Heliocentric Distance	2.43	AU	JPL Small-body Data Browser (2012)
Orbital Eccentricity	0.164		JPL Small-body Data Browser (2012)
Orbit Period	3.80	yr	JPL Small-body Data Browser (2012)
Rotational Period	8.1655	h	JPL Small-body Data Browser (2012)
Mass	1.7	10^{18}kg	Patzold et al. 2011
Mean Radius	47.88	km	JPL Small-body Data Browser (2012)
Mean Density	3400	kg m^{-3}	Patzold et al. 2011
Acceleration of Gravity	0.05	m s^{-2}	JPL Small-body Data Browser (2012)
Spectral Type	C or M		Weiss et al. (2011); Coradini et al. (2011b)

Table 2.3: Lutetia parameters.

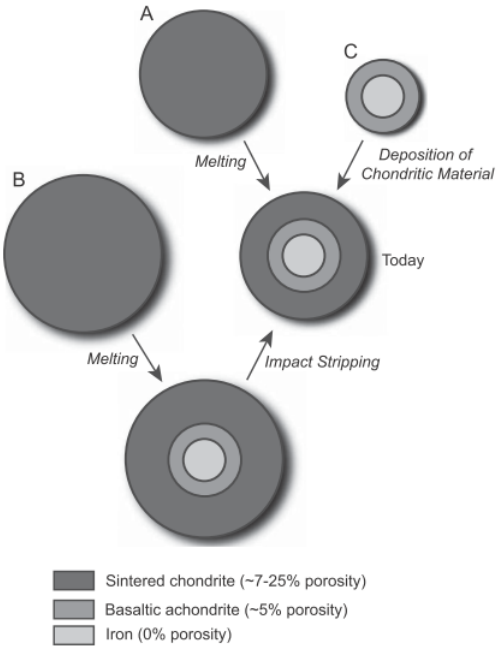

Figure 2.9: Three end-member scenarios that could produce the high bulk density of Lutetia via formation of a partially differentiated body. (A)Proto-Lutetia had nearly the same radius as present Lutetia but was initially undifferentiated (dark gray). Subsequent melting of the interior formed a metallic core (light gray) and silicate mantle (medium gray), decreasing the bulk porosity and therefore increasing the bulk density. (B)Proto-Lutetia was undifferentiated and had a larger radius than present-day Lutetia. A smaller volume fraction of this body experienced melting than the body in (A). Subsequent impacts removed much of the undifferentiated outer layer, thereby increasing the bulk density. (C)Proto-Lutetia differentiated early and either did not initially retain a chondritic crust or else lost such an early crust by early impacts tripping. An outer layer of chondritic debris was subsequently deposited on the body. This figure is schematic and the layer thicknesses are not drawn to scale.

Chapter 3

Thermal Evolution Models of Asteroids

3.1 Differentiation of an Asteroid

Differentiation means to make a homogeneous body heterogeneous. It refers to the processes that cause an essentially homogeneous accreted body that is made up of primordial solar material to become separated into layers having different chemical and/or physical properties. If a planetary body is large enough it will develop a core, mantle and crust each of which may be further subdivided (see Fig.3.1). Differentiation operates as materials of varying density are separated by a body's self gravity, with those of the highest density moving to its center. Melting or partial melting of material is required for the process to occur, which takes place over long time scales. The rate of differentiation depends on buoyancy forces and heat generated in the materials which may be solid, but exhibit fluid properties over geologic time. The minimum size for the differentiation will be set by the rate of conductive heat loss. The characteristic timescale for thermal conduction into body of radius R is R^2/κ (Turcotte & Schubert, 2002) (where κ is the thermal diffusivity of the asteroid): however, this is a poor approximation because this quantity is not constant for a body that reaches melting temperatures. The minimum size for the differentiation will occur when the heat flux is maximum, i.e. instantaneous accretion. The approximate conductive

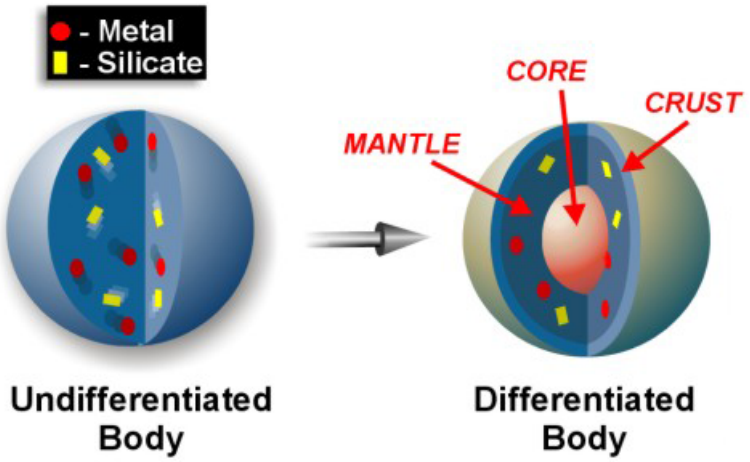

Figure 3.1: Schematization of the differentiation process.

cooling time for a planetesimals with instantaneous accretion is given by (Moskovitz & Gaidos, 2011):

$$\tau_{cool} = 0.014 Ma \left(\frac{R}{1km} \right)^2 . \tag{3.1}$$

Planetesimals with τ_{cool} longer than the most important heating time scale, the half-life of ^{26}Al (τ_{Al}), will sustain melting temperatures and differentiate. For $R = 18$ km in size, τ_{cool} is equal to τ_{Al}. Two important linked questions arise when we talk about asteroid differentiation: are hydrostatic equilibrium and differentiation related? Can we assume that a body in hydrostatic equilibrium (HE) has achieved differentiation? First, we remember that a body is in HE when its self gravitational force is balanced by its internal pressure; the body is neither expanding nor contracting. From a technical perspective, a body in HE will assume a spherical shape to minimize gravitational potential since any deviations from sphericity increases gravitational energy. We can not assume that all differentiated bodies achieve HE. Even if small asteroids are differentiated, it is unlikely they have sufficient mass to reach spherical form. So differentiation does not necessarily imply a body has achieved HE.

3.2 Heat Sources for the Differentiation

The differentiation of an asteroid requires a strong heat source, capable of producing high temperatures in bodies with high surface-to-volume ratios. The heat source must have also operated quite early in the history of the Solar System so the differentiation must have occurred within the first few millions years of the Solar System. Evidence for rapid iron-silicate differentiation, i.e. the formation of the core, come from ^{182}Hf - ^{182}W concentration variations in iron meteorites (Horan et al., 1989; Kleine et al., 2002). Early differentiation is also supported by the presence of excess of ^{26}Mg from the decay of extinct ^{26}Al in the eucrites *Piplia Kalan* (Srinivasan et al., 1999) and *Asuka 881394* (Nyquiest et al., 2001) and angrites (Bizzarro et al., 2005). Several heat sources have been proposed. I analyzed the several contributions, discriminating which are the most significant sources.

3.2.1 Short-Lived Radionuclides

Almost half a century ago, Harold Urey recognized that decay of long-lived radioactive isotopes (K, U, Th), the primary heating mechanism for the differentiation of the planets, was not an effective heat source for asteroids, because the timescale for energy release is long compared to that for conductive loss from small bodies. Urey 1995 suggested decay of the short-lived radionuclide ^{26}Al as the primary heat source for the metamorphism and melting of planetesimals. Lee et al. 1976 discovered evidences for ^{26}Al in CAIs from the Allende meteorite, showing that the ratio of ^{26}Al/^{27}Al was about 5×10^5 supporting Urey's idea of radioactive heating and melting of planetesimals. MacPherson et al. 1995, analyzing CAIs from different classes of chondritic meteorite, showed that the ratio of ^{26}Al/^{27}Al was always equal to 5×10^5, suggesting that ^{26}Al was distributed uniformly in the Milky Way (see Fig.3.2). Evidences for ^{26}Al has now been detected in chondrules, plagioclase fragments in chondrites and basaltic meteorites, in which the inferred initial ratio ^{26}Al/^{27}Al is lower than 5×10^5 of CAIs but it correlates closely with the ages of the objects (independent Pb-Pb dating method). The correlation reinforces the idea that when CAIs formed (the zero time of Solar System) the ratio was equal to 5×10^5 in the Solar Neb-

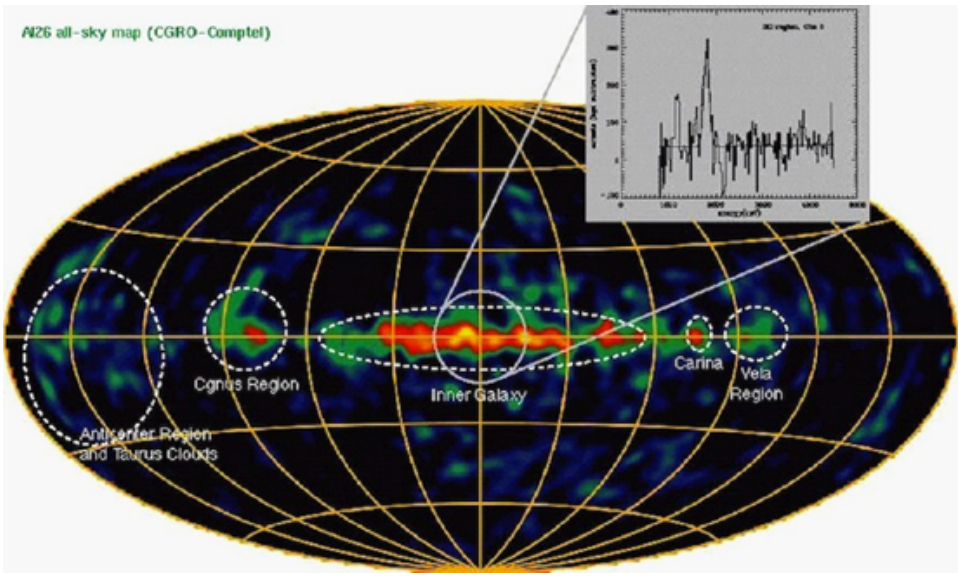

Figure 3.2: Distribution of the ^{26}Al in the Milky Way.

ula. The rapid differentiation and small sizes of planetesimals in early Solar System necessitate a strong heat source that could provide the adequate thermal energy to the planetesimal against the heat conduction losses: in this scenario, a plausible heat source could be the ^{26}Al, which presence in the early Solar System has been established in CAIs and chondrules. There are several mechanisms for the production of the ^{26}Al: it could be produced during core collapse supernovae, during nova outbursts, by asymptotic giant branch stars and by massive stars, in particular during the *Wolf-Rayet* phase. It could also produced by spallation reactions of high energy cosmic ray. The ^{26}Al isotope decays by either positron emission or electron capture with neutrinos carrying away some energy in either case. The daughter ^{26}Mg atom is an excited state and decays to ground level by emitting one or two γ rays, as shown in Fig.3.3. The energy released, following Castillo et al. (2009), per decay suitable for the differentiation is 3.12 MeV. The adopted value for the energy released, as stressed by (Castillo et al., 2009), is very ambiguous in literature: it ranges from 1.21 MeV (McCord & Sotin, 2005) to 4.0 MeV (e.g. Hevey & Sanders 2006). Assuming an half-life (τ_{Al}) of 0.717 Ma, we can convert the energy for decay to a heat production in

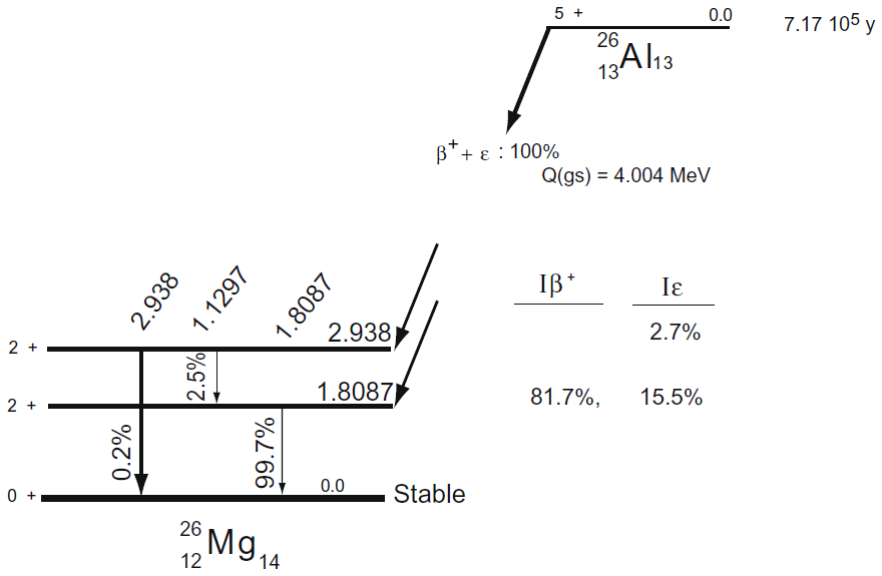

Figure 3.3: ^{26}Al decay scheme Source: National Nuclear Data Center.

W/Kg, through the following relation (Castillo et al., 2009):

$$H = \frac{A}{m_{26}} E_d e_v \lambda, \tag{3.2}$$

where $A = 6.022 \times 10^{23}$ is the Avogadro's number, m_{26} is the mass of one mole of ^{26}Al ($m_{26} = 25.987 \times 10^{-3}$ kg), e_v is the value of one electron volt in Joule and $\lambda = ln(2)/\tau_{Al}$ is the decay constant of ^{26}Al in s^{-1}: H has a value of $\sim$ 0.355 W/kg (Castillo et al., 2009). Then, the volumetric radiogenic heating rate (H_{vol}) in W/m^3 as a function of time is given by:

$$H_{vol}(t) = \rho \chi C_0 H e^{-\lambda t}, \tag{3.3}$$

where ρ is the density of the material, in kg/m^3, χ is the mass fraction of silicates, C_0 is the initial concentration of ^{26}Al in kg per kg of silicates and t is elapsed time in seconds since CAIs formation. Estimates of the ^{60}Fe/^{56}Fe concentration ratio in the early Solar System (Tachibana & Huss, 2003; Mostefaoui et al., 2005) raises the possibility that the short lived radionuclide ^{60}Fe could also contribute significantly to heating and melting even in the absence of other heat sources. In particular, a redistribution of Fe with core formation makes this heat source specifically interesting for the discussion of the thermal evolution of planetesimals. There are several

discrepancies in the literature about the thermal energy per decay used for ^{60}Fe, as noted by Castillo et al. (2009). Some studies use 3.04 MeV÷3.06 MeV which corresponds to the total disintegration energy (e.g. Ghosh & McSween 1998). The actual energy converted to heat locally, using current data (see www.nndc.bnl.gov) is 2.712 MeV per decay. The differences are due to the fact that the former studies did not account for the loss of energy to neutrinos. Anyway, this dispersion in the data have not significant consequences for geophysical modeling, because the main source is represented by the ^{26}Al.

3.2.2 Long-Lived Radionuclides

In contrast to models of the differentiation of terrestrial planets, one must account for significantly lower gravity and significantly smaller radii, implying a much larger surface to volume ratio. As stressed before, this requires early and intense heat sources. These heat sources must have produced much more power than the decay of U, Th and K, the major heat source for the present-day planets (Wadhwa et al., 2006). The main evidence for neglecting the long-lived radionuclides in the thermal evolution history of an asteroid is that most of the known meteorite classes were at least thermally altered in a short period of time after accumulation while the long-lived radionuclides releases heat on a time scale of 1 Ga (McCoy et al., 1997). For long-lived radionuclide decay within small solid bodies it is often adequate to represent the rate of heat production as being in a steady-state balance with the rate of conductive heat loss. This is equivalent to assuming that the time scale for conduction is short compared to the time scale for heat generation. For short-lived radioactive decay, the opposite will be true for large bodies. Let us define a conductive cooling time scale (t_{cond}) as the ratio of the heat content of the solid body to its luminosity:

$$t_{cond} = \frac{c_p M \left(T - T_{surf}\right)}{L}, \tag{3.4}$$

where T is the initial temperature, T_{surf} is the mean surface temperature and L is the thermal luminosity, defined as:

$$L = 4\pi R^2 F = \frac{4\pi R^2 K \left(T - T_{surf}\right)}{R}, \tag{3.5}$$

where F is the flux and K is the thermal conductivity. Considering a spherical body with constant density ($M = 4\pi\rho R^3/3$) and using the eq.(3.5), we can rewrite the eq.(3.4) as:

$$t_{cond} = \frac{c_p \rho R^2}{3K}. \tag{3.6}$$

For thermal conductivities characteristic and specific heat capacities of chondrites ($K = 2$ W m^{-1} K^{-1}; $c_p = 10^3$ J Kg^{-1} K^{-1}) (Yomogida & Matsui, 1984), the conductive cooling time scale becomes about $50R^2$ seconds. A body of radius of 10 km would have a conductive cooling time scale of about 2 Ma. Placing a poorly conducting regolith on the body (lowering K by a factor of, say, 100) could permit much smaller bodies to melt: however, such small bodies probably have great difficulty retaining a thick regolith. In effect, rapid decay is very effective in heating even rather small bodies because the energy is delivered by decay much more rapidly than it can be lost. The body then departs very strongly from steady-state behavior.

3.2.3 Accretion

In any formation process, the total gravitational energy available for the heating of the asteroid is $\alpha GM/R$, where G is the universal gravitational constant, M and R are the mass and the radius of the asteroid, respectively, and α is a constant of order unity which depends of the details of the accretion process: α is 3.5 if the accretion is homogeneous. We consider a small body (with mass m) impacting on the surface of Vesta and depositing all of its incident kinetic energy (E) into stored heat. The energy per unity mass of infalling material is just $0.5v_{esc}^2$, where v_{esc} is the escape velocity, with a value of 0.36 km s^{-1}. The maximum temperature rise possible if all the accretion energy were stored internally is:

$$T_{max} = \frac{E}{m}\frac{h}{c_v} \sim 90K, \tag{3.7}$$

where c_v is the specific heat at constant volume (assuming a value of 720 J/Kg K), and $h = 1$ is the efficiency of the impact. However, only a fraction of this gravitational energy can be retained by the growing planetesimal: the rest is reradiated into space or removed by convection in the surrounding

nebula, in which it formes. The mean impact speed can not be very much larger than the escape velocity, because such violent collisions would have resulted in net erosion of mass rather than net accretion. The parameter h depends on the rate of heat transfer in the nebula and on the temperature of the nebula, on the size distribution of the accreting particles and planetesimals, on their relative velocity and on the time scale of the accretion process (Coradini et al., 1983; Schubert et al., 1986). In terms of h, we can approximate the accretional temperature T_A at radius r within an accumulating planetesimal as:

$$T_A(r) = \frac{hGM(r)}{c_v r}\left[1 + \frac{rv^2}{2GM(r)}\right] + T_E, \tag{3.8}$$

where c_v is the specific heat, T_E the ambient temperature during accretion, $v^2/2$ is the approach kinetic energy per unity mass of planetesimals forming the asteroid and $M(r)$ is the mass of the asteroid internal to r. Assuming an uniform density, we can write $M(r) = 4/3\pi\rho r^3$, where ρ is the density of the asteroid. In Fig.3.4 we show accretional temperature profiles for different value of the parameter h. In the optimistic case in which the 50% of the energy is converted in heat for the differentiation, we observe an increase of the temperature of only $\simeq 50$ K.

3.2.4 Differentiation

In contrast with the accretional energy, all the energy of differentiation is retained within the asteroid. After homogeneous accretion, the silicates are separate from the metallic core. The gravitational energy made available by differentiation of an initially homogeneous asteroid can be written as (Schubert et al., 1986):

$$U_H - U_D = 2\pi \int_0^R \left[\rho_H(r)V_H(r) - \rho_D(r)V_D(r)\right] r^2 dr, \tag{3.9}$$

where U is the gravitational potential energy, V is the gravitational potential, R is the radius of the asteroid, ρ is the density and r is the radial distance from the center of the asteroid, and subscripts H and D refer to the homogeneous and differentiated states, respectively. The potential energy

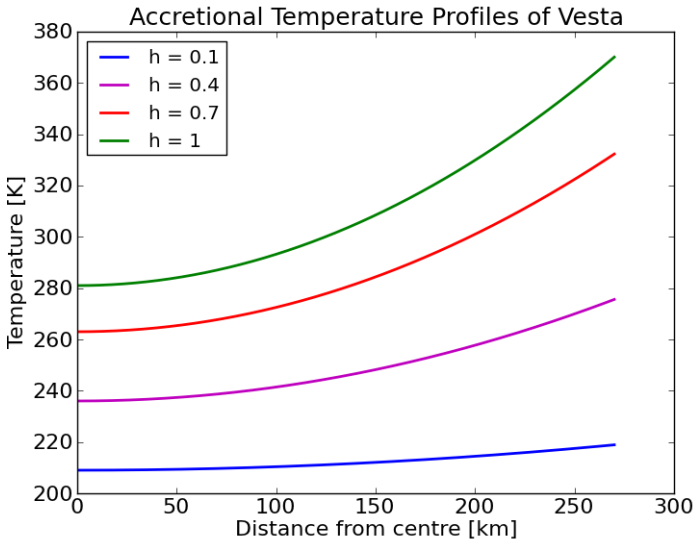

Figure 3.4: Accretional temperature profile for Vesta. The parameter h is the fraction of impact energy retained as heat in an accumulating asteroid.

of a homogeneous asteroid is:

$$U_H = -\frac{16}{15}\pi^2 G R^5 \bar{\rho}^2, \tag{3.10}$$

where $\bar{\rho}$ is the mean density of the asteroid. The potential energy of a two-layer model of the differentiated asteroid is:

$$U_D = -\frac{16}{15}\pi^2 G R^5 \left[\rho_{sil}^2 + \frac{5}{2}\rho_{sil}\left(\bar{\rho} - \rho_{sil}\right) + \left(\frac{3}{2}\rho_{sil} - \rho_{met}\right)\left(-\Delta\rho\right)\left(\frac{\bar{\rho} - \rho_{sil}}{\Delta\rho}\right)^{5/3}\right], \tag{3.11}$$

where $\Delta\rho = \rho_{met} - \rho_{sil}$, with ρ_{sil} and ρ_{met} the density of the silicate and of the metallic components, respectively. Assuming $\rho_{sil} = 3000$ kgm^{-3}, $\rho_{met} = 6300$ kgm^{-3}, $\bar{\rho} = 3456$ kgm^{-3}, $R = 270$ km, $M = 2.58 \times 10^{20}$ kg and $c_v = 720$ J/(kg*K), we obtain for Vesta:

$$\Delta T = \frac{U_D}{M c_v} \simeq 7K, \tag{3.12}$$

that corresponds to less than 10% of the accretional energy.

3.2.5 Electrical Conduction Heating by the T-Tauri Solar Wind

Electrical conduction heating by the T-Tauri solar wind from the pre-main sequence (e.g. Sonett et al. 1968) could have been an effective heating mechanism, because strong magnetic fields were present at the time of meteorite formation in the Solar Nebula. But we have no proof that induction heating by T-Tauri phase of the Sun was an important heat source in meteorite parent bodies. This heating mechanism is especially complex because there are two different heating modes and because the interaction of the solar wind with an asteroidal body depends very sensitively of the electrical conductivity, radius and heliocentric distance of the asteroid. Consider first the case of a spherical body completely covered with a layer of metal. The magnetic field lines will penetrate into the metal and the lines of force will tend to slide around the exterior of the conducting shell while depositing almost no energy in the body. Any heat that is generated by eddy currents near the surface of the shell will be rapidly conducted to the surface and radiated into space. Since the temperature of the nebula in the Main Belt was probably close to the present value during the T-Tauri phase, and since the energy flux carried by solar wind was surely smaller than the radiative energy flux, this mechanism can not have much effect on asteroid surface temperature and even less effect on internal temperature. The second case to consider is that of a spherical body of material that is an excellent insulator, such as pure enstatite. In this case, the magnetic lines of force pass through the asteroid almost as if were not there. No currents are induced because there are no conduction-band electrons available. The surface temperature is again dominated by radiative heating by the Sun.

3.2.6 Impacts

Impacts may have contributed to the heating of asteroids, either through thermal metamorphism or limited melting. Some authors have championed complete melting of asteroids by impacts (e.g. Lodders et al. 1993). It is also possible that impacts produced local heating. Rubin 2004 documented postshock annealing in ordinary chondrites that occurred hundreds of mil-

lions of year after the birth of the Solar System and must have resulted from impact heating. He argued that localized heating of the walls and floors of craters in rubble-pile asteroids might produce sufficient heat for thermal metamorphism. While this idea continues to stimulate debate, it is quite clear that impact did not produce complete differentiation of asteroids and the wide range of achondrites observed in our collections.

3.2.7 Tidal Heating

Tidal dissipation is a negligible heat source for Vesta: it is clearly an important source of energy in some of the moons of Jupiter and Saturn, because of the large masses of these bodies and the small orbital distances and forced orbital eccentricities of some of these satellites. The gravitational field of a planet (or a star) cause the satellites (or the planet) to deform into a prolate spheroid with its long axis pointing toward the planet. If the satellite does not rotate synchronously with its orbital period or if the orbit of the satellite is eccentric, it will experience a periodic forcing with a large part of the deformational energy being dissipated as heat. Internal friction causes angular momentum to be transferred between the planet and its satellite, forcing the rotation and/or eccentricity to be damped (McCoy et al., 1997).

3.2.8 Solar Radiation

Solar heating is responsible for shallow weathering and erosional processes on planets that have atmosphere, but also causes surface warming on planets with thin or no atmosphere. The amount of solar energy that actually reaches the surface depends on several factors, such as the density and composition of clouds. The surface of Venus reaches temperatures of around 900 K due to solar heating. This suggests that the thermal gradient beneath the surface is also quite high due to the elevated starting surface temperature. Thus, the amount of internal heat lost to space may be greatly affected by the surface temperature (McCoy et al., 1997).

3.3 Main Stages of the Life of a Rocky Asteroid

All the terrestrial planets and the Moon experienced igneous differentiation so it appears to have been widespread in the inner Solar System. The records of the differentiation, however, are largely obliterated by the subsequent geologic processes. The nature of the precursor material for a differentiated asteroid can have a profound influence on the process of the differentiation: it is widely assumed that differentiated asteroids began their existence as a *chondritic* materials. This in large parts is owed to the complete lack of any chemically and petrologically primitive materials that fall outside the broad scope of the term *chondritic* (Brearley & Jones, 1998; Scott & Krot, 2003). Ordinary chondrites are well characterized both chemically and mineralogically. Normative mineralogies provide a reasonable approximation of the modal mineralogy for ordinary chondrites (e.g. McSween et al. 1991) and allow comparison across groups with differing oxidation states. Carbonaceous chondrites are more olivine normative, while enstatite chondrites lack olivine in their normative compositions. Moreover, the choice of the chondrite as starting material for a geophysical evolution model is due to the fact that the melting of ordinary chondrites can be reasonably well understood both theoretically (through application of the Fe-FeS and olivine-anorthite-silica phase diagrams (Stolper, 1977)) and experimentally (through partial melting of ordinary chondrites (e.g. Kushiro & Mysen 1979)).

3.3.1 Accretion Process

A crucial role in the geophysical and thermal evolution of an asteroid is played by the accretion process, even if the process by which planetesimals formed in the primordial Solar Nebula is one of the fundamental unresolved problems of cosmogony so several mechanism have been proposed to produce macroscopic bodies from dust. Safronov 1969 invoked gravitational instability in a dense layer of small particles that settled to the midplane of the Solar Nebula. One alternative suggestion is coagulation of aggregate bodies in collisions driven by differential gas drag (Weidenschilling et al., 1997). More recently, variations of gravitational instability have been proposed, involving collapse of concentrations of particles produced by interactions with

the nebular gas (Youdin & Goodman, 2005; Chambers, 2010; Cuzzi et al., 2010). It is not possible to discriminate among these scenarios, because we have not observational constraints: in fact, planetesimals can not be observed directly in protostellar disks and in our Solar System they are largely extinct. Anyway, after reaching a size of about 1 km, the accretion proceeds dominated by mutual gravitational attraction, growing possibly to moon-sized protoplanets at the end of the accretion. It could have taken several million years for bodies with a radius of 500 km to accrete to their final size (Weidenschilling, 1988), although much shorter time scales have been discussed (Kaula, 1988). Essentially, three different scenarios exist: linear, exponential and asymptotic accretion. The linear accretion law corresponds to a constant radial growth rate which is typically about 200 km Ma^{-1} (Encrenaz et al., 1987). The asymptotic accretion law corresponds to a non constant radial growth rate, in which a large amount of material is added in the late stage of accretion: the embryos, in this scenario, accrete in less than 0.1 Ma. Finally, the exponentially accretion law can be considered as a mean between the two described cases. The accretion time is crucial in the geophysical and thermal evolution because it controls the strength of the radiogenic source and it has to be much smaller than the half-life of the ^{26}Al. The reason lies with the competition between heating in the interior of the planetesimal and heat loss through its surface.

3.3.2 Sintering: Reduction of the Porosity and Shrinkage of the Radius

The porosity of a planetesimal, during its evolution, changes from its initial value due to the hot pressure by the self-gravity of the body: this process is labeled *sintering*. This process takes place at about 700 K (Yomogida & Matsui, 1984): the lattice of the solid material is heated by the decay of the radionuclides and the granular components are plastically deformed under pressure and voids are gradually closed. Following (Yomogida & Matsui, 1984), we determine the evolution of the volume filling factor $(1 - \phi)$ by using:

$$\frac{\partial log\,(1-\phi(r))}{\partial t} = A\sigma^{2/3} r_g^{-3} e^{E/R_{gas}T}, \tag{3.13}$$

with $1.6 \times 10^{-5} \leq A \leq 5.4 \times 10^{-5}$, $\sigma(\phi)$ being the effective stress on the contact faces of two grains, r_g the grain radius, E the activation energy, T the temperature and R_{gas} the universal gas constant. As sintering changes the porosity, the size of the planetesimal and thus the radius $R(t)$ are also affected. The radius is hence modified according to:

$$R(t) = R(t) \left(\frac{1 - \phi_0}{1 - \phi(t)} \right)^{1/3}, \tag{3.14}$$

with the initial porosity ϕ_0 and the average porosity $\phi(t)$ of the planetesimal. The sintering also produces a rapid increase of the density (ρ) and a corresponding jump in thermal conductivity from initial values as low as 1×10^{-3} W m^{-1} K^{-1} (Hevey & Sanders, 2006; Sahijpal et al., 2007) (see Fig.3.5). Although this process offers a more realistic picture of the initial heating of the asteroid, there are large uncertainties associated with the assumed initial porosities (and the corresponding thermal conductivities). A value of 1×10^{-3} W m^{-1} K^{-1} is based on laboratory measurements of the lunar regolith in a vacuum (Fountain & West, 1970). This analyzed kind of compaction, the "hot pressing", is what obviously operated in ordinary chondrite material and the different petrologic types 4 to 6 of chondrites are obviously different stages of compaction by hot pressing. There is another kind of compaction, the "cold pressing", that operates already at low temperatures. The granular material can adjust by mutual gliding and rolling of the granular components to the exerted forces and evolves into configurations with closer packing. The ongoing collision with other bodies during the growth process enhances this kind of compaction of the material.

3.3.3 Core Formation

There are two schools of thought regarding core separation from silicatic matrix. The first scenario for the formation of the core assumes that the melt fraction of the silicate is required to be larger than about 50 vol.% (Taylor, 1992; Taylor et al., 1993), arguing for the presence of an early magma ocean in a planetesimal to form a core. This assumption is supported by experimental studies that partial melting of meteorites do not show metal migration (Takahashi, 1983; Walker & Agee, 1988). The second scenario

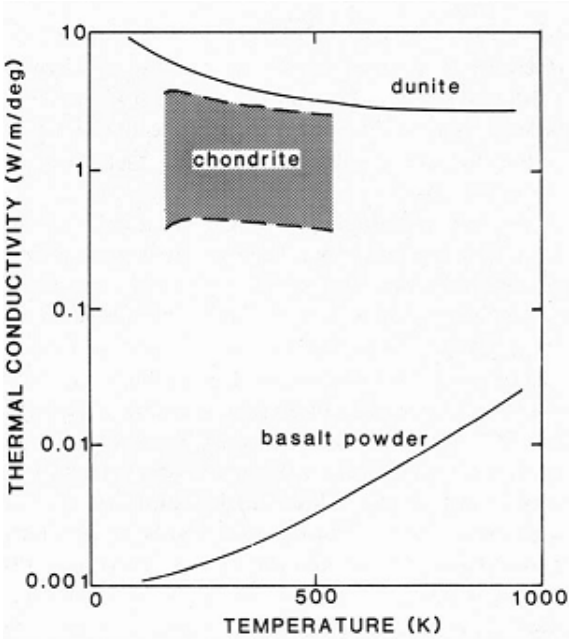

Figure 3.5: Thermal conductivity versus temperature for idealized dunite, chondrites and basaltic powders with a radius of 10 μm and porosity of 40 vol.% under vacuum conditions (below 10^{-6} N/m^2).

suggests that iron segregation and possibly core formation can start already for small melt factions of iron (Larimer, 1995; Hewins & Newsom, 1988) even before silicate starts to melt. This assumption is supported by the observations of Fe, Ni-FeS veins in the acapulcoite-lodanite parent body McCoy et al. (1997) and by recent experiments suggesting an interconnected melt network for pressures below 2-3 GPa Terasaki et al. (2001). Neither approach accounts for the rate of melt generation which, in turn, relates to the thermal environment in the asteroidal interior. For example, latent heat is required to melt the metal-sulfide liquid. How fast the metal sulfide liquid moves as a particular depth will be determined also by how fast it melts, which in turn is determined by the amount of heat that is supplied by ^{26}Al decay and the amount of heat brought into or lost to adjacent layers. When the metallic core is formed, during the phase in which it is melt, advection takes place but this cooling mechanism has no significant effects being small the mass involved.

3.3.4 Rayleigh Taylor Instability

When silicates are partially or completely melted (see Fig.3.6), the *Rayleigh-Taylor instability* (RT) occurs in the interface between the two fluids (metals and silicate melt) that have different densities: the lighter fluid goes to the surface while the heavier one goes to the center. The instability manifests itself with short-wavelength drips that grow from the lower surface, break off, and descend into the warmer, less dense interior (Chandrasekhar, 1961; Elsasser, 1963). We use the following differential equation to solve for the instability between two fluids:

$$\frac{d}{dz}\left(\rho\frac{dw}{dz}\right) - \rho k^2 w = -wg\frac{k^2}{n^2}\frac{d\rho}{dz}, \tag{3.15}$$

where ρ is the density of the fluid, w is the velocity of the fluid in the $z - direction$ (see Fig.3.7), n is the eigenvalue corresponding to the wave number k, g is the acceleration of gravity. For a layer of fluid above (ρ_2) or below (ρ_1) the interface, the density is constant and the governing differential equation reduce to:

$$\frac{d^w}{dz^2} = k^2 w. \tag{3.16}$$

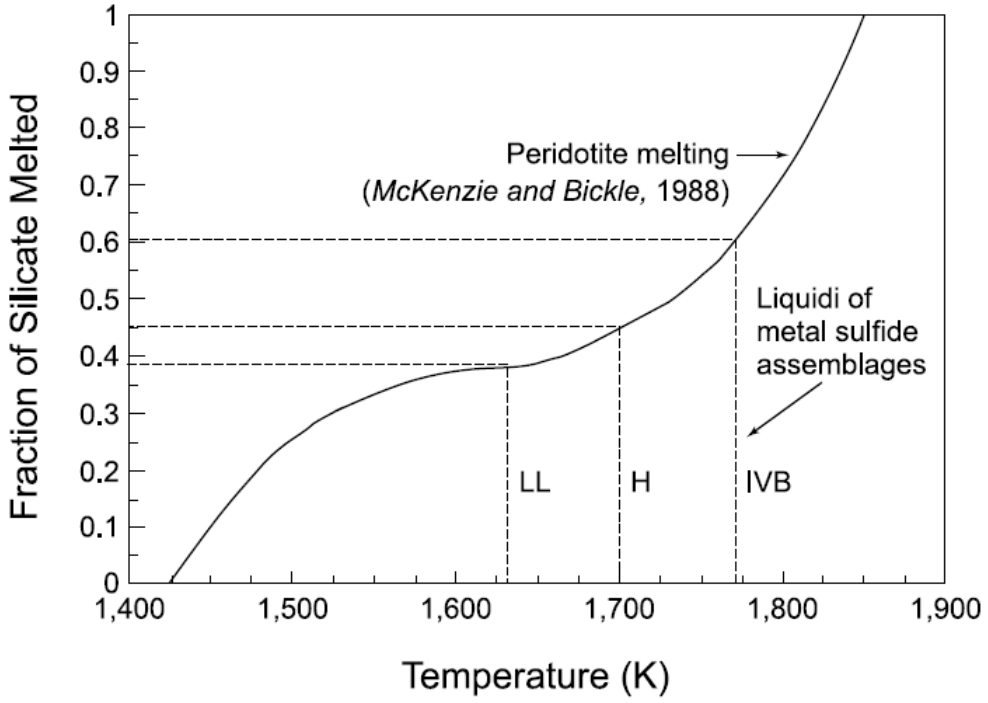

Figure 3.6: Fraction of silicate melted versus temperature for peridotite melting (McKenzie & Bickle, 1988). Liquidi are shown for H and LL chondrites and the S-poor IVB irons. Degrees of partial melting between 39% and 60% are indicated, consistent with the presence of magma oceans on the parent asteroids of most iron meteorites and a residual mantle with $40\% - 60\%$ residual crystals. The residual crystals would be dominantly olivine, although a small pyroxene component might be present at the lower ranges of degrees of partial melting, consistent with the discovery of pyroxene pallasites. Figure from Taylor et al. (1993).

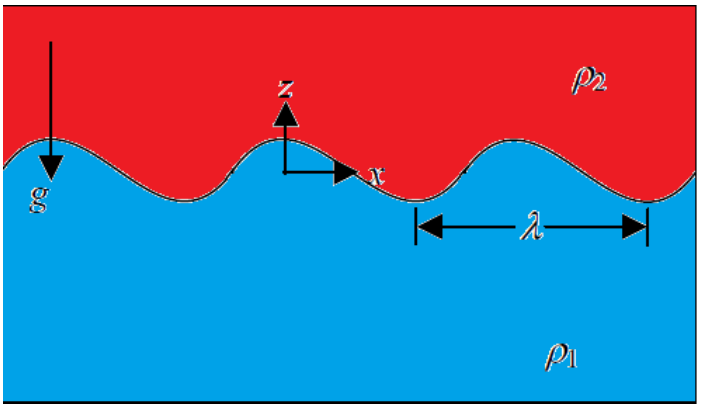

Figure 3.7: Rayleigh-Taylor instability occurs for A ¿ 0.

If the velocity is zero at large distance (above and below the interface) and at the interface is matched for the two solutions (kinematic constrain):

$$w_1 = w_0 e^{kz}$$
$$w_2 = w_0 e^{-kz}. \tag{3.17}$$

Applying the eq.(3.15) at the interface and multiplying by dz and integrating, we obtain:

$$\int d\left(\rho \frac{dw}{dz}\right) - \int \rho k^2 w dz = \int -wg\frac{k^2}{n^2} d\rho. \tag{3.18}$$

If $dz \simeq 0$, we obtain:

$$\Delta\left(\rho \frac{dw}{dz}\right) = -wg\frac{k^2}{n^2}\Delta\rho, \tag{3.19}$$

from which:

$$\rho_2 (-kw) - \rho_1 (kw) = -wg\frac{k^2}{n^2}(\rho_2 - \rho_2). \tag{3.20}$$

Finally, we obtain:

$$(\rho_2 + \rho_1) = \frac{gk}{n^2}(\rho_2 - \rho_1), \tag{3.21}$$

and solving for the eigenvalue n, we write:

$$n = \sqrt{\frac{gk(\rho_2 - \rho_1)}{(\rho_2 + \rho_1)}}. \tag{3.22}$$

The quantity $A = (\rho_2 - \rho_1)/(\rho_2 + \rho_1)$ is called *Atwood number*. If $A > 0$, that means that the heavy fluid is above the lighter one, the instability occurs; if $A < 0$ the interface is stable. The criterion for the onset of the

Rayleigh-Taylor instability is usually described as a local Rayleigh number Ra exceeding a critical value Ra_c that lies between 1000 and 2000 (Korenaga, 2003). The Rayleigh number is the nondimensional ratio of thermal buoyancy forces to viscous and diffusive dissipative effects:

$$Ra = \frac{\rho g \alpha \Delta T L^3}{\mu \kappa}, \tag{3.23}$$

where ρ is fluid density, g is gravitational acceleration, α is thermal expansivity, ΔT is the temperature range across the fluid that drives the convection, L is a characteristic length scale for the fluid body, μ is dynamic viscosity and κ is thermal diffusivity. This instability lead to the formation of a metals-rich core and an overlying silicate-rich mantle.

3.3.5 Crust Formation: Removal of ^{26}Al via Melt Migration

There are two linked requirements for the formation of a compositionally distinct crust on an asteroid: a sufficiently large degree of partial melting of the region that becomes the mantle and efficient spatial separation of melt from the residual mantle. A basaltic crust form either as a result of migration of silicate partial melts to the surface (Walker & Agee, 1988; McKenzie & Bickle, 1988; Taylor et al., 1993) or through fractional crystallization of a magma ocean (McCoy et al., 2006). Molten silicates will migrate in the presence of a density contrast between the melt and the surrounding solid matrix, if the melt is interconnected in a network of pore spaces between the solid grains. Typical density contrasts for silicate partial melts $\Delta\rho$ are 300 - 700 kg m^{-3}. Compaction of a melted region is controlled by the bulk viscosity of the matrix, microscopic shear viscosity of the matrix, viscosity of the melt and permeability of the matrix to fluid flow control. Migration of Al-enriched melts to the surface would produce an ^{26}Al-enriched crust. Migration of these melts can influence internal heating due to the redistribution of ^{26}Al. If partial melting and crust formation occur early, i.e. within one or two ^{26}Al half-lives, this concentration could re-melt the crust. A major issue related to the growth of asteroid crusts is the efficiency of volcanic advection of heat. There are two aspects of this phenomenon. The first is related to the the release of heat at the asteroid surface. Clearly even

shallow intrusions were less efficient than surface eruptions at releasing heat. When surface eruptions occurred, explosive activity was probably more efficient than lava flow formation, but the situation is not clear cut. The negligible atmospheric pressure caused maximal expansion of released gas and hence high velocities of ejected magma droplets and the relatively low gravity allowed wide dispersal of pyroclasts (Wilson & Keil, 1991). However, the high degree of gas expansion would also have fragmented the erupted magma into very small droplets and then there is a wide range of eruption conditions (Wilson & Keil, 1991) that could have produced optically dense fire fountains in which all droplets except those in the outer envelope of the fountain retained their heat and formed uncooled ponds feeding lava flows.

3.3.6 Complete Melting and possible Magma Ocean

The presence of iron meteorites implies high degrees of partial melting (more than 50 vol.%). We have seen that the complete melt of silicates occurs when the temperature inside the planetesimals are higher than 1800 K (see Fig.3.6). This especially occurs in the first stages of large planetesimals through kinetic energy to heat conversion during accretionary impacts with planetary embryos. In this conditions it is possible the creation of magma ocean below the solid crust. Magma oceans can influence the thermal history of the planetesimals, in particular the differentiation and the structure. Taylor & Norman 1992 suggest that a magma ocean can be defined by two criteria. First, the magma behaves rheologically as a liquid, having sufficiently small crystal fraction that the crystals are suspended within the liquid and not fused into a network. Second the magma encompasses a substantial fraction of the body, perhaps more than 10 vol.%. Magma ocean are sufficiently extreme in their condition that they are thought to obtain Rayleigh numbers in the range of 10^{20} - 10^{30}. The processes of solidification of the magma ocean determine initial compositional differentiation of the silicate portion of the planet. The subsequent stability of this differentiation has significance for magmatic source regions, convective instability and magnetic field generation. Solidification of a magma ocean that has a free surface, therefore, would be rapid, possibly as rapid as 10^5 to 10^6 a for a

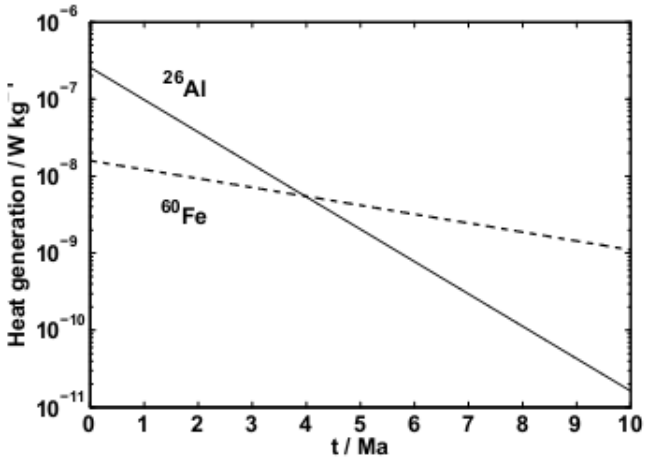

Figure 3.8: Heat generation by the short-lived radionuclides ^{26}Al and ^{60}Fe as a function of time relative to CAIs formation.

deep terrestrial magma ocean (Elkins-Tanton, 2012). If the magma ocean had a solid conductive lid, then heat flux would be reduced by many orders of magnitude and thus cooling and solidification times would be lengthened proportionately.

3.3.7 Cooling Phase

After about 3 Ma the ^{26}Al is extinguished (see Fig.3.8) and the asteroid enters in the cooling phase if there are no other activated radionuclides or heating source, reaching its final internal structure. Successive impacts could locally heat the asteroid and cause mixing of the materials and in some strong cases change the internal structure and the thermal and geophysical history of the asteroid.

3.4 An Overview on the developed Thermal Models

A wide range of thermal models of planetesimals with ^{26}Al as the heat source exists in the literature: we briefly analyze the most significant ones. The first study on the differentiation of asteroid 4 Vesta with a numerical code was presented by Ghosh & McSween 1998. These authors demonstrated

that it is possible to sustain partial melt on Vesta for $\sim$ 100 Ma assuming radiogenic heating by ^{26}Al. They examined the influence of the delay time of accretion with respect to the formation time of the CAIs and they assumed instantaneous accretion. They showed that melting and core formation did not occur if the time accretion is more than 3 Ma after CAIs formation, based on the assumption that the eucrites were generated with no more than 25 vol.% partial melting of silicate (Stolper, 1977). They did not use a fixed temperature at the surface, where the heat loss is governed by the energy balance between the irradiation at the surface and the interior heating due to the decay of short radionuclides. They did not examine the evolution of the internal structure such as the percolation of the iron through the silicatic matrix and consequent core formation. Merk et al. (2002) examined the influence of the accretion process on the thermal evolution. They concluded that the accretion time was not much smaller than the half-life of ^{26}Al. As Ghosh & McSween 1998 they did not analyze the evolution of the internal structure. Hevey & Sanders 2006 also incorporated convection in their thermal evolution models of planetesimals assuming that mantle regions where the degree of partial melting exceeded 50 vol.%, i.e. a magma ocean (Taylor et al., 1993), would be convecting. They simulate mantle convection by assuming that at temperatures greater than 1725 K the thermal conductivity increases by three orders of magnitude. As a result, heat is transferred rapidly from the convecting interior into the overlying rigid, partially molten zone. These authors modeled the primordial history of the planetesimals analyzing the sintering process when the temperature reaches the value of $\sim$ 700 K. Gupta & Sahijpal 2010 and Sahijpal et al. 2011 performed numerical simulations of the differentiation of planetesimals undergoing a linear accretion growth with both ^{26}Al and ^{60}Fe as the heat sources. They studied in particular the dependence of the growth rate of the Fe, Ni-FeS core on the onset time of planetesimal accretion (relative to CAIs formation), the (constant) accretion rate, the final size of the planetesimal, and the ^{60}Fe/^{56}Fe initial ratio. They did not use a radiation boundary condition but they included the sintering and linear accretion. Recently, Moskovitz & Gaidos 2011 studied how the migration of silicate melt and in particular the redistribution of ^{26}Al from the interior

into a crustal layer would affect the thermal evolution of planetesimal. In their model, core formation would require a bulk melting degree of 50 vol.%. They only considered the case of instantaneous accretion but they did not include convection, sintering and they use, like most of the thermal models developed, a fixed temperature at the surface. Sramek et al. 2012 presented a multiphase model for differentiation of planetesimals which takes into account phase separations by compaction driven melt migration and consider accretion. According to these authors, for the bodies with a radius greater than 500 km, impacts provide an additional heat source. Similarly to Merk et al. 2002, accretion rate is a crucial factor. They included accretion, sintering, radiation boundary condition, analyzing the evolution of the internal structure. Neumann et al. (2012) focused on the differentiation of small planetesimals (< 120 km) for melt fractions smaller than 50 vol.%. They combined the calculation of conduction, accretion, sintering, melting, melt segregation by porous flow.
The reasons that led me to develop my code are:

- to improve the treatment of the internal structure, in particular the evolution and the physical properties of the protocore/core (not taking a core already formed);

- to develop scenarios characterized by different physical parameters (available sources of energy, porosity, initial composition, mechanisms of heating/cooling);

- to depict the primordial history of 4 Vesta and 21 Lutetia (and in general of all rocky asteroid partially or completely differentiated) constraining the accretion and differentiation time.

In the next Section, I will explore in detail my geophysical model.

3.5 The Geophysical and Evolution Thermal Model of Vesta and Lutetia

3.5.1 Initial and Boundary Conditions of the Model

My model is based on 1D heat equation with radiogenic heat source and advective heat transport. I assumed Vesta and Lutetia as spherical bodies of fixed radius equal to 270 and 50 km, respectively, and composed of a homogenous mixture of two components, the first one generically referred to as *metals* (∼25 vol.%) and the second generically referred to as *silicates* (∼75 vol.%). This composition is similar to those of the H and L class of the ordinary chondrites, which contain a significative amount of metals (McSween et al., 1991) even if the inferred composition for Vesta is slightly different, as it appears to be strongly depleted in sodium and potassium (Consolmagno & Drake, 1977). The post-sintering porosity ranges from 1 vol.% to 5 vol.% for Vesta, and from 10 vol.% to 30 vol.%, for Lutetia. The initial temperature (T_0) of the body is fixed to 200 K (Lewis, 1974): a change of T_0 to 300 K does not affect the results in any significant way. During the thermal evolution, the silicatic and metallic fraction per unity volume change as a consequence of differentiation. The physical parameters density, specific heat and thermal conductivity of each unity volume also change accordingly. I imposed a radiation boundary condition at the surface and a *Neumann boundary condition* at the center (heat flux equal to zero) expressed in the following equations:

$$T(r, t = 0) = T_0, \tag{3.24}$$

$$\left[\frac{\partial T}{\partial r}\right]_{r=0} = 0, \tag{3.25}$$

$$\left[\frac{\partial T}{\partial r}\right]_{surf} = -\frac{\varepsilon\sigma}{K}\left(T_{surf}^4 - T_0^4\right), \tag{3.26}$$

where T_{surf} is the temperature of the surface, ε is the emissivity and σ is the Stefan-Boltzmann constant (see Tab.4.1).

3.5.2 Physical Description of the Model

To numerically study the thermal evolution of Vesta and Lutetia I considered the heating due to decay of ^{26}Al, ^{60}Fe and long-lived radionuclides (e.g. ^{238}U,^{235}U). The initial concentrations of the two short lived radioactive elements ^{26}Al and ^{60}Fe together with their half-lives are reported in Tab.4.1. The migration velocity of molten metal, following Yoshino et al. 2003, 2004 and Senshu & Matsui 2006, can be expressed:

$$v = \frac{K_D}{\mu} g \Delta\rho \tag{3.27}$$

where K_D is the permeability of the silicate medium, $\mu = 0.005$ Pa·s is the viscosity of molten iron, g is the gravitational acceleration, $\Delta\rho$ is the density contrast between molten metals and silicates (see Tab.4.1). The permeability-porosity relationship is expressed by:

$$K_D = \frac{\phi^n r_g^2}{\beta}, \tag{3.28}$$

where ϕ is the porosity, $r_g = 10^{-3}$ m is the grain size, $\beta = 200$ is a geometrical constant and $n = 2$ is predicted in an isotropic model with regular pore network along the edge of tetrakaidekahedral grains (Yoshino et al., 2004). The equation of heat transfer in a porous medium, assuming local thermal equilibrium so that $T_{sol} = T_{liq} = T$ (here *sol* stands for solid and *liq* for fluid taking averages over an unity volume), becomes (following Nield & Bejan 2006):

$$(\rho c)_m \frac{\partial T}{\partial t} = \vec{\nabla} \cdot \left(K_m \vec{\nabla} T \right) + H, \tag{3.29}$$

where

$$\begin{aligned} (\rho c)_m &= (1-\phi)\,(\rho c)_{sol} + \phi (\rho c)_{liq} \\ K_m &= (1-\phi)\,K_{sol} + \phi K_{liq} \end{aligned} \tag{3.30}$$

are the overall heat capacity and the overall thermal conductivity respectively; H is the overall heat production per unity volume of the medium. The surface temperature is controlled by the radiation boundary condition (see the eq.(3.26)). The volumetric radiogenic heating rate, due to ^{26}Al decay, following Castillo et al. 2009, can be expressed as:

$$H_{Al} = \bar{\rho} C_{Si} \left[{}^{26}Al \right]_0 H^* e^{-\lambda t}, \tag{3.31}$$

where $\bar{\rho}$ is the mean density, C_{Si} is the mass fraction of the silicates, $[^{26}Al]_0$ is the initial concentration of ^{26}Al in kg for kg of silicates, $\lambda = ln(2)/\tau_{Al}$ is the decay constant and H^* is the specific power production (see Castillo et al. 2009 and Tab.4.1). Once the melting temperature of Fe-FeS (or of silicates) is reached, partial or complete melting occurs depending on the parameter

$$\chi = \frac{T - T_{sol}}{T_{liq} - T_{sol}}, \tag{3.32}$$

following Merk et al. (2002) and assuming a linear growth of χ with raising temperature (T). The values of the temperature for the initial (T_{sol}) and complete (T_{liq}) melting temperature of metals (or of silicates) are reported in Tab.4.1. Also following Merk et al. (2002), the specific heat is modified through the Stefan coefficient,

$$Ste = \frac{L}{c_p(T)}\frac{d\chi}{dT} = \frac{L}{c_p(T)}\frac{1}{T_{liq} - T_{sol}}, \tag{3.33}$$

to take into account in a simple way the latent heat during phase transition:

$$\bar{c_p}(T) = c_p(T)(1 + Ste). \tag{3.34}$$

where:

$$c_p(T) = (1 - \chi(T))c_{p,sol} + \chi(T)c_{p,liq}. \tag{3.35}$$

The Stefan number (Ste) normally represents the ratio of latent heat (L) and specific heat (c) and is controlled by the melting rate $d\chi/dT$, where $\chi(T)$ is the melting fraction of solid material $0 \leq \chi \leq 1$. For the sake of simplicity I assumed linear growth of χ with rising temperature, thus leading to a constant melting rate depending only on T_{liq} and T_{sol}, the metallic liquidus and solidus temperatures, respectively. If the temperature is out the windows of melting of metallic or silicate component, the Stefan coefficient is assumed equal to zero. As in Ghosh & McSween 1998, metal melting is initiated at 1213 K, the melting temperature of the eutectic Fe-FeS system, and silicate melt generation is assumed to initiate at 1425 K (see Tab.4.1). The entire latent heat for melting is assumed to be expended in a temperature "window" between *solidus* and *liquidus* (Ghosh & McSween, 1998). This simplification of temperature "windows" does not change the whole thermal history being the exact latent heat supplied to cause silicate

and metallic melting. The percolation of the metals through the silicate matrix, starting at 1213 K, is governed by the advection equation. If Y represents concentration of the metals, the equation reads:

$$\frac{\partial Y}{\partial t} + \vec{v} \cdot \vec{\nabla} Y = 0, \tag{3.36}$$

in which v is the migration velocity of the molten metal. The chemical diffusion is assumed negligible. As noted by Yoshino et al. (2003), if permeable flow is established, segregation velocities (which vary in the range 1-100 m/a) are rapid in comparison with the timescale of core formation predicted from ^{182}Hf-^{182}W isotope system. During the percolation the volume fraction of the metallic component (Y) goes down enriching the forming core region. When the temperature reaches the value of the 50 vol.% melting temperature of the silicate, the separation of two melts occurs and the silicate component (X) moves upwards to the mantle region dragging ^{26}Al with itself. At the end of this phase, the core becomes pure metallic because the melted metals, being more dense than silicatic ones, sink to the center. During the evolution, the concentration of Al grows in the mantle underneath the lithosphere while the density profile varies due to the differentiation and the moment of inertia factor (MoI) decreases starting from the initial characteristic value of 0.4, for a uniform sphere. When the core formation process ends and the thermal evolution becomes simply a heat diffusion problem. With the combined solution of the eqs.(3.29) and (3.36) is possible to study the evolution of the internal structure, constraining formation time, size and mass of the core, the size of the chondritic crust and the temperature profile as a function of the distance from the center and of the time. As noted above, I chose the formation of the core at 50 vol.% of melt fraction of the silicate, that corresponds to a temperature of about 1725 K (Taylor, 1992). I investigated several evolutive scenarios, varying the strength of the radiogenic sources, the accretion time (expressed by Δt_d) and the porosity.

3.5.3 Internal Pressure

To obtain an estimate of a pressure at the distance r from the center of a planetesimal with nearly constant density (meaning homogeneous porosity

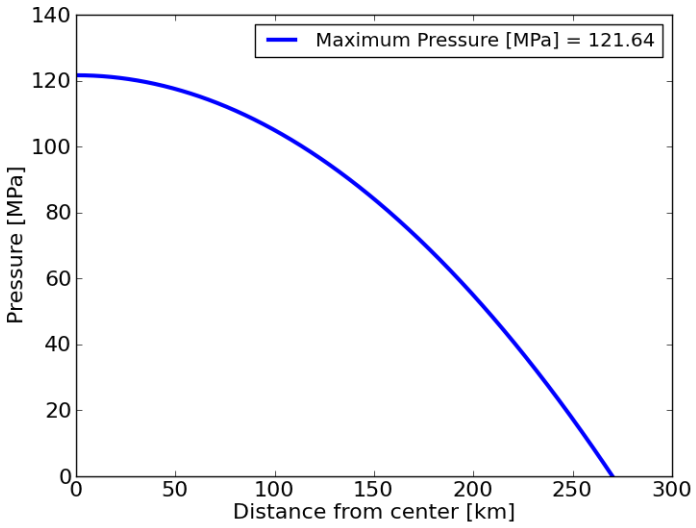

Figure 3.9: Pressure profile vs distance from center.

in the entire body) we can use the following equation:

$$p(r) = \frac{2\pi}{3} G\rho^2 \left[R_p^2(t) - r^2\right], \tag{3.37}$$

where $R_p(t)$ is the radius of the accreting planetesimal. By setting $r = 0$ and $\rho = 3456$ kg/m^3, we obtain an estimate of the pressure in the center equal to $p(r = 0) \simeq 121\ MPa$. The profile of the pressure as a function of the distance from center is shown in the Fig.3.9.

Chapter 4

Numerical Procedure

4.1 Introduction to Numerical Solution of the Heat Equation

The heat transfer equation is the basis for most model calculations. Three methods exist for its numerical solution: the classical series solution, the finite difference method and the finite element method, with the latter being most accurate. Asteroid thermal models must make assumptions that address uncertainties in initial conditions (e.g. asteroids temperature at the beginning of the simulation), boundary conditions (e.g. nebular ambient temperature, asteroid emissivity) and model parameters (e.g. specific heat capacity, thermal diffusivity, presence of regolith, voids or ice). Initial temperatures are usually constrained from nebular models (e.g. Woods & Morfill 1988) and many thermal models assume asteroid accretion was instantaneous. Boundary conditions are implemented in two ways: the Dirichlet boundary condition forces the asteroid surface temperature to that of the ambient nebula and the radiation boundary condition calculates a heat flux depending of temperature difference between the asteroid surface and the nebula. Although the radiation boundary condition is numerically unstable, it is probably more realistic. Model parameters are constrained, to the extent possible, using meteorite and asteroid data (e.g. peak temperatures, cooling rates, closure ages, ^{26}Al contents, asteroid sizes). For the eq.(3.29)

an analytic solution exists (Carlslaw & Jager, 1959):

$$T = T_0 + \frac{\kappa H_0}{K\lambda} e^{-\lambda t} \left[\frac{R sinr \left(\lambda/\kappa\right)^{1/2}}{r sinr \left(\lambda/\kappa\right)^{1/2}} - 1 \right] + \frac{2R^3 H_0}{r\pi^3 K} \sum_{n=1}^{\infty} \frac{(-1)^n}{n\left(n^2 - \lambda R^2/\kappa\pi^2\right)} sin\left(\frac{n\pi r}{R}\right) e^{-\kappa n^2 \pi^2 t/R^2}, \tag{4.1}$$

in which I assume that ρ, c_p and K have constant values and are independent of temperature. In the eq.(4.1), κ is the thermal diffusivity, t is the elapsed time since the asteroid formed, λ is the decay constant of the ^{26}Al and T_0 is the ambient temperature. Fortunately, the eq.(4.1) may be solved numerically as well as analytically as we can see in the next Section.

4.2 Choice of Spatial and Temporal Grid

The numerical solution of the system of differential equations (3.29) and (3.36) is obtained using a 1D finite difference method (*Forward-Time Central-Space* (FTCS) in radial direction. A spatial grid of $\Delta r = 300$ m is used. To avoid numerical stability problems due to the instability of the FTCS scheme I used the *Lax scheme* (Press et al., 2007). Following Toksoz & Solomon (1973), I adopted an *adaptive* time increment according to the *Courant-Friedrichs-Lewy* (CFL) stability condition:

$$\Delta t_T < \frac{c_p \bar{\rho} \Delta r^2}{2\bar{K}}, \tag{4.2}$$

where, at a given time step, $\bar{K}$ is the mean value of the thermal conductivity, $\bar{\rho}$ is the mean density and c_p is the specific heat of the silicatic matrix, at a given time as these quantities ($\bar{K}$, ρ and c_p) evolve during the thermal and internal evolution of the asteroid. At each time step the critical time increment Δt is computed and Δt is assumed equal to 90% of the value obtained by the eq.(4.2). When the melting temperature of the Fe-FeS is reached (and the iron percolation takes place), I need to solve also the eq.(3.36), so I need to introduce another time step respecting the CFL:

$$\Delta t_p < \frac{\Delta r}{v}, \tag{4.3}$$

where Δx is the spatial grid and v is the velocity of the iron percolation. Also in this case I used the 90% of the critical value obtained by the eq.(4.3). I treated the separation of two melts assuming that it occurred when the temperature inside the asteroid reached the critical value for which the 50 vol.% of silicate melted, with a separation rate that is a function of the difference in density of two melts (i.e. $\Delta\rho = 3200$ kgm^{-3}).

4.3 Heat Transfer Equation

In this Section I focused on the solution of the heat equation with the term due to the radiogenic heating by using the finite-difference method in *Python language*. I solved the eq.(3.29) in which I expanded the right derivative, obtaining (Nield & Bejan, 2006):

$$(\rho c_p)_T \frac{\partial T}{\partial t} = \frac{\partial K(r)}{\partial r}\frac{\partial T}{\partial r} + K(r)\frac{\partial^2 T}{\partial r^2} + \frac{2}{r}K(r)\frac{\partial T}{\partial r} + H(r,t). \tag{4.4}$$

In the Tab.4.1, we find the values for the several physical parameters introduced in the model. Using the finite-difference method, we obtain:

$$(\rho c_p)_T \frac{\partial T}{\partial t} = \left[\frac{\partial K(r)}{\partial r} + \frac{2}{r}K(r)\right]\frac{\partial T}{\partial r} + K(r)\frac{\partial^2 T}{\partial r^2} + H(r,t). \tag{4.5}$$

The indexes m and n represent the temporal and spatial coordinate, respectively. Let us to analyze every terms of the eq.(4.5):

$$\frac{\partial T}{\partial t} = \frac{3T_m^{n+1} - 4T_m^n + T_m^{n-1}}{2\Delta t}, \tag{4.6}$$

in which I approximated the first temporal derivative of temperature with the unknown coefficient method. I approximated the first spatial derivative of the temperature as:

$$\frac{\partial T}{\partial r} = \frac{T_{m+1}^{n+1} - T_{m-1}^{n+1}}{2\Delta r}, \tag{4.7}$$

by using the centered difference method. Similarly, the derivative of the diffusivity is:

$$\frac{\partial K(r)}{\partial r} = \frac{K_{m+1}^{n+1} - K_{m-1}^{n+1}}{2\Delta r}. \tag{4.8}$$

The second spatial derivative of the temperature is approximated as:

$$\frac{\partial^2 T}{\partial r^2} = \frac{T_{m+1}^{n+1} - 2T_m^{n+1} + T_{m-1}^{n+1}}{\Delta r^2}. \tag{4.9}$$

Quantity	Value	Unit	Reference
Vesta final primordial radius (R_{Vesta})	270×10^3	m	Ghosh & McSween (1998)
Lutetia final primordial radius ($R_{Lutetia}$)	50×10^3	m	Weiss et al. (2011)
Density of metal (solid) ($\rho_{met,sol}$)	6300	$Kg\ m^{-3}$	Neumann et al. (2012)
Density of silicate (solid) ($\rho_{sil,sol}$)	3000	$Kg\ m^{-3}$	Neumann et al. (2012)
Density of metal (liquid) ($\rho_{met,liq}$)	6200	$Kg\ m^{-3}$	Neumann et al. (2012)
Density of silicate (liquid) ($\rho_{sil,liq}$)	2900	$Kg\ m^{-3}$	Neumann et al. (2012)
Specific heat of metal (solid) ($c_{met,sol}$)	600	$JKg^{-1}K^{-1}$	Sahijpal et al. (2007)
Specific heat of metal (liquid) ($c_{met,liq}$)	2000	$JKg^{-1}K^{-1}$	Sahijpal et al. (2007)
Specific heat of silicate(solid) ($c_{sil,sol}$)	720	$JKg^{-1}K^{-1}$	Sahijpal et al. (2007)
Specific heat of silicate (liquid) ($c_{sil,liq}$)	720	$JKg^{-1}K^{-1}$	Sahijpal et al. (2007)
Latent heat of metal (L_{met})	270	$KJ\ Kg^{-1}$	Ghosh & McSween (1998)
Latent heat of silicate (L_{sil})	400	$KJ\ Kg^{-1}$	Ghosh & McSween (1998)
Metal solidus (T^{met}_{sol})	1213	K	Ghosh & McSween (1998)
Metal liquidus (T^{met}_{liq})	1233	K	Ghosh & McSween (1998)
Silicate solidus (T^{sil}_{sol})	1425	K	Taylor (1992)
Silicate liquidus (T^{sil}_{liq})	1850	K	Taylor (1992)
50 vol.% silicate melting (T^{sil}_{50})	1725	K	Hevey & Sanders (2006)
Thermal conductivity of metal (K_{met})	50	$W\ m^{-1}\ K^{-1}$	Sramek et al. (2012)
Thermal conductivity of silicate (K_{sil})	3	$W\ m^{-1}\ K^{-1}$	Sramek et al. (2012)
Initial metal volume fraction (Y)	25%		
Initial silicate volume fraction (X)	75%		
Vesta post-sintering porosity (ϕ_{Vesta})	1% - 5%		
Lutetia post-sintering porosity ($\phi_{Lutetia}$)	10% - 30%		
Temperature of Solar Nebula (T_0)	200	K	Lewis (1974)
Stefan-Boltzmann constant (σ)	5.67×10^{-8}	$W\ m^{-2}\ K^{-4}$	
Emissivity (ε)	1		
Half-life of ^{26}Al (τ_{Al})	0.717	Ma	Castillo et al. (2009)
Specific heat production of ^{26}Al	0.355	WKg^{-1}	Castillo et al. (2009)
Initial isotopic abundance of ^{26}Al in ordinary chondrites ($[^{26}Al]_0$)	6.20×10^{-7}	ppb	Castillo et al. (2009)
Half-life of ^{60}Fe (τ_{Fe})	2.62	Ma	Rugel et al. (2009)
Specific heat production of ^{60}Fe	$0.068 \div 0.074$	WKg^{-1}	Castillo et al. (2007)
Initial isotopic abundance of ^{60}Fe in ordinary chondrites ($[^{60}Fe]_0$)	$(22.5 \div 225)\times10^{-9}$	ppb	Castillo et al. (2007)

Table 4.1: Physical parameter values used in my work.

We have to solve a set of equations, written in a matrix form:

$$AT = b. \tag{4.10}$$

Separating the unknown terms (in temperature), at fixed index $n+1$, $m-1$, m and $m+1$ in temperature, we write:

$$\begin{cases} A[m,m-1] = \dfrac{2\Delta t}{2\left(\rho_m^{n+1}c_p\right)_T \Delta r^2}\left(\dfrac{K_{m+1}^{n+1}-K_{m-1}^{n+1}}{4}\right) \\ -\dfrac{2\Delta t}{\left(\rho_m^{n+1}c_p\right)_T \Delta r^2}\times\left(\dfrac{m-1}{m}\right)K_m^{n+1} \\ A[m,m] = 3+\dfrac{4\Delta t}{\left(\rho_m^{n+1}c_p\right)_T \Delta r^2}K_m^{n+1} \\ A[m,m+1] = -\dfrac{2\Delta t}{2\left(\rho_m^{n+1}c_p\right)_T \Delta r^2}\left(\dfrac{K_{m+1}^{n+1}-K_{m-1}^{n+1}}{4}\right)- \\ \dfrac{2\Delta t}{\left(\rho_m^{n+1}c_p\right)_T \Delta r^2}\left(\dfrac{m+1}{m}\right)K_m^{n+1} \\ b_m = 2\Delta t\dfrac{H_m^n}{(c_p)_T}+4T_m^n-T_m^{n-1}. \end{cases} \tag{4.11}$$

4.3.1 Boundary Condition at $r = 0$

Rewrite the eq.(4.4) as:

$$\frac{\partial T}{\partial t} = \frac{1}{(\rho c_p)_T}\frac{\partial K(r)}{\partial r}\frac{\partial T}{\partial r}+\frac{K(r)}{(\rho c_p)_T}\left(\frac{\partial^2 T}{\partial r^2}+\frac{2}{r}\frac{\partial T}{\partial r}\right)+\frac{H(r,t)}{(c_p)_T}. \tag{4.12}$$

By de l'Hôpital's rule:

$$\left[\frac{2}{r}\frac{\partial T}{\partial r}\right]_{r=0} = 2\frac{\dfrac{\partial}{\partial r}\left(\dfrac{\partial T}{\partial r}\right)}{\dfrac{\partial r}{\partial r}} = 2\frac{\partial^2 T}{\partial r^2}, \tag{4.13}$$

and by using the condition:

$$\left[\frac{\partial T}{\partial r}\right]_{r=0} \Rightarrow \frac{T_1^{n+1}-T_{-1}^{n+1}}{2\Delta r} = 0 \Rightarrow T_1^{n+1} = T_{-1}^{n+1}, \tag{4.14}$$

the coefficients of the matrix A become:

$$\begin{cases} A[0,0] = 3 + \dfrac{2\Delta t}{(\rho_0^{n+1} c_p)_T \Delta r^2} \left(K_1^{n+1} + 5K_0^{n+1}\right) \\ \\ A[0,1] = -\dfrac{2\Delta t}{(\rho_0^{n+1} c_p)_T \Delta r^2} \left(K_1^{n+1} + 5K_0^{n+1}\right) \\ \\ b[0] = \dfrac{2\Delta t H_0^{n+1}}{(c_p)_T} + 4T_0^n - T_0^{n-1}. \end{cases} \tag{4.15}$$

4.3.2 Radiation Boundary Condition at the surface

We can introduce the heat loss by radiative transfer by using the following relation:

$$\frac{\partial T}{\partial r} = -\frac{\varepsilon\sigma}{K}\left(T_{surf}^4 - T_{neb}^4\right) \tag{4.16}$$

in which ε and σ are the emissivity and the Stefan-Boltzmann constant, respectively. We rewrite the eq.(4.16) as:

$$\frac{\partial T}{\partial r} = \frac{\varepsilon\sigma}{K}\left[\left(T_{surf}^2 + T_{neb}^2\right)\left(T_{neb} - T_{surf}\right)\left(T_{neb} + T_{surf}\right)\right], \tag{4.17}$$

and by using Taylor's approximation:

$$\frac{\partial T}{\partial r} = \frac{\varepsilon\sigma}{K}\left[\left(2T_{neb}^2 + 2T_{neb}\left(T_{surf} - T_{neb}\right)\right)\left(T_{neb} - T_{surf}\right)\left(T_{neb} + T_{surf}\right)\right], \tag{4.18}$$

we obtain:

$$A[N,N] = 1$$

$$b[N] = \frac{\varepsilon\sigma\Delta t}{(\rho c_p)_N^n \Delta r}\left(\frac{K_N^n - K_{N-1}^n}{\Delta r}\right) \times$$

$$\left[\left(2T_{neb}^2 + 2T_{neb}\left(T_N^n - T_{neb}\right)\right)\left(T_{neb} - T_N^n\right)\left(T_N^n + T_{neb}\right)\right] - \frac{4\varepsilon\sigma T_{neb}^3 \Delta t}{(\rho c_p)_N^n}\left(T_N^n - T_{N-1}^n\right)$$

$$+\frac{2\varepsilon\sigma\Delta t}{N\,(\rho c_p)_N^n}\left[\left(2T_{neb}^2 + 2T_{neb}\left(T_N^n - T_{neb}\right)\right)\left(T_{neb} - T_N^n\right)\left(T_{neb} + T_N^n\right)\right] + \frac{\Delta t H_N^n}{c_{p_N}^n}. \tag{4.19}$$

Though a radiative boundary condition offers a more robust approach (Ghosh & McSween, 1998), it is numerically unstable. The greater the difference

between peak temperature and nebular temperature, the greater will be the error with a *Dirichlet boundary condition* is used. This happens because in order to make the temperature on the surface of the asteroid equal to the temperature of the surrounding nebula, a higher heat flux than is allowed by the radiation boundary condition must be invoked. A Dirichlet boundary condition will result in lower peak temperature and higher cooling rates.

4.4 Iron Percolation: Advection Equation

I approximated the eq.(3.36) with the FTCS scheme:

$$\frac{Y_m^{n+1} - Y_m^n}{\Delta t} = -v \left(\frac{Y_{m+1}^n - Y_{m-1}^n}{2\Delta x} \right) \tag{4.20}$$

from which:

$$Y_m^{n+1} = -\frac{v\Delta t}{2\Delta x} \left(Y_{m+1}^n - Y_{m-1}^m \right) + Y_m^n. \tag{4.21}$$

To fix numerical oscillation due to the instability of the FTCS scheme, I used the Lax method (see Fig.4.1 for the schematic representation) by replacing Y_m^n on the right-hand side by the spatial average of Y_m^n taken over the neighboring grid points. Thus, we obtain:

$$Y_m^{n+1} = -\frac{v\Delta t}{2\Delta x} \left(Y_{m+1}^n - Y_{m-1}^m \right) + \frac{1}{2} \left(Y_{m+1}^n + Y_{m-1}^n \right). \tag{4.22}$$

At $r = 0$, I simply fixed the concentration to the initial value.

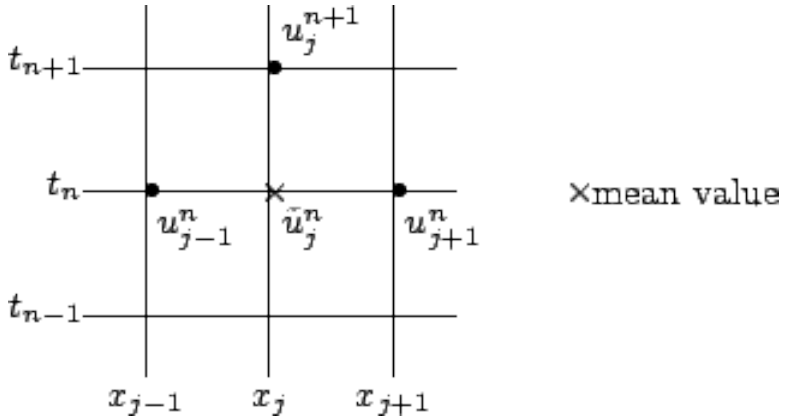

Figure 4.1: Schematic representation of the Lax method applied to a FTCS scheme.

Chapter 5

Results: the case of Vesta

The results of my geophysical and thermal model depends on all the various physical parameters that I reported in Tab.4.1: luckily, while most of these parameters are still poorly known, their variation does not affect the overall evolution of Vesta in any significant way. In Tab.5.1, I report the results obtained for different values of Δt_d and post-sintering porosity, in particular the time at which the metal (τ_{met}) and the silicate (τ_{sil}) melting begins, the time of formation of core (τ_{core}), the size of the surviving chondritic crust, the size of the solid layer (labeled as *SL*) after 3 and 5 Ma, the maximum degree of the silicate melting and the maximum temperature reached inside the asteroid after 5 Ma. I define the chondritic crust as the thickness of the region of Vesta that never melt. It is identified by the intersection between the temperature profile with the line corresponding to the onset of metals melting. This behavior is present also in the modeling of Ghosh & McSween (1998), who assumed that this point is fixed. In this work, instead, the location of this intersection moves in time depending on the characteristics of the scenarios (see Tab.5.1). I define the solid layer (SL) as the the thickness of the region of Vesta that is solid at a given time. In the following discussion I focused on the dependence of the evolution of Vesta on the post-sintering porosity and on the delay time Δt_d. The delay time is essentially an unknown parameter, but it is critical in determining the initial overall abundance of short lived radioactive elements, i.e. the intensity of the source of energy, the maximum temperature reached during

the evolution and then the cooling behavior of the object. The chosen values of Δt_d sample a long time interval and therefore very different intensities of the radioactive sources. I investigated seven scenarios, labeled as N0-N6: as shown in Tab.5.2, I considered values for Δt_d equal to 0, 0.5, 1, 1.5, 2, 2.5 and 3 times the half-life of ^{26}Al, corresponding to values in the range 0-2.15 Ma. My first analysis of the results obtained for the different scenarios is based on the compatibility of the simulated evolution of Vesta with the constrains supplied by the HEDs. As we can see in Figs.5.4, 5.5 and 5.6, in N0-N2, which implies accretion time less than 1 Ma, the complete melting of silicates is achieved across the whole of the asteroid. In N3, where Vesta took 1 Ma to form, complete melting of silicates is achieved in a limited region of the mantle of Vesta but in the rest of the asteroid the degree of melting is larger than 50 vol.% with the only exception of the case where the porosity is equal to 5 vol.%. Similarly, in N4 where Vesta took 1.4 Ma to form, the degree of melting is generally lower than 50 vol.%, except possibly in the limited region of the mantle. Finally, if Vesta took more than 1.5 Ma to form, silicate melting is either not possible or is limited only to a small region of the asteroid. The N0-N3 are compatible with the results of (Greenwood et al., 2005) which link the formation of the eucrite and diogenite to a large scale ($>$ 50 vol. %) melting of the silicates. This would implied Vesta formed in no more 1 Ma. It is be noted that in those scenarios in which the differentiation takes place, the melting of the silicatic component begins in the first 1 Ma and the differentiation is completed in about 3 Ma. Accretion times of Vesta of about 1.5 Ma are compatible with the formation of HEDs if eucrite and diogenites can form from a partial melt ranging from 25 to 50 vol.%. Formation time larger than 1.5 Ma are not compatible with petrogenesis of HEDs. The conditions to start the formation of eucrites and diogenites are always obtained within 1 to 2 Ma from the accretion of Vesta. In Figs.5.4, 5.5 and 5.6 I set the maximum temperature to 4000 K to ease the comparison: I refer the reader to Figs.5.1(e), 5.2(e) and 5.3(e) for the maximum temperature reached in the different cases. We observe that the maximum temperature reached in the N0-N2 far exceeds the liquidus silicates melting temperature (1850 K): this happens because in my model I do not take into account other cooling

mechanisms (convection and effusive phenomena) than the conduction and the irradiation at the surface. In Figs.5.1, 5.2, 5.3 for three different initial post-sintering porosity, I report in (a), (b), (c), (d) and (e) temperature profiles at different time (0.1, 0.5, 1.5, 3 and 5 Ma), in (f) the maximum temperature vs time profile. In (a), (b), (c), (d) and (e) the horizontal lines represent: the windows for the melting of metals (green and red) and of the silicates (cyan and magenta). Note that I report in Figs. 5.1 - 5.3 (in (a) - (e)) the profiles of N0-N4 while I neglect N5 and N6 because in those scenarios the differentiation of the asteroid does not take place. The general trend we observe in the different cases is the following. The first phase is characterized by a homogeneous heating of the asteroid. The second one is an increase of the temperature in the region in which the metals is depleting and migrating to the center of the asteroid. The final phase is the formation of the metallic core followed by the migration of the silicates (with the ^{26}Al) towards the surface and the increase of the temperature in the mantle of the asteroid. When the formation of Vesta takes less than 1 Ma, the formation of a pure metallic core, with a density of $\simeq$6200 kgm^{-3} is possible: its mass represents about the 2 vol.% of the total mass, slightly lower than the minimum value (4 vol.%) given by (Ruzicka et al., 1997), while the moment of inertia (MoI) is 0.33. For a delay of about 1.5 Ma, the formation of the metallic core is possible only if the porosity is lower than 5 vol.%. In Fig.5.1(a) Vesta heats up maintaining an almost unform temperature due to the initially homogeneous distribution of ^{26}Al, in all the scenarios. Due to the strong heating source, after 0.5 Ma (see Fig.5.1(c)), very high temperatures are reached in N0 and N1 and this trend continues after 1.5 Ma (see Fig.5.1(c)) and also involves N2. In N3 and N4 the silicate melting is still partial. After 3 Ma (see Fig.5.1(d)), only in N4 the complete melting of silicates is not reached and the temperature profile is inside the melting temperature of silicates. In Fig.5.1(e), after 5 Ma, the general trend for all the profiles is similar to that after 3 Ma. I report in Fig.5.1(f) the maximum temperature vs time profile and we observe that the differentiation is possible only in N0-N3, for which the separation of two melts occurs. The size of the chondritic crust, defined as the region of asteroid never melts, ranges from 3 to 17 km, while the size of the solid layer ranges from 7 to 21

km (after 3 Ma) and from 8 to 27 (after 5 Ma), as we can see in Tab.5.1. The formation of the core takes place between 0.45 and 3.06 Ma (in N0-N3). We can observe in Figs.5.2 and 5.3 (in (a) - (e)) that the evolution of the temperature in the first 5 Ma from CAIs is quite similar to the previous case (i.e. porosity of 1 vol.%). In the case of porosity of 2 vol.%, after 5 Ma, Vesta is in the cooling phase in N3 and N4, while if the porosity is equal to 5 vol.% the asteroid undergoes the cooling phase in all scenarios, except N0 and N1. The chondritic crust, in both cases, ranges from 4 to 19 km while the solid layer, after 3 Ma, ranges from 8 to 21 km. After 5 Ma, the solid layer ranges from 9 to 30 km (see Tab.5.1). It is be noted that the irradiation at the surface (I have fixed $\varepsilon = 1$) allows the presence of a primitive chondritic crust of maximum value of about 20 km, while as previously observed the SL can achieve the maximum value of about 30 km: the temperature at the surface, while never reaching the solid temperature of metals, can reach values as high as 1000 K. It is also noteworthy that the SL thickness implies a 5-10 km thick eucritic layer can already form between 3 and 5 Ma, in agreement with the dating of the oldest eucrites described by (Bizzarro et al., 2005).

	τ_{met} [Ma]	τ_{core} [Ma]	τ_{sil} [Ma]	Crust [km]	SL_{3Ma} [km]	SL_{5Ma} [km]	vol.% Silicate melt	T_{max} [K]
N0								
$\phi = 1.0$ vol.%	0.14	0.45	0.34	3	7	8	100	$\simeq 10000$
$\phi = 2.0$ vol.%	0.14	0.47	0.34	4	8	9	100	$\simeq 9500$
$\phi = 5.0$ vol.%	0.15	0.51	0.43	4	8	9	100	$\simeq 8700$
N1								
$\phi = 1.0$ vol.%	0.21	0.72	0.52	5	10	11	100	$\simeq 6500$
$\phi = 2.0$ vol.%	0.21	0.73	0.52	5	10	13	100	$\simeq 6000$
$\phi = 5.0$ vol.%	0.22	0.80	0.52	6	11	13	100	$\simeq 5800$
N2								
$\phi = 1.0$ vol.%	0.30	1.20	0.84	7	12	17	100	3848
$\phi = 2.0$ vol.%	0.31	1.27	0.88	7	12	17	100	3529
$\phi = 5.0$ vol.%	0.31	1.43	0.83	8	13	18	100	3643
N3								
$\phi = 1.0$ vol.%	0.46	3.06	1.60	11	15	20	100	2253
$\phi = 2.0$ vol.%	0.47	3.42	2.20	11	16	20	100	1964
$\phi = 5.0$ vol.%	0.47	- -	1.56	11	16	20	100	2316
N4								
$\phi = 1.0$ vol.%	0.72	- -	- -	17	21	27	$\simeq 40$	1679
$\phi = 2.0$ vol.%	0.73	- -	- -	18	21	30	$\simeq 35$	1597
$\phi = 5.0$ vol.%	0.74	- -	- -	19	21	30	$\simeq 50$	1737

Table 5.1: Summary of scenarios.

Scenario	**Delay** [Ma]	**Delay**[τ_{Al}]
N0	0.00	0.0
N1	0.36	0.5
N2	0.72	1.0
N3	1.08	1.5
N4	1.43	2.0
N5	1.79	2.5
N6	2.15	3.0

Table 5.2: Seven scenarios have been studied, where the delay-parameter Δt_d is expressed in Ma and in half-lives of ^{26}Al.

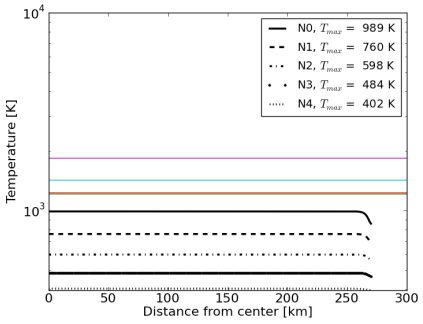

(a) t = 0.1 Ma

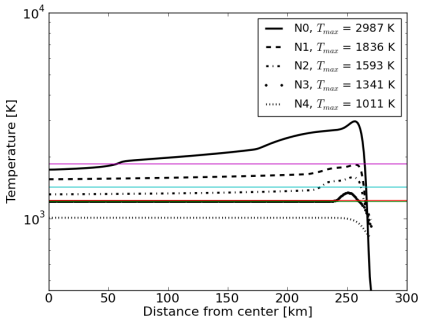

(b) t = 0.5 Ma

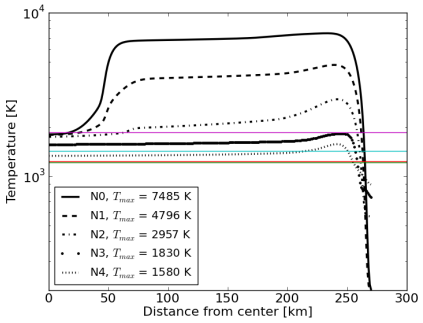

(c) t = 1.5 Ma

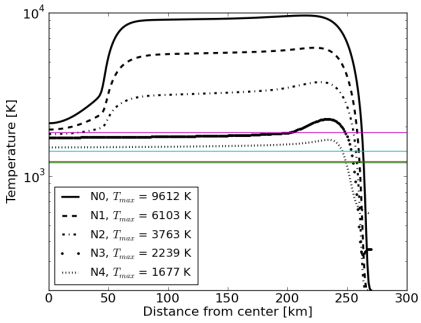

(d) t = 3.0 Ma

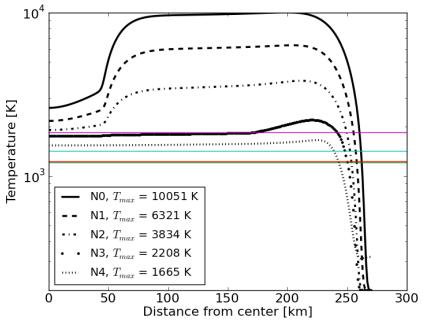

(e) t = 5.0 Ma

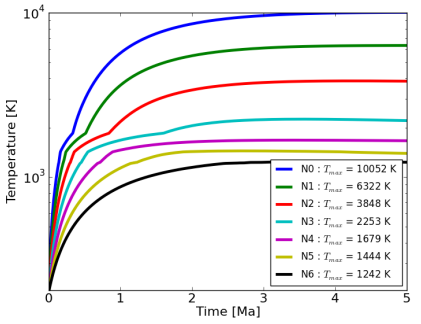

(f) Maximum temperature

Figure 5.1: Temperature vs distance from center (a-b-c-d-e), maximum temperature vs time (f), for $\phi = 1$ vol.%.

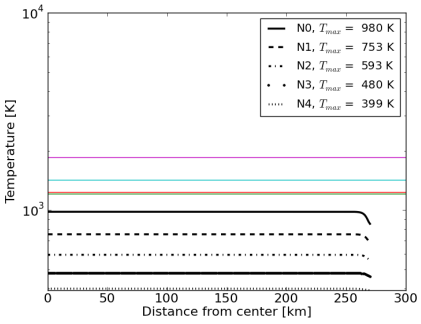

(a) t = 0.1 Ma

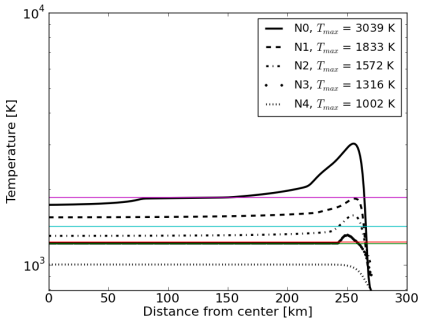

(b) t = 0.5 Ma

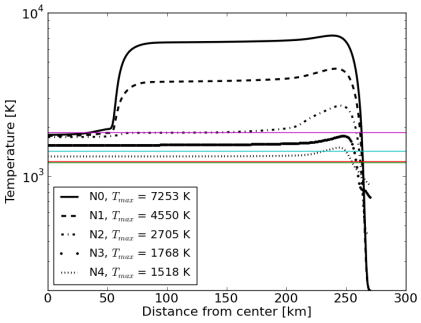

(c) t = 1.5 Ma

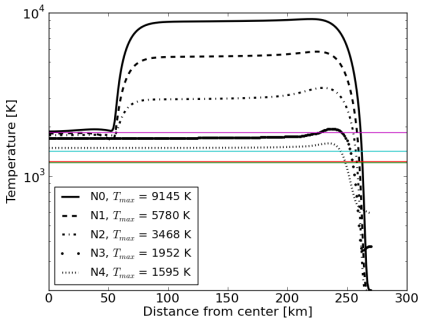

(d) t = 3.0 Ma

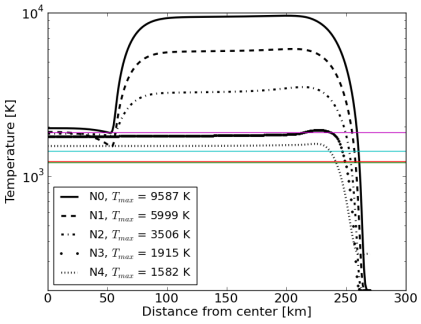

(e) t = 5.0 Ma

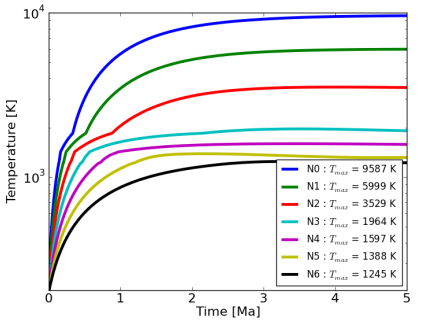

(f) Maximum temperature

Figure 5.2: Temperature vs distance from center (a-b-c-d-e), maximum temperature vs time (f), for $\phi = 2$ vol.%.

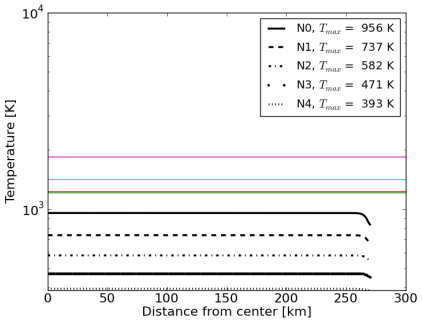

(a) t = 0.1 Ma

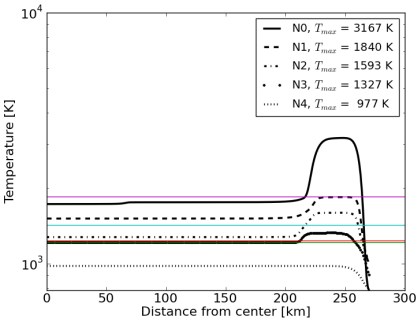

(b) t = 0.5 Ma

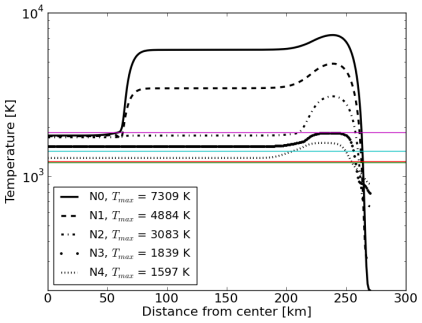

(c) t = 1.5 Ma

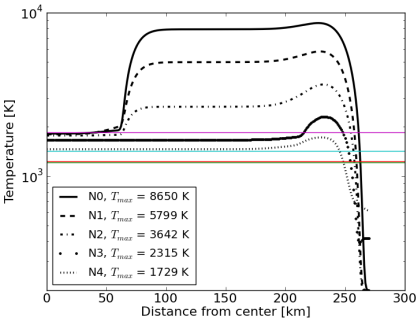

(d) t = 3.0 Ma

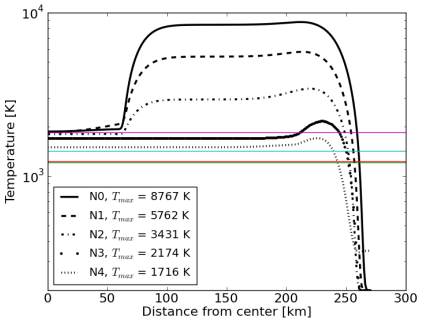

(e) t = 5.0 Ma

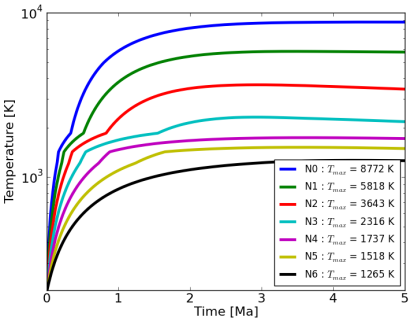

(f) Maximum temperature

Figure 5.3: Temperature vs distance from center (a-b-c-d-e), maximum temperature vs time (f), for $\phi = 5$ vol.%.

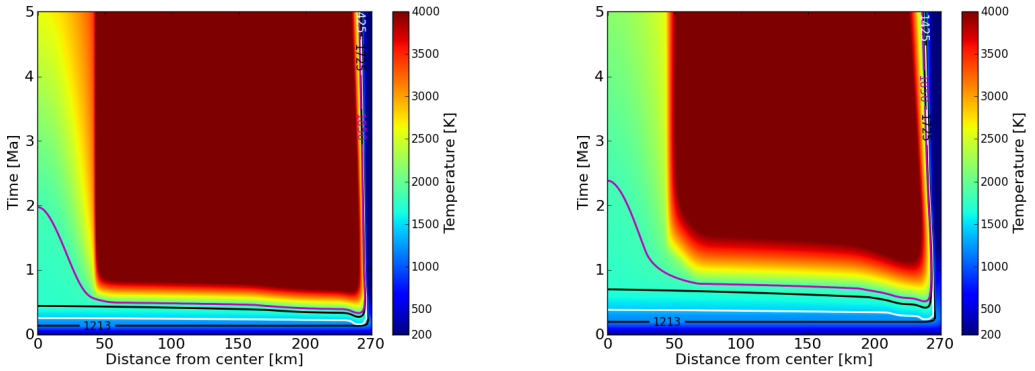

(a) Scenario 0

(b) Scenario 1

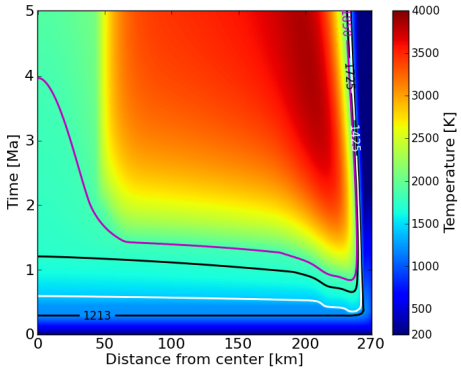

(c) Scenario 2

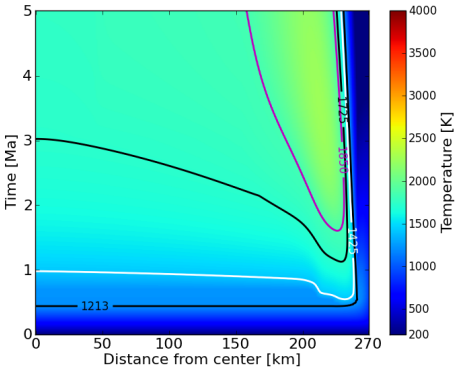

(d) Scenario 3

Figure 5.4: Thermal history maps for $\phi = 1$ vol.%

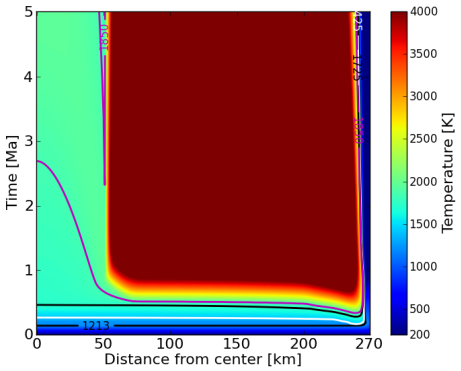

(a) Scenario 0

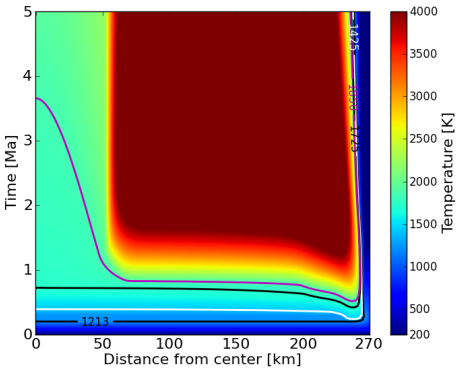

(b) Scenario 1

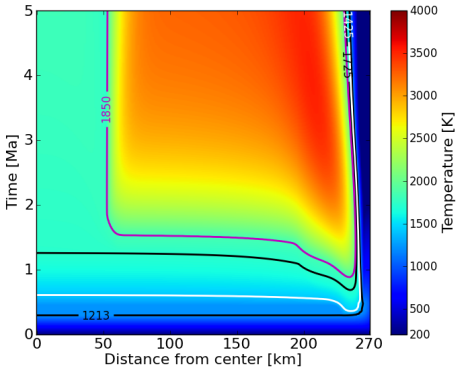

(c) Scenario 2

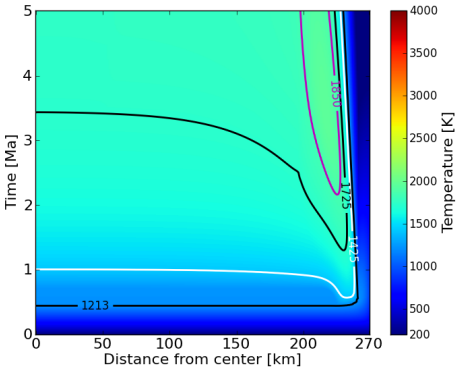

(d) Scenario 3

Figure 5.5: Thermal history maps for $\phi = 2$ vol.%

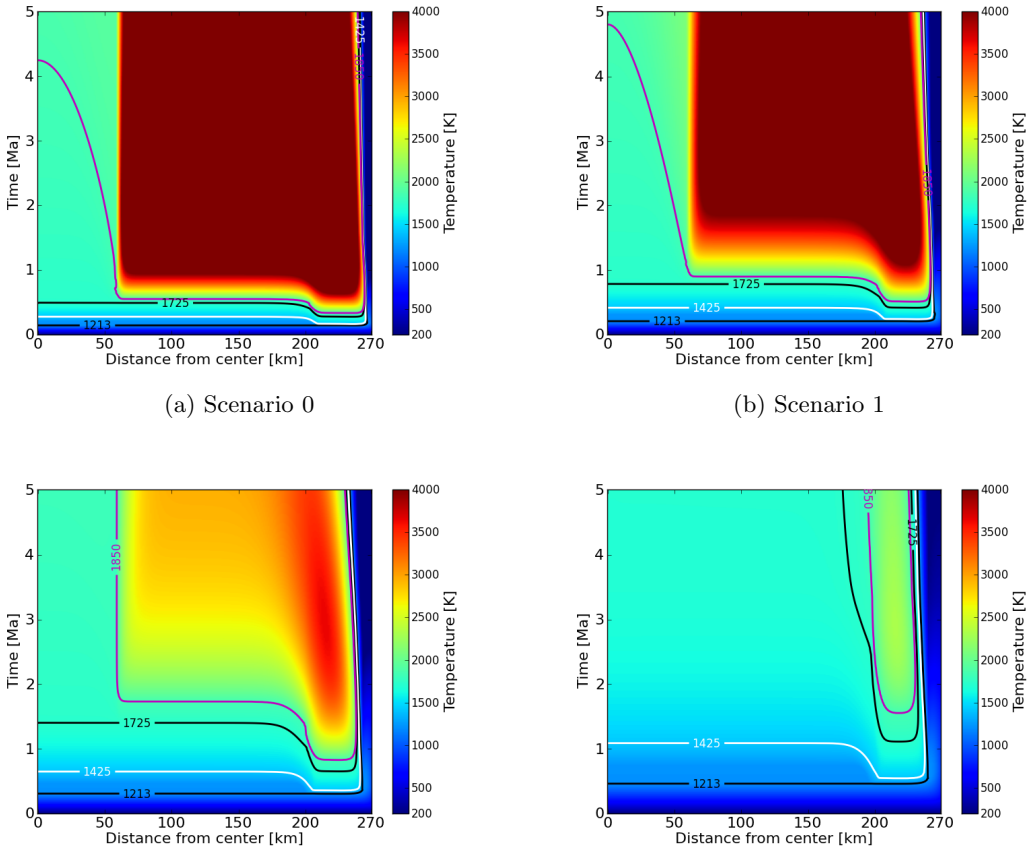

(a) Scenario 0

(b) Scenario 1

(c) Scenario 2

(d) Scenario 3

Figure 5.6: Thermal history maps for $\phi = 5$ vol.%

Chapter 6

Results: the case of Lutetia

As in discussing the geophysical history scenarios of Vesta, I explored several scenarios characterized by different strength of the energy sources (the radiogenic heat due to the decay of ^{26}Al) and values of post-sintering macroporosity (10, 20 and 30 vol.%). The scenarios are labeled N0 (instantaneous accretion, i.e $\Delta t_d = 0$, N1 ($\Delta t_d \simeq 0.3$ Ma) and N2 ($\Delta t_d \simeq 0.7$ Ma). The main results are showed in Tab.6.1, in which I reported the size and the time of formation of the proto-core (i.e. a structure enriched in metals and containing pristine silicates), the proto-core relative mass and maximum temperature reached after 5 Ma. I do not calculate the moment of inertia factor, because in all the explored scenarios the complete differentiation never does take place.

	Size [km]	Δt_{core} [Ma]	M_{core} [$\%M_{tot}$]	T_{max}
N0				
$\phi = 10$ vol.%	31	1.2	$\simeq 36$	1455
$\phi = 20$ vol.%	21	1.7	$\simeq 11$	1444
$\phi = 30$ vol.%	13	2.3	$\simeq 3$	1338
N1				
$\phi = 10$ vol.%	28	1.6	$\simeq 27$	1448
$\phi = 20$ vol.%	18	2.3	$\simeq 7$	1358
$\phi = 30$ vol.%	11	2.8	$\simeq 2$	1282
N2				
$\phi = 10$ vol.%	25	2.2	$\simeq 19$	1387
$\phi = 20$ vol.%	14	3.2	$\simeq 3$	1284
$\phi = 30$ vol.%	6	3.6	< 1	1240

Table 6.1: Summary of scenarios.

In all the case I analyzed, the maximum degree of silicate melting (about 10 vol.%, corresponding to about 1450 K, Taylor (1992)) is reached only in a limited region of the asteroid. In the case of post-sintering porosity of 10 vol.%, we can observe that in all scenarios Lutetia does not completely differentiate and only a proto-core forms (see the maximum temperature versus time profiles of Fig.6.1(f)). In Fig.6.1(a), after 0.1 Ma in the three scenarios the temperature is lower than the solidus temperature of silicates and the asteroid is homogeneously heated. After 0.5 Ma (Fig.6.1(b)), N0 enters in the melting temperature of silicates, while in N1 and N2 the temperature are lower than 1425 K. After 1 Ma (Fig.6.1(c)) in N1 the temperature reaches the solidus temperature of silicates, while in N2 the values are still low. In Fig. 6.1(d), after 3 Ma we observe a slight general increase of the temperature in all scenarios and than, after 5 Ma, in N0 the temperature has almost the same value while in N1 and N2 we observe a general decrease of the temperature. The core size ranges from 25 to 31 km with a density of $\simeq 4900$ kg m^{-3}: the time of formation ranges from 1.2 to 2.2 Ma. The maps of Fig.6.4 summarize the results obtained, showing that maximum temperatures are reached in the middle region of the asteroid (from 30 to 40 km from the center) as a consequence of the partial differentiation: in

this region, in fact, there is less mass to be heated and so the temperatures are high. The general trend, for a porosity of 20 vol.%, is similar to the previous case, but the values of temperature reached in this case are lower because of the lower amount of material (and therefore energy sources) per unity volume. (see Fig.6.2(a)). As we can observe in Fig.6.2(b), after 0.5 Ma in N0 and N1, the temperatures overcomes the liquidus temperature of metallic component, while in N2 the temperature is in the window of melting of metals. After 1.5 Ma (see Fig.6.2(c)) Lutetia is in the heating phase for all the scenarios and after 3 Ma (see Fig.6.2(d)) the general trend is the same. In Fig.6.2(e) after 5 Ma we observe a general decrease of the temperature, for N1 and N2. In Fig.6.2(f) the maximum temperature versus time profile is reported. We observe that the maximum temperature is reached in the hottest scenario, characterized by instantaneous accretion (i.e N0), and the time of formation of the core ranges from 1.7 to 3.2 Ma while the core size ranges from 14 to 21 km. In Fig.6.5 we can see that the general trend is the same of Fig.6.4 but the temperatures reach lower value than the previous case because the porosity is increased (i.e. 20 vol.%). In N0 the melting of silicates is possible while in N1 and N2 only the melting of metals occurs. If I choose a value of porosity of 30 vol.%, we can observe that after a isothermal phase (see Fig.6.3(a)) for all scenarios, at 0.5 Ma the temperature overcomes the liquidus melting temperature of metals in N0, while in N1 is in the windows of melting of metals and in N2 is lower than 1213 K (see Fig.6.3(b)). After 1.5 Ma (see Fig.6.3(c)), N1 overcomes the liquidus temperature of metals and N2 enters in the windows of melting of metals. The general trend is the same after 3 Ma and 5 Ma (see Fig.6.3(d)) and (e), respectively). In no scenarios the temperature reaches the solidus temperature of silicates (see Fig.6.3(f)). The formation of the proto-core occurs from $\simeq$ 2 Ma to $\simeq$ 4 Ma. Fig.6.6 shows that high values of porosity (i.e. 30 vol.%) prevent the reaching of silicate melting temperature and in particular, when the delay in the injection of ^{26}Al is larger (i.e. 0.72 Ma), also the melting of metals is possible in a narrow region of Lutetia, ranging from 5 km to 15 km.

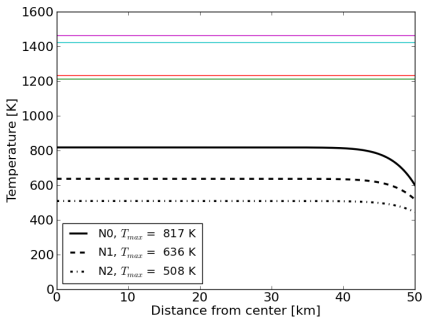

(a) t = 0.1 Ma

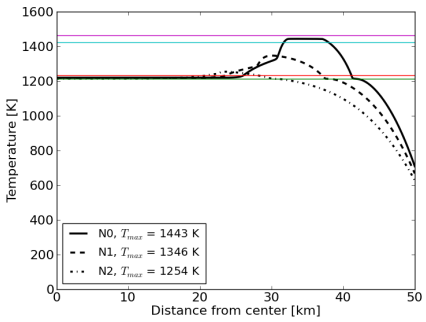

(b) t = 0.5 Ma

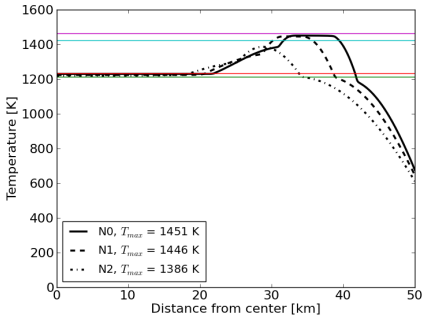

(c) t = 1.5 Ma

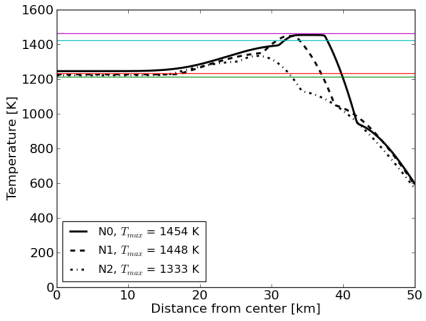

(d) t = 3.0 Ma

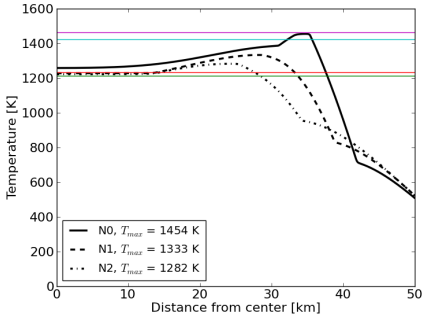

(e) t = 5.0 Ma

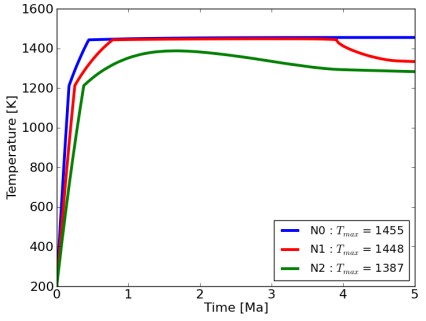

(f) Maximum temperature

Figure 6.1: Temperature vs distance from center (a-b-c-d-e), maximum temperature vs time (f) profile, for $\phi = 10$ vol.%.

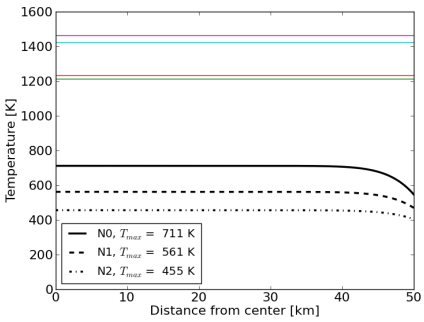

(a) t = 0.1 Ma

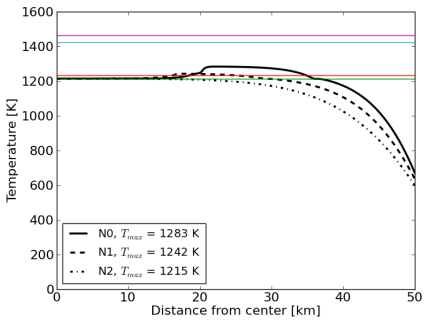

(b) t = 0.5 Ma

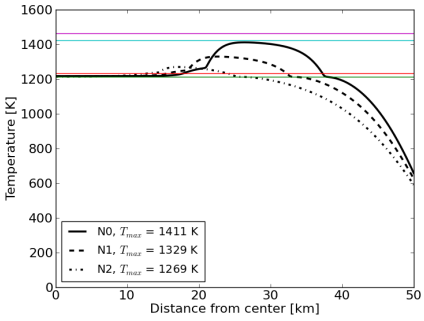

(c) t = 1.5 Ma

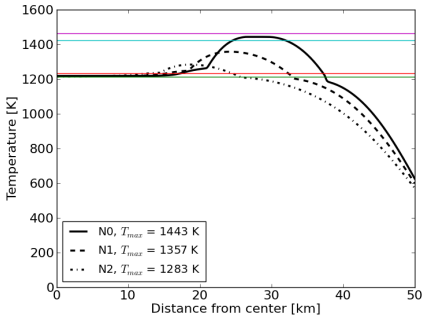

(d) t = 3.0 Ma

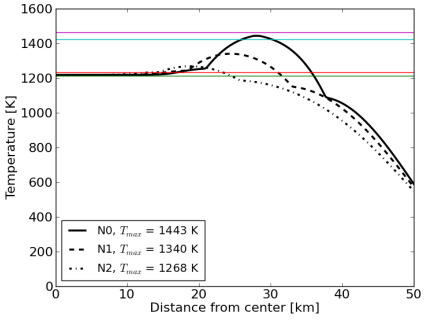

(e) t = 5.0 Ma

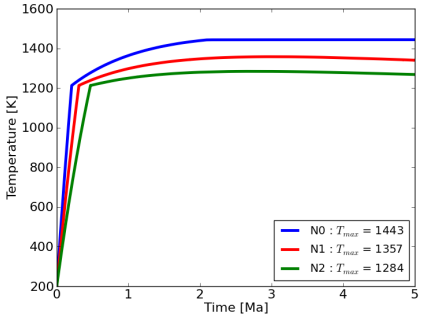

(f) Maximum temperature

Figure 6.2: Temperature vs distance from center (a-b-c-d-e), maximum temperature vs time (f) profile, for $\phi = 20$ vol.%.

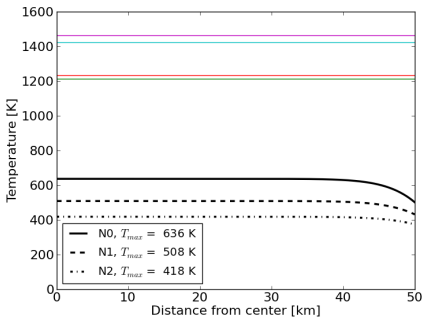

(a) t = 0.1 Ma

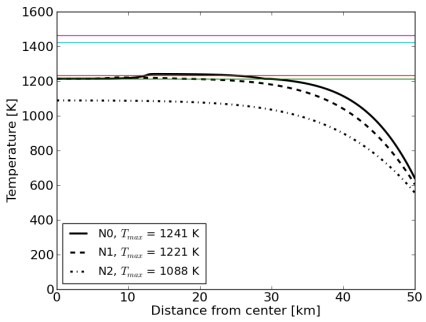

(b) t = 0.5 Ma

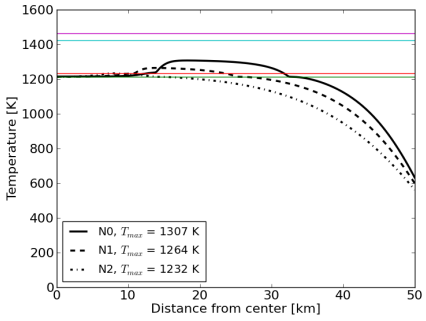

(c) t = 1.5 Ma

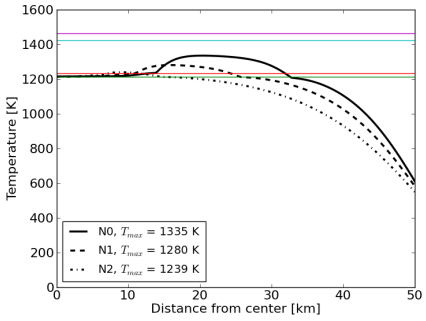

(d) t = 3.0 Ma

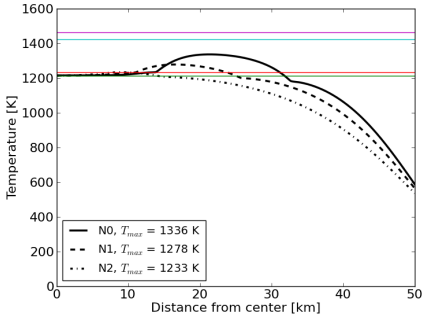

(e) t = 5.0 Ma

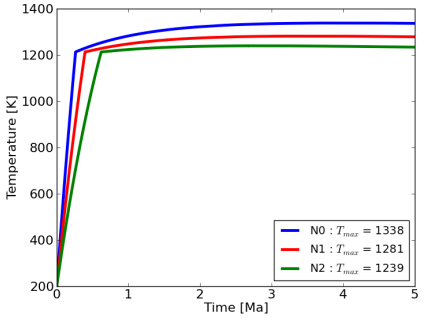

(f) Maximum temperature

Figure 6.3: Temperature vs distance from center (a-b-c-d-e), maximum temperature vs time (f) profile, for $\phi = 30$ vol.%.

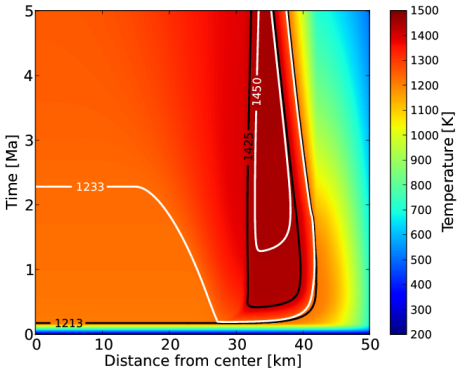

(a) Scenario 0

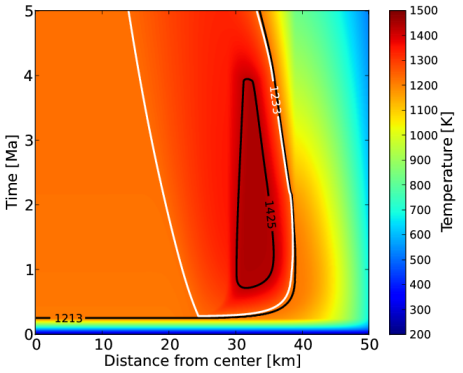

(b) Scenario 1

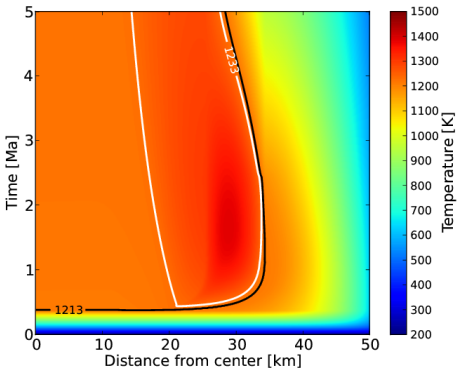

(c) Scenario 2

Figure 6.4: Thermal history maps for $\phi = 10$ vol.%

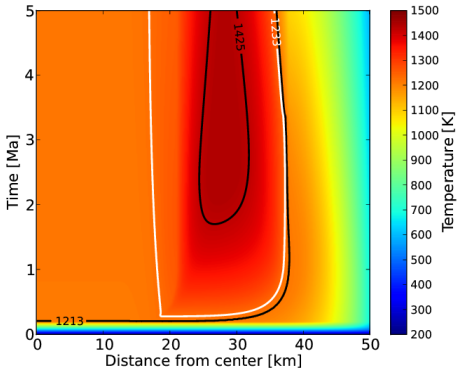

(a) Scenario 0

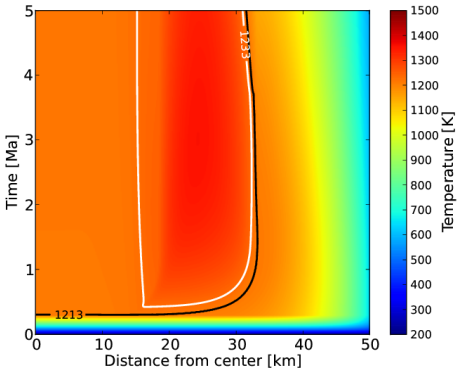

(b) Scenario 1

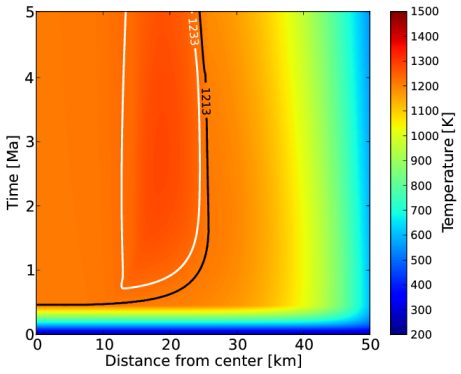

(c) Scenario 2

Figure 6.5: Thermal history maps for $\phi = 20$ vol.%

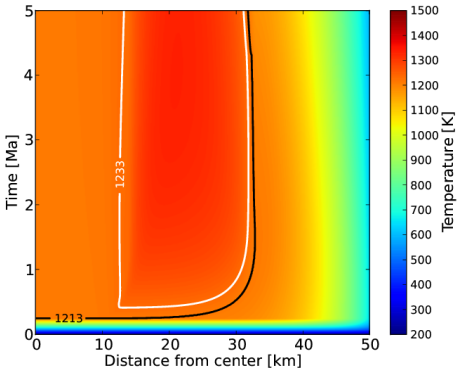

(a) Scenario 0

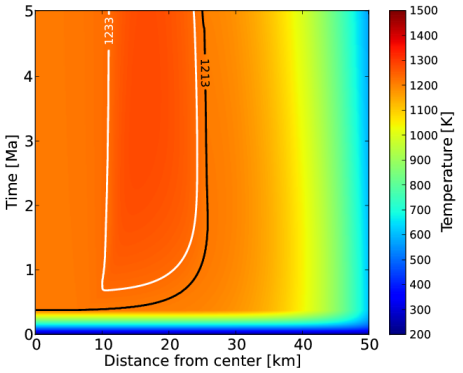

(b) Scenario 1

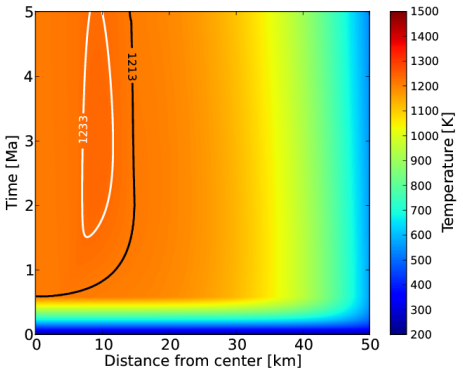

(c) Scenario 2

Figure 6.6: Thermal history maps for $\phi = 30$ vol.%

Conclusions

English Version

In this work I analyzed the thermal histories of Vesta and Lutetia across the first 5 Ma from their formation. I considered several scenarios differing in the available strength of energy and in the post-sintering macroporosity and I focused my analysis on the effects on the evolution of the internal structure (percolation of metals and separation of silicatic and metallic melts) and of crust (chondritic and achondritic) and on the heat distribution due to the radiogenic sources. I observed that the main source of energy is represented by ^{26}Al while the contribution of the other radionuclides (^{60}Fe,^{238}U and ^{235}U) are negligible and the same holds true for the contribution of the accretional heating. In fact, in the case of Vesta the maximum temperature rise, if all the accretional energy was stored internally, is $\simeq 90\ K$ and of the impacts that only produce a local heating on the surface of the asteroid. The differentiation process, i.e. the separation of the metallic core from the silicatic part, does produce a temperature rise less than 10 % of the accretional energy. At the surface the balance between thermal heating and the black-body irradiation into space offers a more realistic picture of the thermal history than a simple case in which the temperature of the surface is fixed to a constant value.

In the case of Vesta I explored several scenarios (N0-N6) characterized by different radiogenic strengths, expressed by a delay-parameter (Δt_d) ranging from 0 to 2.16 Ma. I opted for an initial composition, similar to those of the H and L classes of the ordinary chondrites, of about 75 vol.% of silicates and about 25 vol.%: the chosen values of the porosity are 1, 2

and 5 vol.%. In the scenarios in which the differentiation takes place the metallic core has a radius of about 60 km, density of about 6200 kgm^{-3} and moment of inertia of 0.33. In these scenarios the formation time of the core ranges from about 0.5 to 3.5 Ma. I observed the solidification of a surface layer whose maximum thickness is about 30 km. This solid layer is composed by a chondritic crust with its thickness reaching the maximum of about 20 km and the exact value strongly depends on the formation time of Vesta. A 5-10 thick eucritic layer can already form beneath the chondritic crust between 3 and 5 Ma, in agreement with the dating of the oldest eucrites described by Bizzarro et al. (2005). The solidification of this solid layer is possible even in absence of convection and volcanism, but only with conduction of heating mechanism and irradiation at the surface. The survival of the chondritic crust and the rate of solidification of the underlying eucritic layer are of particular importance to understand the geophysical and thermal evolution of Vesta as, across the temporal interval here investigated, the asteroid underwent a bombardment caused by the formation of Jupiter Turrini et al. (2011, 2012). The Jovian Early Bombardment, in fact, causes a global erosion of the primordial crust of Vesta (Turrini 2012, submitted) and the chondritic crust plays an important role in preserving the eucritic layer. Moreover, the Jovian Early Bombardment can trigger local or large-scale effusive phenomena due to the excavation of craters and the formation of impact basins Turrini et al. (2011), thus affecting the cooling history of Vesta.

The complete melting of silicates is achieved if Vesta takes less than 0.8 Ma to form while it is achieved in a limited region of the mantle if the formation is completed in about 1 Ma and in the rest of the asteroid a 50 vol.% melting of silicates occurs. If the formation is completed in about 1.4 Ma the degree of melting is generally lower than 50 vol.% and for formation time of more than 1.5 Ma the melting, when occurring, is limited to a small region of the asteroid. The formation time should not exceed 1 Ma if the crystallization of eucrites and diogenites are linked to a large degree (more than 50 vol.%) of silicates as suggested by Greenwood et al. 2005. If eucrites and diogenites can form from a partial melt ranging to 25-50 vol.%, accretion times of less than 1.5 Ma are still compatible with

the formation of HEDs. The global picture depicted of my results supplies new tools for the interpretation of the data gathered the Dawn mission to investigate the internal structure as well as the composition of the crust and of the underlying mantle of Vesta and to constrain the surface evolution of the asteroid.

In the case of Lutetia, observational data do not provide stringent constraints about the internal structure. Currently we know that Lutetia possesses a chondritic crust (carbonaceous or enstatitic) and its high bulk density suggests the presence of a metallic core. The results of my model suggest partial differentiation (in fact, the maximum degree of silicate melting is about 10 vol.% in a limited region of the mantle) if the current macroporosity (10 - 30 vol.%) is the same at the time of formation as proposed by Weiss et al. 2011. In all scenarios only the formation of a proto-core, i.e. a structure enriched in metals, occurs. The proto-core formed from 1 to about 4 Ma and its size ranges from 6 to 30 km. The relative proto-core mass ranges from about 1 to about 36 % of the total mass. My results suggest that the accretion time does not exceed 0.7 Ma from CAIs and the post-sintering macroporosity does not exceed 30 vol.%.

Italian Version

Nel mio lavoro ho analizzato le storie termiche degli asteroidi Vesta e Lutetia, appartenenti alla Fascia Principale. Gli scenari considerati differiscono per l'energia (rilasciata dal decadimento del radionuclide ^{26}Al) a disposizione per la differenziazione e per la macroporosità post-sintering.

La temperatura alla superficie non è fissata ma è regolata dal bilancio energetico tra il calore prodotto all'interno e quello irraggiato come un corpo nero.

Sia per Vesta che per Lutetia ho scelto una composizione simile a quella delle condriti H o L, ma gli intervalli di porosità analizzati sono differenti.

Nel caso di Vesta, si osserva in quasi tutti gli scenari la formazione di un nucleo metallico di raggio di circa 60 km. Il suo tempo di formazione va da 0.5 a 3.5 Ma. La crosta ha uno spessore massimo di circa 30 km, di cui circa 20 km composto da materiale condritico e circa 10 km da materiale eucritico

successivamente cristallizzato. Il grado di fusione è sempre maggiore del $\simeq$ 50 % dell'intero volume nella quasi totalità dei casi esplorati.

Nel caso di Lutetia, invece, non si posseggono molti dati osservativi: i pochi di cui si dispone indicano la presenza di una crosta primitiva e la presenza di un nucleo ferroso. I miei risultati suggeriscono che, se l'attuale macroporosità fosse quella al tempo della sua formazione, Lutetia in nessun caso riuscirebbe a differenziare completamente, arrivando a fondere una piccolissima regione al suo interno. E' soltanto possibile, quindi, la formazione di un proto-core, ossia una struttura arricchita di metalli ma ancora contenente materiale silicatico al suo interno.

Appendix A

Von Neumann stability analysis for FTCS scheme

The FTCS scheme is always unstable as we can show by using the following test solution:

$$C_j^n = \xi(k)^n e^{ikj\Delta x} \tag{A.1}$$

in the eq.(4.21), where $\xi(k)$ is the amplification factor and k is a real spatial wave number. We suppose that the coefficients of the difference equations are so slowly varying as to be considered constant in space and time, so the *eigenmodes* of the difference equations are all of the form of the eq.(A.1). The *von Neumann's stability condition* for the amplification factor $\xi(k)$ reads:

$$\xi(k) \leq 1 \tag{A.2}$$

for all k. In FTCS scheme, we obtain:

$$\xi(k)^{n+1} e^{ikj\Delta x} = \xi(k)^n e^{ikj\Delta x} - \frac{v\Delta t}{2\Delta x}\left(\xi(k)^n e^{ik(j+1)\Delta x} - \xi(k)^n e^{ik(j-1)\Delta x}\right). \tag{A.3}$$

By dividing for ξ^n we get:

$$\xi(k) e^{ikj\Delta x} = e^{ikj\Delta x}\left[1 - \frac{v\Delta t}{2\Delta x}\left(e^{ik\Delta x} - e^{-ik\Delta x}\right)\right] \tag{A.4}$$

writable as:

$$\xi(k) = 1 - i\frac{v\Delta t}{\Delta x}\left(sin(k\Delta x)\right). \tag{A.5}$$

Finally, we have the following expression for the amplification factor:

$$\mid \xi(k) \mid = \sqrt{1 + \left(\frac{v\Delta t}{\Delta x}\right)^2 sin^2(k\Delta x)} \tag{A.6}$$

and we can observe that:

$$\mid \xi(k) \mid > 1. \tag{A.7}$$

In the *von Neumann stability analysis* we would still treat v as a constant (v slowly varying). One can see that the magnitude of the amplification factor $\xi(k)$ is greater than unity for all k. This implies that the instability occurs for all given v, Δt and Δx, i.e., the FTCS scheme is unconditionally unstable. By adjusting the FTCS scheme with the Lax correction, we note that the final scheme is stable. Applying the Von Neumann stability analysis to eq.(4.22) we get:

$$\begin{aligned} \xi(k)^{n+1} e^{ikj\Delta x} &= \frac{1}{2}\left(\xi(k)^n e^{ik(j+1)\Delta x} + \xi(k)^n e^{ik(j-1)\Delta x}\right) \\ &-\frac{v\Delta t}{2\Delta x}\left(\xi(k)^n e^{ik(j+1)\Delta x} - \xi(k)^n e^{ik(j-1)\Delta x}\right). \end{aligned} \tag{A.8}$$

By dividing for ξ^n and rearranging the terms:

$$\xi(k) e^{ikj\Delta x} = e^{ikj\Delta x}\left[\frac{e^{ik\Delta x} + e^{-ik\Delta x}}{2} - \frac{v\Delta t}{\Delta x}\left(\frac{e^{ik\Delta x} - e^{-ik\Delta x}}{2}\right)\right] \tag{A.9}$$

writable as:

$$\xi(k) = \left[cos(k\Delta x) - i\frac{v\Delta t}{\Delta x} sin(k\Delta x)\right]. \tag{A.10}$$

The amplification factor, in this case, is:

$$\mid \xi(k) \mid = \sqrt{cos^2(k\Delta x) + \left(\frac{v\Delta t}{\Delta x}\right)^2 sin^2(k\Delta x)} \tag{A.11}$$

or:

$$\mid \xi(k) \mid = \sqrt{1 - \left[1 - \left(\frac{v\Delta t}{\Delta x}\right)^2\right] sin^2(k\Delta x)}. \tag{A.12}$$

It follows that the Lax scheme is unconditionally stable (i.e. $\mid \xi \mid < 1$ for all k), provided that:

$$\Delta t < \frac{\Delta x}{v}. \tag{A.13}$$

This is the famous *Courant-Friedrichs-Lewy* (or CFL) stability criterion. In fact, all stable explicit differencing schemes for solving the advection equation are subject to the CFL constraint, which determines the maximum allowable time-step. To understand the physical meaning of the Lax method, we rewrite the eq.(4.22) by adding and subtracting the terms C_m^n:

$$C_m^{n+1} - C_m^n = -\frac{v\Delta t}{2\Delta x}\left(C_{m+1}^n - C_{m-1}^m\right) + \frac{1}{2}\left(C_{m+1}^n + C_{m-1}^n\right) - C_m^n. \quad \text{(A.14)}$$

By dividing for Δt and rearranging the expression:

$$\frac{C_m^{n+1} - C_m^n}{\Delta t} = -\frac{v}{2\Delta x}\left(C_{m+1}^n - C_{m-1}^m\right) + \frac{1}{2\Delta t}\left(C_{m+1}^n - 2C_m^n + C_{m-1}^n\right). \quad \text{(A.15)}$$

The eq.(A.15) has the following "physical" form:

$$\frac{\partial C}{\partial t} = -v\frac{\partial C}{\partial x} + \frac{(\Delta x)^2}{2\Delta t}\frac{\partial^2 C}{\partial x^2}, \quad \text{(A.16)}$$

where the last term on the right is the *numerical viscosity* introduced by the Lax method. If $\Delta t \leq \dfrac{\Delta x}{v}$, the artificial viscosity ensures that the method is stable (it smooths out the instabilities). But, if Δt is too small the viscosity term dominates and pulse dies away (it smooths out everything).

List of Figures

List of Tables

Bibliography

Alexander C.M.O'D. et al., *Evolution of the inner solar system: A meteoritic perspective*, Science 293 (2001).

Amelin Y. et al., *Lead isotopic ages of chondrules and calcium-alluminum-rich inclusions*, Science 297 (2002).

Asphaug E., *Impact origin of Vesta family*, Meteoritics and Planetary Science 32 (1997).

Asphaug E. et al., *Asteroid Interiors*, Asteroids III, Arizona Press (2003).

Asphaug E. et al., *Growth and evolution of Asteroids*, Annual Review of Earth and Planetary Science 37 (2009).

Barucci M.A. et al., *Classification of asteroids using G-mode analysis*, Icarus 72 (1987).

Belskaya I.N et al., *Puzzling asteroid 21 Lutetia: our knowledge prior to the Rosetta fly-by*, Astronomy & Astrophysics 515 (2010).

Binzel R.P., Xu S., *Chips off of asteroid 4 Vesta: Evidence for the parent body of basaltic achondrite meteorites*, Science 260 (1993).

Binzel R.P. et al., *Geologic mapping of Vesta from 1994 Hubble Space Telescope images*, Icarus 128 (1997).

Bizzarro M. et al., *Rapid Timescales for Accretion and Melting of Differentiated Planetesimals Inferred from ^{26}Al - ^{26}Mg Chronometry*, The Astrophysical Journal 632 (2005).

Bottke Jr. W.F. et al., *An Overview of the Asteroids: The Asteroids III Perspective*, Asteroids III, Arizona Press (2003).

Bottke Jr. W.F. et al., *Linking the collisional history of the main asteroid belt to its dynamical excitation and depletion*, Icarus 179 (2005).

Bouvier A. et al., *Pb-Pb dating constraints on the accretion and cooling history of chondrites*, Geochimica et Cosmochimica Acta 71 (2007).

Brearley A.J., Jones R.H., *Chondritic meteorites*, in Planetary Materials (J.J. Papike, ed.), Reviews in Mineralogy 36, Mineralogical Society of America (1998).

Britt D.T. et al., *Asteroid Density, Porosity, and Structure*, Asteroids III, Arizona Press (2003).

Brophy J.R. et al., *Status of Dawn ion propulsion system*, AIAA paper 2004-3433, 40th AIAA/ASME/SAE/ASEE Joint Propulsion Conference and Exhibit, Fort Lauderdale, FL, USA (2004).

Bus S.J. & Binzel R.P., *Phase II of the small main-belt asteroid spectroscopic survey: A feature-based taxonomy*, Icarus 158 (2002).

Cameron A.G.W., *Origin of the Solar System*, Annual Review of Astronomy & Astrophysics 26 (1988).

Castillo-Rogez J. et al., *Iapetus'geophysics: Rotation rate, shape, and equatorial ridge*, Icarus 190 (2007).

Castillo-Rogez J. et al., ^{26}*Al decay: Heat production and a revised age for Iapetus*, Icarus 204 (2009).

Carlslaw H.S., Jager J.C., *Conduction of heat in solids*, Oxford University Press (1959).

Carpozen L. et al., *Magnetic evidence for a partially differentiated carbonaceous chondrite parent body*, Proceedings of the National academy of Sciences of the United States of America 108 (2011).

Chambers J., *Planetesimal formation by turbulent concentration*, Icarus 208 (2010).

Chandrasekhar S., *Hydrodynamic and Hydromagnetic Stability*, Dover Publications, Inc., New York (1961).

Chaudisson M. & Gounelle M., *Short-lived radioactive nuclides in meteorites and early solar system process*, Comptes Rendus Geoscience 339 (2007).

Cloutis E.A. et al., *Reflectance spectra of iron meteorites: Implications for spectral identification of their parent bodies*, Meteoritics and Planetary Science 45 (2010).

Consolmagno G.J. et al., *The significance of meteorite density and porosity*, Chemie der Erde 68 (2008).

Consolmagno G.J., Drake M.J., *Composition and evolution of the eucrite parent body - Evidence from rare earth elements*, Geochimica et Cosmochimica Acta 41 (1977).

Coradini A. et al., *Earth and Mars: early thermal profiles*, Physics of the Earth and Planetary Interiors 31, Elsevier Scientific Publishing Company, Amsterdam (1983).

Coradini A. et al., *Vesta and Ceres: Crossing the History of the Solar System*, Space Science Review 163 (2011).

Coradini et al., *The Surface Composition and Temperature of Asteroid 21 Lutetia As Observed by Rosetta/VIRTIS*, Science 334 (2011).

Cuzzi J.N. et al., *Towards initial mass functions for asteroids and Kuiper belt objects*, Icarus 208 (2010).

DeMeo F. et al., *An extension of the Bus asteroid taxonomy into the near-infrared*, Icarus 202 (2009).

De Sanctis M.C. et al., *Spectral and mineralogical characterization of inner main-belt V-type asteroids*, Astronomy & Astrophysic 533 (2011)

De Sanctis M.C. et al., *Spectoscopic Characterization of Mineralogy and Its Diversity Across Vesta*, Science 336 (2012).

Drake M.J., *The Eucrite Vesta Story*, Meteoritics and Planetary Science 36 (2001).

Drummond J. et al., *Speckle Interferometer of Asteroids. IV - Reconstructed images of 4 Vesta*, Icarus 73 (1988).

Elkins-Tanton L.T. et al., *Chondrites as samples of differentiated planetesimals*, Earth and Planetary Science Letters 305 (2011).

Elkins-Tanton L.T., *Magma Oceans in the Inner Solar System*, Annual Review of Earth Planetary Science 40 (2012).

Elsasser W.M., *Early history of the Earth*, in Earth Science and Meteorites, ed. by Geiss J. and Goldberg E., 1-30, North Holland (1963).

Encrenaz T. et al., *The Solar System*, Springer Berlin (1987).

Farinella P. & Vokrouhlick Y.D, *Semimajor Axis Mobility of Asteroidal Fragments*, Science 283 (1999).

Foderà Serio G. et al., *Giuseppe Piazzi and the Discovery of Ceres*, Asteroids III, Arizona Press (2003)

Fountain J.A., West E.A., *Thermal conductivity of particulate basalt as a function of density in simulated lunar and Martian environments*, Journal of Geophysical Research 75 (1970).

Gaffey M.J., *Surface Lithologic Heterogeneity of Asteroid 4 Vesta*, Icarus 127 (1997).

Ghosh A. & McSween Jr. H.Y., *A Thermal Model for the Differentiation of Asteroid 4 Vesta, Based on Radiogenic Heating*, Icarus 134 (1998).

Ghosh A. & McSween Jr. H.Y., *Temperature dependence of specific heat capacity and its effect on asteroid thermal models*, Meteoritics & Planetary Science 34 (1999).

Greenwood R.C. et al., *Widespread Magma Oceans On Asteroidal Bodies In The Early Solar System*, Nature 435 (2005).

Gupta G. & Sahijpal S., *Differentiation of Vesta and the parent bodies of other achondrites*, Journal of Geophysic Research 115 (2010)

Harmann W.K. et al., *The time dependent intense bombardment of the primordial Earth/Moon system.*, in: Canup, R. and Righter, K. (Eds.), Origin of the Earth and Moon, The University of Arizona Press, Tucson, Arizona (2000).

Hewins R.H. & Newsom H.E., *Igneous activity in the early solar system. Meteorites and the early solar system*, Tucson, AZ, University of Arizona Press (1988).

Hevey P. J & Sanders I.S., *A model for planetesimals meltdown by ^{26}Al and its implications for meteorite parent bodies*, Meteoritics & Planetary Science 41 (2006).

Hilton J.L., *Asteroid Masses and Densities*, Asteroids III, Arizona Press (2003).

Horan M. F. et al., *W-182 and Re(187)-Os-187 systematics of iron meteorites - Chronology for melting, differentiation, and crystallization in asteroids*, Geochimica et Cosmochimica Acta 62 (1998).

Howell E.S. et al., *Classification of asteroid spectra using a neural network*, Journal of Geophysical Research 99 (1994).

Kaula W.M., *Formation of the terrestrial planetes in Planetary Systems, the long View*, ed. L.M. Celnikier & J.Tran Thanh Van (Edition Frontieres, Paris) (1998).

Keil K. et al., *Constraints on the Role of Impact Heating and Melting in Asteroids*, Meteoritcs and Planetary Science 32 (1997).

Kleine T. et al., *Rapid accretion and early core formation on asteroids and the terrestrial planets from Hf-W chronometry*, Nature 418 (2002).

Konopliv A.S. et al., *Gravity investigation*, Space Science Review (2011).

Korenaga J., *Energetics of mantle convection and the fate of fossil heat*, Geophysical Research Letters 30 (2003).

Kushiro I. & Mysen B.O., *Melting experiments on a Yamato chondrite*, Proc.4th Symp. Antartic Met., Mem. Natl. Inst. Polar Res. 15 (1979).

Kuzmanoski M. et al., *The mass of(4) Vesta derived from its largest gravitational effects.*, The Astronomical Journal 140 (2010).

Larimer J.W., *Core formation in asteroid-sized bodies*, Meteoritics 30 (1995).

Lazzaro D., *Basaltic Asteroids: A New Look On The Differentiation Process In The Main Belt*, Rev.Mex.AA. (Serie de Conferencias) 35 (2009).

Lazzaro D. et al., *The visible spectroscopic survey of 820 asteroids*, Icarus 172 (2004).

Lee T. et al., *Demonstrating of* ^{26}Mg *excess in Allende and evidence for* ^{26}Al, Geophysical Research Letters 3 (1976).

Leinhardt Z.M. et al., *Direct, N-body simulations of rubble pile collisions*, Icarus 146 (2000).

Lewis J.S., *The temperature gradient in the solar nebula*, Science 186 (1974).

Li J.Y. et al., *Photometric mapping of Asteroid (4) Vesta's southern hemisphere with Hubble Space Telescope*, Icarus 208 (2010).

Lissauer J.J., *Planet Formation*, Annual Review of Astronomy and Astrophysics 31 (1993).

Lodders K. et al., *Trace elements in mineral separates of the Pena Blanca Spring aubrite - Implications for the evolution of the aubrite parent body*, Meteoritics 28 (1993).

Lugmair G.W. & Shukolyukov A., *Early solar system events and timescales*, Meteoritics and Planetary Science 36 (2001).

Lunine J.I., *Processing of material in the solar nebula*, ASP Conference Series 122 (1997).

Marcy G.W. et al., *Extrasolar Planets around Main Sequence Stars*, ASP Conference Series 213, G.Lemarchand, K. Meech eds. (2000).

Marzari F. et al.,*Origin and evolution of the Vesta asteroid family*, Astronomy and Astrophysics 316 (1996).

McCord T.B. & Sotin C., *Ceres: Evolution and current state*, Journal of Geophysical Research 110 (2005).

McCoy T.J. et al., *Partial melting and melt migration in the acapulcoite-lodranite parent body*, Geochimica et Cosmochimica Acta 61 (1997).

McCoy T. J., Mittlefehldt D. W. and Wilson L., *Asteroid differentiation.* In Meteorites and the early solar system II, ed. by Lauretta D. S. and McSween H. Y. Tucson, AZ: The University of Arizona Press (2006).

McKenzie D. & Bickle M. J., *The volume and composition of melt generated by extension of the lithosphere*, The Journal of Petroleum Science and Engineering 29 (1988).

MacPherson G. J. et al., *The distribution of aluminum-26 in the early Solar System - A reappraisal*, Meteoritics 30 (1995).

McSween Jr. H.Y. et al., *The mineralogy of ordinary chondrites and implications for asteroid spectrophotometry*, Icarus 90 (1991).

McSween Jr. H.Y. et al., *Thermal Evolution Models of Asteroids*, Asteroids III, Arizona Press (2003).

McSween Jr. H.Y. et al., *HED meteorites and their relationship to the geology of Vesta and the Dawn Mission*, Space Science Review (2011).

Merk R. et al., *Numerical Modeling of* ^{26}*Al-Induced Radioactive Melting of Asteroids Considering Accretion*, Icarus 159 (2002).

Migliorini F. et al., *Vesta fragments from* ν_6 *and* $3:1$ *resonances; Implications for V-type near-Earth-asteroids and howardite, eucrite and diogenite meteorites*, Meteoritics Planetary Science 32 (1997).

Milani A. et al., *Asteroid Close Approaches: Analysis and Potential Impact Detection*, Asteroids III, Arizona Press (2003).

Millis R.L. & Elliot J.L., *Direct determination of asteroid diameters from occulation observations*, in Asteroids, ed. by Gehrels T., Arizona Press, Tucson (1979).

Moskovitz N. & Gaidos E., *Differentiation of planetesimals and the thermal consequences of melt migration*, Meteoritics & Planetary Science 46 (2011).

Mostefaoui S. et al., ^{60}Fe*: A Heat Source for Planetary Differentiation from a Nearby Supernova Explosion*, The Astrophysical Journal 625 (2005).

Navrotsky A., *Thermodynamic properties of minerals. In Mineral physics and crystallography: A handbook of physical constants*, edited by Ahrens T. J. Washington, D.C.: American Geophysical Union (1995).

Neumann W. et al., *Differentiation and core formation in accreting planetesimals.* Astronomy & Astrophysics 543 (2012).

Nield D.A. & Bejan A., *Convection in Porous Media - Third Edition*, Springer Science+Business Media, Inc. (2006).

Nyquist L. E. et al., *Ages and Geologic Histories of Martian Meteorites*, Space Science Reviews 96 (2001).

Ockert-Bell M.E. et al., *The composition of M-type asteroids: Synthesis of spectroscopic and radar observations*, Icarus 210 (2010).

Patzold M. et al., *Asteroid 21 Lutetia: Low Mass, High Density*, Science 28 (2011).

Perna D. et al., *Inhomogeneities on the surface of 21 Lutetia, the asteroid target of the Rosetta mission - Ground-based results before the Rosetta fly-by*, Astronomy & Astrophysics 513 (2010).

Petit J.M. et al., *Primordial Excitation and Depletion of the Main Belt*, Asteroids III, Arizona Press (2003).

Pravec P. et al., *Asteroid Rotations*, Asteroids III, Arizona Press (2003).

Press W.H., Teukolsky S.A., Vetterling W.T., Flannery B.P., *Numerical Recipes Third Edition*, Cambridge University Press (2007).

Raymann M.D. et al., *Dawn:Amission in development for exploration of main belt asteroids Vesta and Ceres*, Acta Astronautica 58 (2006).

Richardson D.C. et al., *Gravitational Aggregates: Evidence and Evolution*, Asteroids III, Arizona Press (2003).

Rubin A.E., *Postshock annealing and postannealing shock in equilibrated ordinary chondrites: implications for the thermal and shock histories of chondritic asteroids*, Geochimica et Cosmochimica Acta 68 (2004).

Rugel G. et al., *New measurement of the ^{60}Fe half-life*, Physycal Review Letters 103 (7), (2009).

Russel C.T. et al., *Dawn at Vesta: Testing the Protoplanetary Paradigm*, Science 11 (2012).

Ruzicka A. et al., *Vesta as the howardite,eucrite and diogenite parent body: Implications for the size of a core and for large scale differentiation*, Meteoritics and Planetary Science 32 (1997).

Safronov V.S., *Evolution of the protoplanetary cloud and formation ofthe Earth and planets*, NASA Tech.Transl., TT-667 (1969).

Sahijpal S. et al., *Numerical simulations of the differentiation of accreting planetesimals with ^{26}Al and ^{60}Fe as the heat sources*, Meteoritics & Planetary Science 42 (2007).

Schenk P. et al., *The Geologically Recent Giant Impact Basins at Vesta's South Pole.* Science 336 (2012).

Sahijpal S. et al., *Did the carbonaceous chondrites evolve in the crustal regions of partially differentiated asteroids?*, Journal of Geophysical Research 116 (2011).

Schiller M. et al., *Rapid Timescales for Magma Ocean Crystallization on the Howardite-Eucrite-Diogenite Parent Body*, The Astrophysical Journal Letters 740 (2011).

Scott E.R.D. & Krot A.N., *Chondrites and their Components*, Treatise on Geochemistry 1. Editor: Andrew M. Davis. Executive Editors: Heinrich D. Holland and Karl K. Turekian (2003)

Scott E.R.D., *Chondrites and the protoplanetary disk*, Annual Review of Earth and Planetary Science 35 (2007).

Scott E.R.D. et al., *Oxygen isotopic constraints on the origin and parent bodies of eucrites, diogenites, and howardites*, Geochimica et Cosmochimica Acta 73 (2009).

Schubert G. et al., *Thermal histories, compositions and internal structures of the moons of the solar system*, in Satellites ed. by Burns J.A., Shapley M.S., Arizona Press, Tucson (1986).

Senshu H. & Matsui T., *Possible core formation within planetesimals due to permeable flow*. Workshop on Planetary Differentiation 4021 (2006).

Sonett C. P. et al., *Electrical Heating of Meteorite Parent Bodies and Planets by Dynamo Induction from a Pre-main Sequence T Tauri "Solar Wind"'*, Nature 291 (1968).

Šrámek O. et al., *Thermal evolution and differentiation of planetesimals and planetary embryos*, Icarus 217 (2012).

Srinivasan G. et al., *^{26}SAl in Eucrite Piplia Kalan: Plausible Heat Source and Formation Chronology*, Science 284 (1999).

Stolper E., *Experimental petrology of eucritic meteorites*, Geochimica et Cosmochimica Acta 41 (1977).

Tachibana S. & Huss G. R., *The Initial Abundance of ^{60}Fe in the Solar System*, The Astrophysical Journal 588 (2003).

Takahashi E., *Melting of a Yamato L3 chondorite (Y-74191) up to 30 kbar*, National Institute of Polar Research, Memoirs, Special Issue 30 (1983).

Taylor G.J. & Norman M.C., *Evidence for magma oceans on asteroids, the moon, and Earth*, in Lunar and Planetary Inst., Workshop on the Physics and Chemistry of Magma Oceans from 1 Bar to 4 Mbar (1992).

Taylor G.J., *Core formation in asteroids*, Journal of Geophysical Research 97 (1992)

Taylor G.J. et al., *Asteroid differentiation - Pyroclastic volcanism to magma oceans*, Meteoritics 28 (1993).

Tedesco E.F. et al., *A three-parameter asteroid taxonomy*, The Astronomy Journal 97 (1989).

Terasaki H. et al., *The effect of temperature, pressure, and sulfur content on viscosity of the Fe-FeS melt*, Earth Planetary Science 190 (2001).

Terasaki H. et al., *Percolative core formation in planetesimals*, Earth and Planetary Science Letters 273 (2008).

Tholen D. J., *Asteroid taxonomic classifcations*, in Asteroids II (R.P. Binzel, T. Gehrels, and M. S. Matthews, Eds.), Arizona Press, Tucson (1989).

Thomas P.C. et al., *Impact Escavation on Asteroid 4 Vesta: Hubble Telescope results*, Science 277 (1997a).

Thomas P.C. et al. *Vesta: Spin Pole, Size, and Shape from HST Images*, Icarus 128 (1997b).

Toksoz M.N. & Solomon S.C., *Thermal history and evolution of the moon*, The Moon 7 (1973).

Turcotte D.L. & Schubert G., *Geodynamics, 2nd ed.*, Cambridge University Press (2002).

Turrini D. et al., *Probing the history of Solar system through the cratering records on Vesta and Ceres* Monthly Notices of the Royal Astronomical Society 413 (2011).

Turrini D. et al., *Jovian Early Bombardment: Planetesimal Erosion in the Inner Asteroid Belt*, The Astrophysical Journal 750 (2012).

Turrini D.. *The primordial collisional evolution of Vesta: crater saturation, surface evolution and survival of the basaltic crust.* Submitted to Planetary & Space Science, special issue on the cratering of Vesta.

Urey H.C., *The cosmic abundances of potassium, uranium and thorium and the heat balances of the earth, the Moon and Mars*, Proc. Natl. Acad. Sci. 41 (1955).

Wadhwa M. et al., *Meteorites and the Early Solar System II*, ed. by Lauretta D.S., McSween H.Y Jr., Arizona Press, Tucson (2006).

Walker D. & Agee C.B., *Ureilite compaction*, Meteoritics 23 (1988).

Weidenschilling S.J., *Dust to planetesimals*, Icarus 44 (1980).

Weidenschilling S.J., *Formation processes and time scales for meteorite parent bodies, in Meteorites nad the Early Solar System*, ed. J.F. Kerridge & M.S. Matthews, University of Arizona Press, Tucson (1988).

Weidenschilling S.J. & Cuzzi J.N., *Formation of planetesimals in the solar nebula*, in Protostar and Planets III, ed by Levy E.H., Lunine J.I., Arizona Press, Tucson (1993).

Weidenschilling S.J. et al., *Accretional evolution of a planetesimal swarm 2. The terrestrial zone.*, Icarus 128 (1997).

Weidenschilling S.J., *Formation of Planetesimals and Accretion of the Terrestrial Planets*, Space Science Reviews 92 (2000).

Weiss B.P. et al., *Paleomagnetic records of meteorites and early planetesimal differentiation*, Space Science Reviews 152 (2010).

Weiss B.P. et al., *Possible evidence for partial differentiation of asteroid Lutetia from Rosetta*, Planetary and Space Science 66 (2011).

Wetherill G.W., *Origin of the asteroid belt*, in Asteroid II, ed. by Binzel R.P., Gehrels T., Matthews M.S., Arizona Press, Tucson (1989).

Whiffen G.J., Sims J.A., *Application of a novel optimal control algorithm to low-thrust trajectory optimization*, AAS paper 01-209, AAS/AIAA Space Flight Mechanics Conference, San Antonio, TX, USA (2003).

Williams J. G., *Asteroids II*, ed. Binzel R.P., Gehrels T. & Matthews M.S., Tucson, Arizona Press 1034 (1989).

Wilson L. & Keil K., *Consequences of explosive eruptions on small solar system bodies–The case of the missing basalts on the aubrite parent body*, Earth and Planetary Science Letters 104 (1991).

Woods J.A. & Morfill G.E., *A review of solar nebula*, In Meterorites and the Early Solar System, ed. J. F. Kerridge and M.S. Matthews, Arizona Press (1988).

Xu S. & Binzel R.P., *Small main-belt asteroid spectroscopic survey: Initial Results*, Icarus 115 (1995).

Yomogida K. & Matsui T., *Multiple parent bodies of ordinary chondrites*, Earth and Planetary Science Letters 68 (1984).

Yoshino T. et al., *Core formation in planetesimals triggered by permeable flow*, Nature 422 (2003).

Yoshino T. et al., *Connectivity of molten Fe alloy in peridotite based on in situ electrical conductivity measurements: implications for core formation in terrestrial planets*, Earth and Planetary Science Letters 222 (2004).

Youdin A.N. & Goodman J., *Streaming Instabilities in Protoplanetary Disks*, The Astrophysical Journal 620 (2005).

Zappalà V. et al., *Asteroid families*, The Astronomical Journal 100 (1990).

Zellner N.E.B. et al., *Near-IR imaging of asteroid 4 Vesta*, Icarus 177 (2005).

Zuber M.T. et al., *Origin, Internal Structure and Evolution of 4 Vesta*, Space Science Review 163 (2011).